Dottorato in Biologia Umana e Genetica Medica, XXIX ciclo

C. elegans as a model to identify and functionally characterize novel genes causing RASopathies and other developmental diseases

Candidato

Luca Pannone

Tutor interno:

Prof.ssa Viviana Caputo

Coordinatore:

Prof. Antonio Pizzuti

Tutor esterno

Dott. Simone Martinelli

Index

Summary

RASopathies are a family of syndromes affecting development and growth, sharing RAS signaling dysregulation as pathogenetic mechanism. Past work of our group and others have significantly contributed to our understanding of the molecular causes of these diseases. However, a large fraction of RASopathy cases remains unexplained molecularly. Here, I used the nematode *C. elegans* to reveal novel molecular mechanisms underlying RASopathies, as well as to identify new candidate genes for these group of developmental disorders. *C. elegans* is an excellent model to study RASopathies since the RAS-MAPK pathway is well conserved in worms, where it plays a crucial role in vulval development.

Based on a gene candidacy approach, we identified two germline mutations in *RRAS*, a gene encoding a small monomeric GTPase controlling cell adhesion, spreading and migration, underlying a rare and atypical form of Noonan syndrome (NS), the most common RASopathy. We also identified somatic *RRAS* mutations in 2 cases of non-syndromic juvenile myelomonocytic leukaemia (JMML), a childhood myeloproliferative/myelodysplastic disease caused by upregulated RAS signaling. Two of the three identified mutations affected known oncogenic hotspots of RAS genes and conferred variably enhanced RRAS function and stimulus-dependent MAPK activation. Expression of an RRAS mutant homolog in *C. elegans* enhanced RAS signaling causing a multivulva (Muv) phenotype, and engendered protruding vulva (Pvl), a phenotype previously linked to the RASopathy-causing SHOC2^{S2G} mutant. These findings provided evidence of a functional link between RRAS and MAPK signaling and reveal an unpredicted role of enhanced RRAS function in human disease.

Epistatic analyses performed on *C. elegans* transgenic lines allowed us to establish that the RASopathy-causing SHOC2 and RRAS mutants belong to the same pathway. Within this signaling network, both RAS-1/RRAS and RAS-2/MRAS are downstream to constitutively active SHOC2, with the former being epistatic to the latter. By using a reverse genetic approach based on RNA interference experiments, we demonstrated that the Muv phenotype was completely mediated by LET-60/RAS, while the Pvl phenotype was modulated by the RHO-family small GTPases CDC-42 and RAC1. We then confirmed these results in fibroblasts derived from patients with Mazzanti syndrome (NS with loose anagen hair) and transfected cell lines. In these models, we observed constitutive RAC1 activation and aberrant lamellipodia formation in cells expressing SHOC2^{S2G} compared to wild-type cells.

These results suggested RHO GTPases as excellent candidate genes to be mutated in RASopathies. To explore this hypothesis, mutation scanning of *RAC1*, *RAC2* and *CDC42* genes was performed in RASopathy patients by targeted resequencing and identified seven different

germline *CDC42* mutations in 11 unrelated subjects with a variable phenotype partially overlapping NS and predisposing to thrombocytopenia. *In vitro* biochemical characterization demonstrated a variable impact of the mutations on GTPase activity and defective binding to WASP. *In vitro* and *in vivo* (*C. elegans*) functional characterization of these mutants allowed to define their impact on cell migration and proliferation, as well as on vulval induction and morphogenesis. A first class of mutations was shown to have an hypomorphic effect on processes mediating cell polarized migration, with no effect on the RAS-MAPK signaling, while a second class of mutations had a gain-of-function effect on both cell migration/proliferation and LET-60/RAS-mediated vulval induction. Overall, our data highlighted the possible contribution of dysregulated signaling controlling cell spreading and migration to certain features of RASopathies, such as lymphedema, cardiac defects and lymphocytes infiltration in non-hematopoietic tissues in case of JMML.

1. Introduction

1.1 The RAS/mitogen-activated protein kinase (MAPK) pathway

The RAS/mitogen-activated protein kinase (MAPK) pathway plays a pivotal role in several biological processes with a key role in development, including cell proliferation, survival, senescence and differentiation (Rauen, 2013), and is activated by extracellular inputs in the form of growth factors, citokines and hormons (Figure 1) (Kratz *et al.,* 2007).

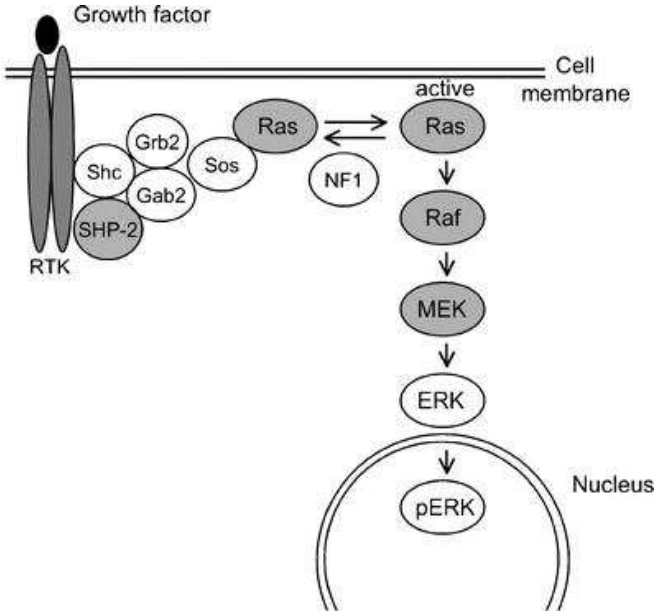

Figure 1. The RAS signaling pathway relays growth signals from activated growth factor receptors to the nucleus. Kratz *et al.,* 2007

RAS genes constitute a multigene family that includes *HRAS*, *NRAS* and *KRAS*. RAS proteins are small guanosine nucleotide-bound GTPases that function as a critical signaling hub within the cell. RAS proteins act as molecular switches by cycling between an active guanosine triphosphate (GTP)-bound and an inactive guanosine diphosphate (GDP)-bound state. Stimulated growth factor receptors recruit a number of adaptor proteins that activate guanosine nucleotide exchange factors (GEFs) to remove guanine nucleotides from RAS. RAS is then activated by binding to GTP, which is present at a ten fold higher concentration than GDP. In the GTP-bound state, the two switch regions of RAS (switch I and II) modify their conformation. This conformational switch allows RAS to bind and activate RAS effector proteins such as RAF1. The “on” position is turned “off” by an intrinsic GTPase activity, which hydrolyses and releases a phosphate group from RAS·GTP to produce RAS·GDP. The conformational transition of the switch I and II regions that is associated with this reaction disrupts the interaction between RAS and its effectors. The intrinsic GTPase

activity of RAS is slow and accelerated about 105-fold by GTPase activating proteins (GAPs), such as neurofibromin or p120 GAP. These GAPs mediate Ras·GTP hydrolysis by inserting an arginine residue (arginine finger) into the phosphate binding pocket of RAS (Figure 2).

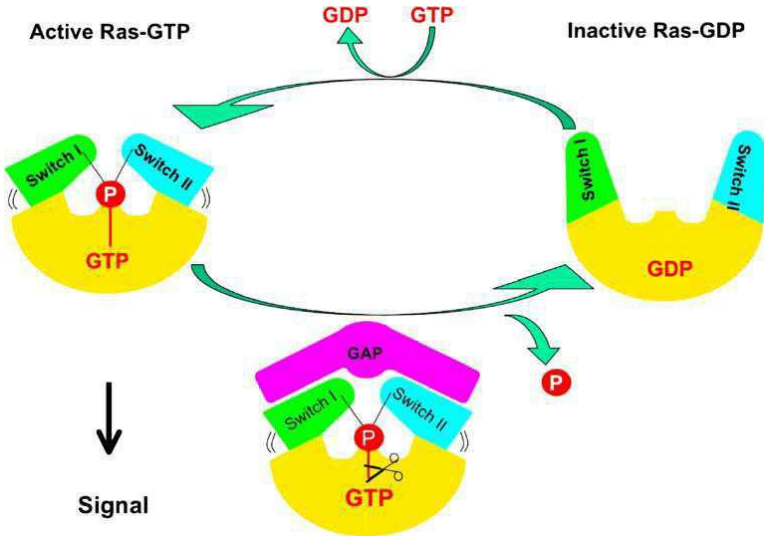

Figure 2. RAS cycles between an active GTP-bound and an inactive GDP-bound conformation. In the active state, the two switch regions, switch I and II, change their conformation allowing RAS to activate effector proteins. The intrinsic GTPase hydrolyzes a phosphate group to produce RAS·GDP. This reaction is accelerated by GTPase activating proteins (GAPs).
Kratz *et al.*, 2007.

The MAPK pathway is one of the many critical downstream signaling cascades of RAS. Activated RAS leads to the activation of RAF (ARAF, BRAF and/or CRAF), the first MAP kinase kinase kinase of the pathway. RAF phosphorylates and activates the MAP kinase kinase MEK1 and/or MEK2 which, in turn, phosphorylate and activate the MAP kinase ERK1 and/or ERK2,which exert their function on a large number of downstream molecules, both nuclear and cytosolic. ERK1 and ERK2 substrates include nuclear components, transcription factors, membrane proteins, and protein kinases that in turn control vital cellular functions, including cell cycle progression, differentiation and growth (Yoon and Seger, 2006).

The Ras/MAPK pathway has been studied extensively in the context of oncogenesis because its somatic dysregulation is one of the primary causes of cancer. *RAS* is somatically mutated in at least 20% of human cancers (Bos, 1989), and BRAF is mutated in approximately 7% of malignancies (Pritchard *et al.*, 2007).

1.2 The RASopathies

The RASopathies are a class of autosomal dominant developmental disorders caused by germline mutations in genes encoding RAS genes themselves, or RAS regulators or effectors involved in the RAS/MAPK pathway. These disorders are considered cancer predisposition syndromes, with the majority of associated mutations resulting in enhanced pathway activation or dysregulated

signaling. However, biochemical studies have demonstrated that a large fraction of the novel germline mutations identified in the pathway are not as robustly activating as those associated with oncogenesis. This is likely due to the embryonic lethality arising from these germline mutations.

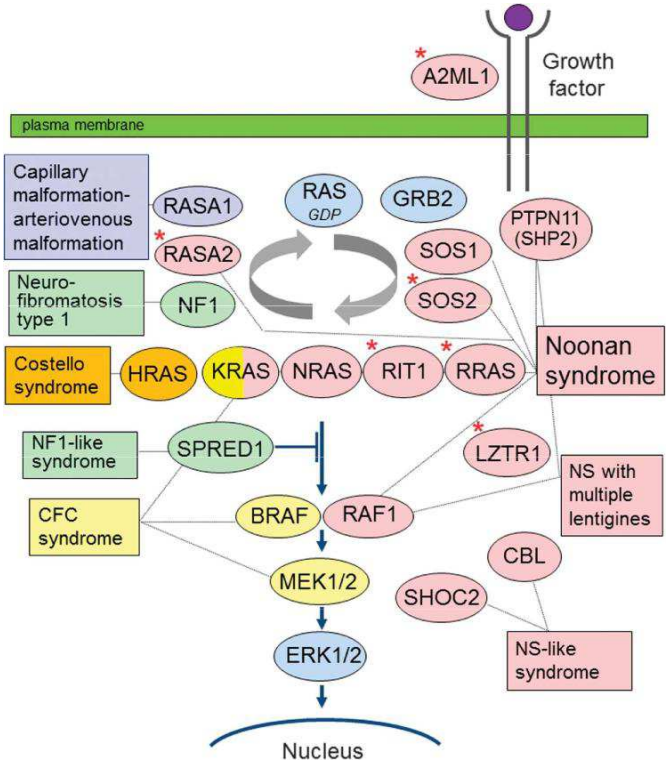

Figure 3. RAS/MAPK cascade and disorders involving germline mutations of related genes. MAPK, mitogen-activated protein kinase; NF1, neurofibromatosis type 1; NS, Noonan syndrome. *Indicates additional causative genes that have been reported since 2013.
Aoki *et al.*, 2016

Each RASopathy exhibits a unique phenotype, but owing to the common mechanisms of RAS/MAPK pathway dysregulation, they share many overlapping features, including craniofacial dysmorphisms, cardiac defects, ectodermal, skeletal and ocular abnormalities, variable neurocognitive disabilities, and an overall increased cancer risk (Figure 4).

Figure 4. Clinical images of patients with RASopathies. (*a*) A young boy who has a clinical diagnosis of neurofibromatosis type 1. (*b*) A young girl with Noonan syndrome who has a *PTPN11* mutation. (*c*) A young adult woman with Costello syndrome who has the common p.G12S *HRAS* mutation. (*d*) A school-age boy with cardio-facio-cutaneous syndrome who has a *MEK2* mutation.
Rauen, 2013

Taken together, the RASopathies are one of the largest family of genetic disorders affecting development and growth, with an estimated prevalence of approximately 1 in 1,000 individuals.

1.3 Molecular mechanisms underlying RASopathies

Although RAS signals to multiple intracellular pathways, hyperactivation of the MAPK pathway represents the common pathogenic feature of most RASopathies (Tartaglia *et al.*, 2011), although enhanced signaling through the PI3K/AKT cascade has been documented (Edouard *et al.*, 2010) (Table 1). However, each syndrome results from mutations in specific genes associated with the MAPK pathway and distinct mutations within these genes affect RAS signaling through different molecular mechanisms. Neurofibromatosis type 1 (NF1) was the first syndrome identified as being caused by heterozygous loss-of-function mutations of a gene involved in the RAS/MAPK pathway (*NF1*) (Cawthon *et al.*, 1990; Viskochil *et al.*,1990; Wallace *et al.*, 1990), and numerous other syndromes have subsequently been identified (Figure 3). These disorders include (*a*) Noonan syndrome (NS), caused by activating mutations in *PTPN11* (Tartaglia *et al.*, 2001), *SOS1* (Roberts *et al.*, 2007; Tartaglia *et al.*, 2007), *SOS2* (Cordeddu *et al.*, 2015; Yamamoto *et al.*, 2015) *RAF1* (Pandit *et al.*, 2007; Razzaque *et al.*, 2007), *KRAS* (Schubbert *et al.*, 2007), *NRAS* (Cirstea *et al.*, 2010); (*b)* atypical NS, caused by mutations in *SHOC2* (Cordeddu *et al.*, 2009), *CBL (*Martinelli *et al.*, 2010; Niemeyer *et al.*, 2010), *RIT1* (Aoki *et al.*, 2013) and *LZTR1* (Yamamoto *et al.*, 2015); (*c*)

Noonan syndrome with multiple lentigines (NSML), caused by allelic mutations in *PTPN11* (Digilio *et al.,* 2002) or, rarely, in *RAF1* (Pandit *et al.,* 2007); (*d*) capillary malformation-arteriovenous malformation syndrome (CM-AVM), caused by haploinsufficiency of *RASA1* (Eerola *et al.,* 2003); (*e*) Costello syndrome (CS), caused by activating mutations in *HRAS* (Aoki *et al.,* 2005); (*f*) cardio-facio-cutaneous syndrome (CFC), caused by activating mutations in *BRAF* (Niihori *et al.,* 2006; Rodriguez-Viciana *et al.,* 2006) and *MAP2K1 (MEK1)* or *MAP2K2 (MEK2)* (Rodriguez-Viciana *et al.,* 2006); and (*g*) Legius syndrome, caused by inactivating mutations in *SPRED1* (Brems *et al.,* 2007).

1.3.1 Small GTPases: HRAS, KRAS, NRAS, RIT1

RAS GTPases

HRAS, *KRAS* and *NRAS* encode the main GTPases belonging to the RAS subfamily, which cycle between an active GTP-bound state to an inactive GDP-bound state. *HRAS* is located on 11p15.5 and encodes the Harvey rat sarcoma viral oncogene homologue. The vast majority of *HRAS* mutations underlying CS result from amino acid substitutions affecting glycine residues at positions 12 or 13. These changes disrupt the guanine nucleotide binding site and cause a reduction in intrinsic and GAP-stimulated GTPase activity, resulting in constitutive activation of RAS and sustained signaling through the MAPK cascade (Gibbs *et al.,* 1984; McGrath *et al.,* 1984; Sweet *et al.,* 1984). Germline *HRAS* mutations involve the same residues affected by somatic lesions occurring in cancer. However, individual amino acid substitutions rarely overlap, with those associated with CS having a milder effect than cancer-causing lesions. *KRAS* is located on chromosome 12p12.1 and consists of two different isoforms encoded through alternative splicing. It encodes the V-Ki-Ras2 Kirsten rat sarcoma viral oncogene homolog. Biochemical analyses of *KRAS* activating mutations associated with NS or CFC demonstrated a general hypermorphic role of *KRAS* mutation (Schubbert *et al.,* 2007). Of note, germline and somatic lesions do not overlap, the former being weak hypermorphs due to their impaired binding to a plethora of effectors (Gremer *et al.,* 2011).

Finally, the *NRAS* gene encode the neuroblastoma Ras viral (V-Ras) oncogene homolog (NRAS) and is located on chromosome 1p13.2. Mutations in *NRAS* have been found in a very small number of individuals with NS (Cirstea *et al.,* 2010). Mutations have been identified within or near the switch II region of NRAS and are thought to interfere with GTPase function. Also for *NRAS*, germline mutations do not overlap lesions found in malignancies.

Table 1. Functional classificationof genes associated with RASopathies or suggested to be associated with this group of diseases (red).
Tidyman WE and Rauen KA, 2016

Class	Gene	Protein name	Protein function	Pathogenetic mechanism
GTPase	*HRAS*	HRAS: Harvey rat sarcoma viral oncogene homologue	Hydrolyzes GTP) and activates Raf by recruiting to the cell membrane	Activating mutations
	KRAS	KRAS: the V-Ki-Ras2 Kirsten rat sarcoma viral oncogene homolog	Hydrolyzes GTP and activates Raf by recruiting to the cell membrane	Activating mutations
	NRAS	NRAS: neuroblastoma Ras viral (V-Ras) oncogene homolog	Hydrolyzes GTP and activates Raf by recruiting to the cell membrane	Activating mutations
	RRAS	RRAS: Related Ras viral R-Ras) oncogene homologue	Hydrolyzes GTP and activates Raf by recruiting to the cell membrane	Activating mutations
	RIT1	RIT1; Ras-like protein in tissue	Hydrolyzes GTP and participates in Ras/MAPK and p38 signaling	Activating mutations
RasGAP	*NF1*	Neurofibromin	Binds activated G-proteins and stimulate their GTPase activity switching the active GTP-bound Ras to the inactive GDP-bound form	Loss of function
	RASA1	RASA1: p120-RasGTPase-activating protein	Binds activated G proteins and stimulate their GTPase activity switching the active GTP-bound Ras to the inactive GDP-bound Ras	Loss of function
	RASA2	RASA2: Ras p21 proteinactivator 2	Binds activated G proteins and stimulates GTPase activity switching the active GTP-bound Ras to the inactive GDP-bound Ras	Loss of function
	SYNGAP1	SynGAP: Synaptic Ras GAP	Neuron-specific RasGAP that binds activated G proteins and stimulates GTPase activity switching the active GTP-bound Ras to the inactive GDP-bound Ras	Loss of function
RasGEF	*SOS1*	SOS1: Son of sevenless homologue 1	RasGEF that stimulates the conversion of Ras from the inactive GDP-bound form to the GTP-bound active form	Activating mutations
	SOS2	SOS2: Son of sevenless homologue 2	Ras-GEF that stimulates the conversion of Ras from the inactive GDP-bound form to the GTP-bound active form	Activating mutations
Scaffolding	*SHOC2*	SHOC2: Homologue of suppressor of clear (SOC-2) in *Caenorhabditis elegans*	Binds GTP-Ras and mediates protein phosphatase 1 translocation to the cell membrane.	Activating mutation
Ubiquitin Ligase	*CBL*	CBL: casitas B-lineage lymphoma	E3 ubiquitin ligase that inhibits Ras activity by targeting phosphorylated substrates for proteasome degradation	Loss of function
Phosphatase	*PTPN11*	SHP2: Tyrosine-protein phosphatase non-receptor type 11; Src Homology 2	Non-receptor protein tyrosine phosphatase that in its active form, increases downstream Ras activity	Activating mutations
Kinase	*BRAF*	BRAF: v-Raf murine sarcoma viral oncogene homolog B	Serine/threonine protein kinase that activates MEK1 and/or MEK2 by phosphorylation	Activating mutations
	RAF1	CRAF: v-Raf-1 murine leukemiaviral oncogene homolog 1	Serine/threonine protein kinase that activates MEK1 and/or MEK2 by phosphorylation	Activating mutations
	MAP2K1	MEK1: Mitogen-activated protein kinase kinase 1	Threonine/tyrosine kinase that activates ERK1 and/or ERK2 by phosphorylation	Activating mutations
	MAP2K2	MEK2: Mitogen-activated protein kinase kinase 2	Threonine/tyrosine kinase that activates ERK1 and/or ERK2 by phosphorylation	Activating mutations
	MAP3K8	MAP3K8: Mitogen-activated protein kinase kinase kinase 8	Serine/threonine protein kinase which can activate both the Ras/MAPK and JNK pathways.	Activating mutation
Sprouty Related protein	*SPRED1*	SPRED1: Sprouty-related EVH1 domain containing 1	Negative regulator of Ras by inhibiting phosphorylation of Raf. Also, SPRED1 binds to the RasGAP, NF1, inducing the membrane localization of NF1 which in turn inhibits Ras	Loss of function
	SPRY1	SPRY1/Sprouty1	Negative regulator of Ras/MAPK pathway signaling	Loss of function
Acetyltransferase	*MYST4*	MYST4: Histone Acetyltransferase (Monocytic Leukemia-4)	Epigenetic modification of DNA by transferring an acetyl group from acetyl-CoA to histone proteins.	Loss of function
Adaptor protein	*LZTR1*	LZTR1: Leucine-zipper-like transcriptional regulator 1	Unknown	Unknown
Protease inhibitor	*A2ML1*	A2ML1: Alpha-2-macroglobulin-like 1	Protease inhibitor that binds lipoprotein receptor-related protein 1, which is an upstream activator of the Ras/MAPK pathway	Unknown

Other GTPases: RIT1

RIT1 is located on chromosome 1q22 and encodes RIT1 (RAS-like protein in tissues), which is a member of a novel branch of RAS-related GTPase proteins of the RAS family. RIT1 shares approximately 50% structural homology with RAS, but lacks a C-terminal lipidation site. Most of the RIT1 mutations are in the switch I or II regions and are predict to result in a constitutively active protein (Aoki *et al.,* 2015)

1.3.2 RasGAP : Neurofibromin, RASA1, RASA2

Neurofibromin

The *NF1* gene is located on chromosome 17q11.2. *NF1* is large with 60 exons covering approximately 350 Kb and encodes neurofibromin. NF1 is a GTPase-activating protein (GAP) that belong to a family of RAS regulatory proteins that stimulate RAS-GTPase activity. This results in a negative regulation of activated RAS. Neurofibromatosis type 1 is an autosomal dominant genetic syndrome caused by various types of loss-of-function mutations in the *NF1* gene resulting in neurofibromin haploinsufficiency within the cell (Cawthon *et al.,* 1990; Viskochil *et al.,* 1990; Wallace *et al.,* 1990). This reduces RAS-GTPase activity and, therefore, results in an overall increase in active GTP-bound RAS.

RASA1

RASA1, like *NF1*, encodes a RAS-GAP, specifically the p120-RAS-GTPase-activating protein (p120-RAS-GAP). The N-terminus contains a Src (sarcoma) homology region and the C-terminus contains a pleckstrin homology domain and the RAS-GTPase-activating domain. Like neurofibromin, RASA1 increases the intrinsic GTPase activity of RAS, behaving as a negative regulator of the RAS/MAPK signal transduction pathway. Heterozygous inactivating mutations in *RASA1* was shown to cause the autosomal dominant CM-AVM (Eerola *et al.,* 2003)

RASA2

RASA2 is located on chromosome 3q23 and encodes the RAS-GAP protein Ras P21 Protein Activator 2, RASA2, which is a negative regulator of the RAS/MAPK pathway. The three mutations associated with NS affect two different residues, Y326 and R511, located in the conserved RASA2 GAP domain, and are predicted to have a dominant negative effect on RAS.

1.3.3 RasGEF : SOS1, SOS2

SOS1

SOS1 is located on chromosome 2p22.1 and consists of 23 exons encoding son of sevenless homolog 1, SOS1. SOS1 is a RAS-specific guanine exchange factor (RAS-GEF). The majority of *SOS1* mutations associated with NS affects residues that are responsible for stabilizing SOS1 in its autoinhibited conformation. Therefore, alteration of these residues disrupts interactions mediating autoinhibition, causing increased GDP/GTP exchange that, in turn, lead to hyperactivation of signal flow through RAS and the MAPK cascade.

SOS2

SOS2 is located on chromosome 14q21.3 and consists of 23 exons encoding the son of sevenless homolog 2, SOS2; SOS2 is a RAS-GEF and homologue to SOS1. The murine and human SOS1 and SOS2 proteins have an overall 65% amino acid identity. The heterozygous autosomal dominant *SOS2* mutations observed in NS are located in the Dbl homology (DH) domain, that is responsible for maintaining SOS2 in its auto-inhibited conformation (Cordeddu *et al.*, 2015; Yamamoto *et al.*, 2015). Functional studies demonstrated that mutations cause higher levels of GTP-bound RAS and, therefore, increase signaling through the RAS/MAPK pathway, which is consistent with the mechanism associated with NS causative *SOS1* mutations.

1.3.4 Scaffolding : SHOC2

SHOC2 is a homolog of *suppressor of clear* (*SOC-2*) in *Caenorhabditis elegans*, which encodes a protein whose primary structure consists almost entirely of leucine-rich repeats. SHOC2 functions as a scaffold protein linking RAS to RAF1, its downstream effector in the RAS/MAPK pathway. SHOC2 is ubiquitously expressed and serves as the regulatory subunit of protein phosphatase 1C (PP1C) (Rodriguez-Viciana *et al.*, 2006). SHOC2 binds RAS-GTP and mediates PP1C translocation to the cell membrane. This enables PP1C dephosphorylation of residue S259 of RAF1, which is required for RAF1 translocation to the cell membrane and catalytic activity. A single germline mutation in *SHOC2*, which results in a p.S2G substitution, has been shown to underlie a rare subset of NS individuals with an atypical phenotype characterized by loose anagen hair and Attention-Deficit/Hyperactivity (ADHD)-like disorder (Cordeddu *et al.*, 2009). This unique p.S2G mutation causes the abnormal addition of a 14-carbon saturated fatty acid chain, myristate, to the N-terminal glycine of SHOC2, which results in the aberrant translocation of SHOC2 to the cell

membrane, prolonged PP1C dephosphorylation of RAF1, and sustained MAPK pathway activation. In *C. elegans*, ectopic expression of $SHOC2^{S2G}$ engendered protruding vulva, a neomorphic phenotype previously associated with aberrant signaling.

1.3.5 Ubiquitin Ligase : CBL

CBL is located on chromosome 11q23.3 and consists of 16 exons encoding the tumor suppressor casitas B-lineage lymphoma, CBL. CBL is an E3 ubiquitin ligase which is an enzyme that targets substrates for degradation by the proteasome. CBL mediates the association of ubiquitin with activated RTKs, which is necessary for receptor internalization and degradation and, therefore, acts as a negative regulator of RAS/MAPK signaling (Dikic *et al.,* 2007). Missense mutations of*CBL* associated with a NS-like phenotype characterized by susceptibility to myeloid malignancies alter the RING finger domain or the linker connecting this domain to the N-terminal tyrosine kinase binding domain and behave as dominant negative proteins. Mutations in CBL reduce the turnover of activated RTK increasing MAPK activation.

1.3.6 Phosphatase : PTPN11

PTPN11, the first-discovered and major gene underlying NS (Tartaglia *et al.*, 2001), encodes SHP2, a non-receptor protein tyrosine phosphatase (PTP) composed of two *N*-terminal Src Homology 2 (SH2) domains and a catalytic PTP domain. The N-SH2 domain acts as an allosteric switch. Basally, the catalytic function of the protein is auto-inhibited through a blocking interaction of the N-SH2 domain and the catalytic PTP domain (Hof *et al.,* 1998). Following binding of the N-SH2 domain with SHP2's signaling partners containing phosphorylated tyrosines, the phosphatase switches towards an open, catalitycally active conformation. Most of the disease-causing mutations cluster residues involved in the interface between the N-SH2 and PTP domain, altering the stability of the catalytically inactive state (Keilhack *et al.,* 2005; Tartaglia *et al.,* 2006).

1.3.7 Kinase : BRAF, CRAF/RAF1, MEK1, MEK2

BRAF

BRAF is located on chromosome 7q34, contains 18 exons and spans approximately 190 Kb. *BRAF* encode v-Raf murine sarcoma viral oncogene homolog B (BRAF) which is a serine/threonine protein kinase and is one of the many direct downstream effectors of RAS. Heterozygous mutations in BRAF cause CFC with the most common mutations occurring in the cysteine-rich domain in exon 6 and in the protein kinase domain. Germline mutations do not overlap somatic lesions found in melanoma. *In vitro* functional analyses of BRAF demonstrated that most of them have increased kinase activity (Niihori *et al.,* 2006; Rodriguez-Viciana *et al.,* 2006).

CRAF/RAF1

CRAF, like BRAF, is a downstream effector of RAS and is a member of the Raf family of serine/threonine protein kinases. *RAF1* is the gene that encodes the v-raf-1 murine leukemia viral oncogene homolog 1 (CRAF/RAF1) and is located on chromosome 3p25.2. Like BRAF, CRAF also has three conserved regions and can phosphorylate to activate the dual specificity protein kinases MEK1 and MEK2, which, in turn, phosphorylate to activate the serine/threonine specific protein kinases, ERK1 and ERK2. Mutations in this gene are associated with NS and, rarely, NSML (Pandit *et al.,* 2007; Razzaque *et al.,* 2007). The majority of *RAF1* mutations in NS cluster in the Conserved Region 2 flanking p.S259 and the Conserved Region 3, surrounding the activation segment. These mutations have a gain-of-function since the phopshorylation of residues p.S259 and p.S621 are responsible for regulation of CRAF.

MEK1 and MEK2

The *MAP2K1* gene is located on chromosome 15p22.31 and spans approximately over 11 exons. The *MAP2K1* gene encodes the mitogen-activated protein kinase kinase 1 (MEK1) which is a threonine/tyrosine kinase and is a downstream effector of BRAF. MEK1 activates both ERK1 and ERK2 by phosphorylation. Missense mutations in MEK1 cause CFC (Rodriguez-Viciana *et al.,* 2006). The majority of them are missense mutations affecting residues located in exons 2 and 3. Functional studies of CFC mutant proteins have shown that they are more active than wild-type MEK1 in stimulating ERK phosphorylation (Rodriguez-Viciana *et al.,* 2006).

The *MAP2K2* gene is located on chromosome 19p13.3, spans approximately 34 Kb and contains 11 exons. The *MAP2K2* gene encodes the mitogen-activated protein kinase kinase 2 (MEK2). MEK2 is a threonine/tyrosine kinase that, like MEK1, has the ability to phosphorylate and activate both

ERK1 and ERK2. Like MEK1, MEK2 mutants are hyperactive proteins increasing signaling through the MAPK cascade (Rodriguez-Viciana *et al.,* 2006; Anastasaki *et al.,* 2009).

Overall, heterozygous missense mutations in *MAP2K1* and *MAP2K2* are present in approximately 25% of CFC individuals in which a gene mutation has been identified.

1.3.8 Sprouty related protein : SPRED1

SPRED1 is located on chromosome 15q14 and encodes sprout-related EVH1 domain containing 1, SPRED1. SPRED1 functions as a negative regulator of RAS by inhibiting phosphorylation of RAF (Wakioka *et al.,* 2001). Heterozygous inactivating mutations in *SPRED1* cause Legius syndrome which is an autosomal dominant RASopathy that shares many phenotypic features with NF1 (Brems *et al.,* 2007). The vast majority of SPRED1 mutations associated with Legius syndrome cause truncation of the protein, a loss of SPRED1 function and dysregulated RAS/MAPK pathway signaling.

1.3.9 Adaptor protein : LZTR1

LZTR1 is located on chromosome 22q11.21 and has 21 exons. The encoded protein is leucine-zipper-like transcriptional regulator 1 (LZTR1) which belongs to a functionally diverse family of proteins containing BTB-kelch domains that are thought to localize to the cytoplasmic surface of the Golgi membrane (Nacak *et al.,* 2006). Heterozygous missense mutations have been identified in individuals with a clinical diagnosis of NS (Chen *et al.,* 2014; Yamamoto *et al.,* 2015). The mutations are in the highly conserved kelch domain and are predicted to disrupt protein function. Interestingly, the link between this protein and the RAS/MAPK cascade has not been elucidated yet. Based on this consideration, the possibility that *LZTR1* mutations might be associated with a phenocopy of NS cannot be ruled out.

1.4 Use of the nematode *Caenorhabditis elegans* as an animal model for human diseases

Characterization of the nature of RAS/MAPK signal dysregulation is essential to understanding the molecular mechanisms underlying RASopathies. The use of animal model is useful to study and characterize how individual gene mutations can affect the protein properties and alter intracellular signaling.

1.4.1 *Caenorhabditis elegans*

In 1963, Sydney Brenner observed that the success of molecular biology was due to the existence of model systems, defined as extremely simple organisms, such as bacterial phage that can be handled in large numbers. With the awareness of how important model systems are in biological research, he introduced *Caenorhabditis elegans* (*C. elegans*) as a model organism for pursuing research in developmental biology and neurology.

Ever since its introduction by Brenner, *C.elegans* has been widely used in research laboratories (Wood, 1988). Due to its value as a research tool, a sophisticated knowledge infrastructure has been developed, with freely disseminated research methods and protocols.

Caenorhabditis elegans (*Caeno*, recent; *habditis*, rod; *elegans*, nice), is a free-living, non-parasitic soil nematode. It is small (about 1 mm in length), transparent for ease manipulation and observation, feeds bacteria, such as *E. coli*, and can be easily and cheaply housed and cultivated in large numbers (10,000 worms/petri dish) in the laboratory. *C. elegans* has five pairs of autosomes and one pair of sex chromosome. There are two sexes (Figure 5) determined by the number of X chromosomes: hermaphrodites have two X chromosomes and males have just one X chromosome.

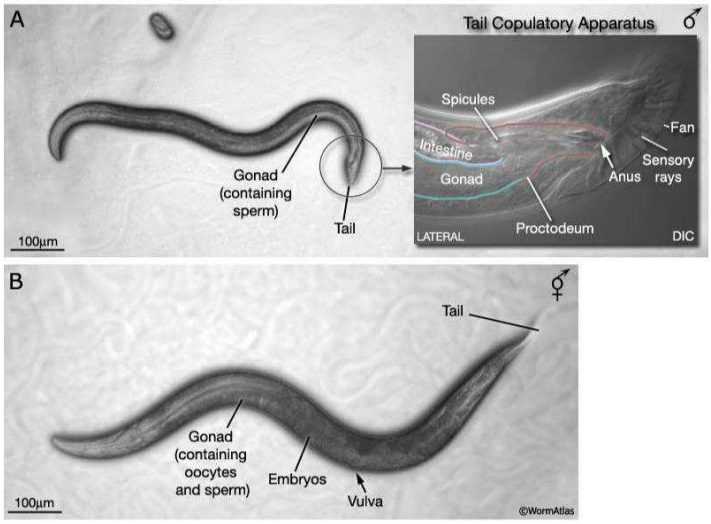

Figure 5. A) A *C. elegans* male with description of tail copulatory apparatus. B) A *C. elegans* hermaphrodite.
Modified from WormAtlas

In wild populations living in the soil, most *C. elegans* are hermaphrodites (XX), with males (XO) being just 0.05% of the total population on average. Hermaphrodites produce both eggs and sperm and, as a result, can self-fertilize. Self-fertilization in a hermaphrodites results in 99.95% hermaphrodite offspring. Males are produced only when an offspring inherits only one X chromosome, due to a mistake during meiosis, and their role is to guarantee the genetic variability. Males cannot produce offspring by themselves, but they may mate with hermaphrodites to produce offspring. When hermaphrodites mate with males, 50% of the progeny will be males and 50% will be hermaphrodites. In the laboratory, self-fertilization of hermaphrodites or crossing with males can be manipulated to produce progeny with desired genotypes that are especially useful for genetic study. In addition, *C. elegans* is extremely fecund: a hermaphrodite can produce about 300 to 350 offspring under self-fertilization and even more if it mates with males.

Under laboratory conditions, the average life span of the individuals is ~ 2-3 weeks, depending on the temperature, while the development time is 3 to 4 days. The short life cycle of *C. elegans* consists of four larval stages (L1, L2, L3 and L4) (Figure 6).

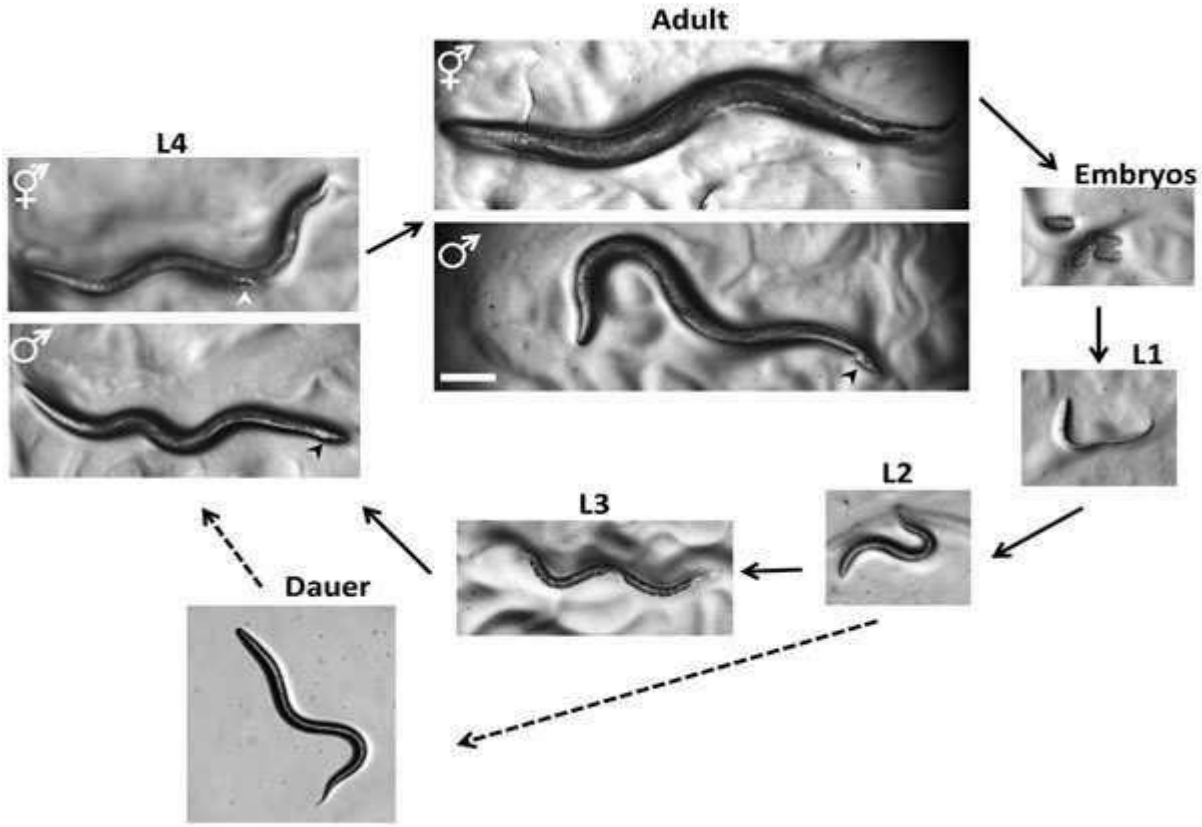

Figure 6. Life cycle of *C.elegans*. Modified from WormBook.

First, regardless of whether the sperm that fertilizes the oocyte comes from the spermatheca of the hermaphrodite or from mating with a male, the embryo begins development inside the hermaphrodite. Once the embryo has approximately 28–30 cells, it is typically laid into the environment through the vulval opening. Embryogenesis is then completed outside the hermaphrodite during an approximately 13-hour period. Just prior hatching, the egg contains a fully formed larva of 558 cells that can be seen tumbling inside the eggshell in a 3-fold pretzel configuration. At hatching, this L1 larva will arrest in development if there is no food available. In the presence of food, the larva proceeds through four stages that are punctuated by intervening molts when the animal sheds its cuticle to accommodate increasing body growth. During the larval period, a number of blast cells divide and the germline and sexually dimorphic features such as the hermaphrodite vulva and male tail develop so that the animal will be able to reproduce when it reaches young adulthood. An alternative pathway in the life cycle is taken when the animal encounters poor conditions such as a limited food supply at the L1/L2 larval molt. In this scenario rather than developing into an L3 larva, the animal enters into dauer or diapause pathway. This stage is an adaptation to survive at extreme conditions (mainly lack of food). Dauer larval development is induced by crowding, temperature and genetics (there are many loci that control dauer development, and there is variation between wild strains in the propensity for dauer development). Dauer larvae are highly resistant to stress and will reenter the normal life cycle at the L4 stage when conditions improve such as when food becomes available. The genes that control the decision to enter the dauer pathway are interesting because they are homologs of the vertebrate insulin-signaling pathway and many of them play an independent role in the longevity of *C. elegans*.

C.elegans was the first multicellular eukaryotic organism to have its genome sequenced (*C. elegans* Sequencing Consortium, 1998). As sequence information from additional *Caenorhabditis* species as well as more distantly-related nematodes has become available in the past decade, the information from *C. elegans* has provided the basis for rich comparative genomics studies. The entire *C. elegans* genome is 100 Mb (*C. elegans* Sequencing Consortium, 1998) and has 20,444 protein-coding genes (WormBase release WS245, Oct. 2014). Both *C. elegans* sexes contain five autosomal chromosomes named linkage group (LG) I, II, III, IV, and V and the X chromosome. Individual genes of *C. elegans* are arranged in conventional eukaryotic fashion with 5’ untranslated regions, open reading frames (ORFs) containing exons and introns, and 3’ untranslated regions. Compared to vertebrate genes, *C. elegans* genes are relatively small with the average gene size of 3 kb due primarily to the presence of very small introns; *C. elegans* genes also have many normal-sized introns. The chromosomes do not contain traditional centromeres; during mitosis the microtubule

spindle attaches to more than one position along the chromosome (these attachments are said to be holocentric or polycentric). In fact, a specific sequence does not seem to be required for attachment since extrachromosomal DNA-containing transgenes can be inherited throughout many cell divisions. Despite their simple anatomy, these animals show a large repertoire of behaviors included locomotion, feeding, defecation and egg laying, besides more complex abilities such as thermosensitivity, attraction or repulsion to several substances (chemotaxis), the response to mechanical stimulation, the ability to perceive light despite the absence of the eyes, and social behavior (Rankin, 2002; De Bono, 2003).

The developmental fate of all somatic cells (959 in the adult hermaphrodite, 1,031 in the adult male) have been mapped out. These patterns of cell lineage are largely invariant between individuals, in contrast to what occurs in mammals (Figure 7). *C. elegans* is one of the simplest organisms with a nervous system. The hermaphrodite has a total of 302 neurons. These can be divided into the pharyngeal nervous system containing 20 neurons and the somatic nervous system containing 282 neurons; the somatic nervous system contains 6,393 chemical synapses, 890 gap junctions, and 1,410 neuromuscular junctions.

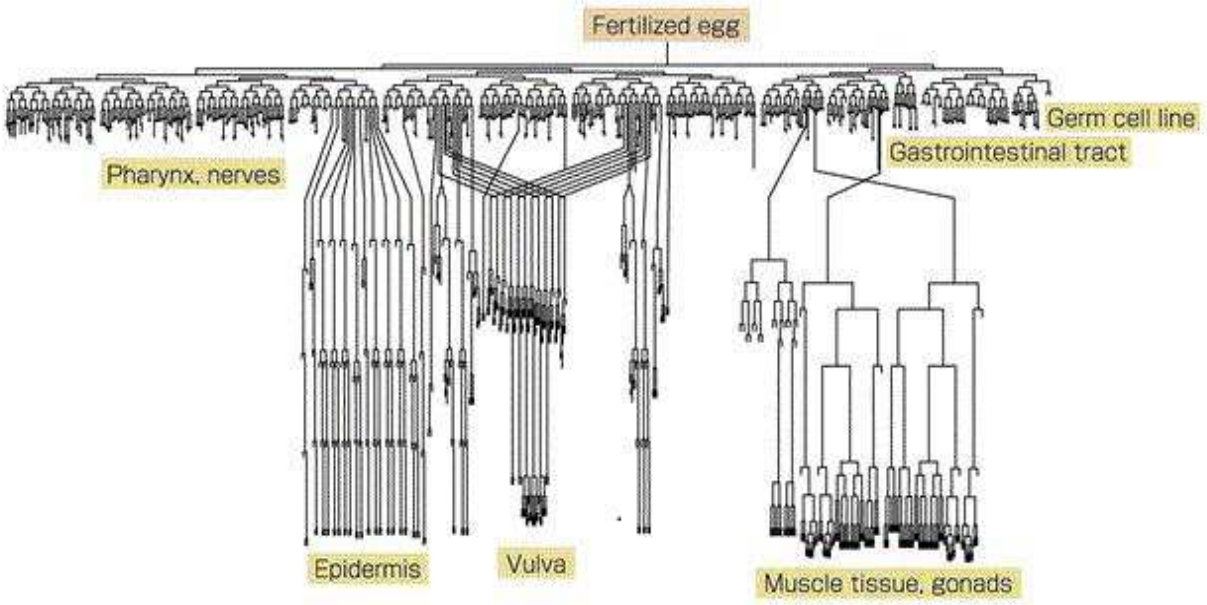

Figure 7. ***C.elegans*** **cell lineage.** Out of one zygote, 1,090 cells are created, and they differentiate into various cells.During this process, 131 cells die according to the developmental program.
Modified from WormBook

The animals can be maintained in culture in the lab where they grow at 20°C on plates or liquid medium using *Escherichia coli* as a food source; mutant animals can be obtained through chemical mutagenesis, radiation exposure (Anderson, 1995; Jorgensen and Mango, 2002) or RNA

interference (RNAi). The sexual dimorphism and the production of a broad progeny (each hermaphrodite lays about 300 eggs) allow to easily perform genetic crosses. All these features, along with easy manipulation and the possibility to hibernate the larvae at -80 °C or in liquid nitrogen, make this animal an ideal model organism in genetic studies, notoriously difficult in more complex organisms such as vertebrates.

Historically, the first researches on *C. elegans* were conducted by Sydney Brenner since 1965. For the discoveries on the spatial and temporal development of the organism, and apoptosis, the same Brenner, Robert Horvitz and John Sulston received in 2002 the Nobel prize for medicine. In 2006, Andrew Fire and Craig Mello received the same recognition for the discovery of RNA-interference, and a few years later the worm received its third Nobel prize thanks to Chalfie's research on the first use of GFP *in vivo*.

1.4.2 Modeling human diseases in *Caenorhabditis elegans*

At least 50% of worm genes have human homologs, and *C. elegans* orthologs exist for ~70% of known human disease related genes (Schwarz, 2005) (partially summarized in Table 2). The genetic overlap between *C. elegans* and *Homo sapiens*, although not as significant as the overlap between humans and more complex model organisms, enables researchers to use this simple model system to study the functions and interactions of genes contributing to basic cellular pathways relevant to human disease.

Table 2 . Human disease-related genes conserved in *C. elegans*

Disorder	Human gene	*C. elegans*gene
INBORN ERRORS OF METABOLISM/SIMPLE MENDELIAN DISORDERS		
Aarskog-Scott syndrome	*FGD1* (guanine nucleotide exchange factor)	*exc-5*
Achondroplasia	*FGFR3* (FGF receptor tyrosine kinase)	*egl-15*
Alzheimer's disease	*AD3* and *4* (presenilins)	*sel-12*
	APP (amyloid precursor protein)	*apl-1*
Amyotrophic lateral sclerosis	*SOD1* (super oxide dismutase)	*sod-4*
Aniridia	*PAX6* (paired homeobox domain)	*vab-3*
Ataxia telangiectasia	*AT* (PI-3 kinase-like domain)	*atl-1*
Barth syndrome	*TAZ* (phosphate acyl transferase)	*acl-2*
Beckwith-Weidemann syndrome	*GFI1/2* (C2H2 zinc-finger protein)	*pag-3*
Charcot-Marie-Tooth disease, type 4B2	*SBF1* (SET-binding factor)	*mtm-5*
Cystic fibrosis	*CFTR* (ABC transporter)	*mrp-2*
Diabetes mellitus	*IRF4* (insulin)	*Y53F4B.10*
Glucose-6-phosphate 1-dehydrogenase deficiency	*G6PD (*glucose-6-phosphate dehydrogenase)	*B0035.5*
Hermansky-Pudlak syndrome	*AP-3* (adaptin)	*apm-3*

Huntington's disease	*HD* (huntingtin)	*F21G4.6*
Hypogonadotropic hypogonadism	*GNRHR* (gonadotropin releasing hormone receptor)	*gnrr-1*
Lissencephaly/Miller-Diekersundrome	*LIS1* (platelet activating factor acetylhydrolase)	*lis-1*
Marfan syndrome	*FBN1* (fibrillin)	*fbn-1*
Menkes syndrome	*ATP7A* (Cu2+ transporting ATPase)	*cua-1*
McArdle disease	*PYGM* (muscle glycogen phosphorylase)	*T22F3.3*
Muscular dystrophy, Duchenne/Becker	*DMD* (dystrophin)	*dys-1*
Muscular dystrophy, Fukuyama	*FCMD* (fukutin)	*T07D3.4*
Muscular dystrophy, limb-girdle, type 2D	*SGCA* (sarcoglycan alpha)	*sgca-1*
Muscular dystrophy, limb-girdle, type 2E	*SGCB* (sarcoglycan beta)	*sgcb-1*
Myotonic dystrophy	*CUGBP1* (RNA binding protein)	*etr-1*
Neimann-Pick disease type B (NPB)	*ASM* (acid sphingomyelinase)	*asm-2*
Neimann-Pick disease type C1 (NPC1)	*NPC1* (patched membrane domain-containing permease)	*ncr-1* and *-2*
Neimann-Pick disease type C2 (NPC2)	*NPC2* (cholesterol-binding protein)	*heh-1*
Pallister-Hall syndrome	*GLI3* (GLI-Kruppel family transcription factor)	*tra-1*
Parkinson's disease	*PARK2* (parkin)	*pdr-1*
Phenylketonuria	*PAH* (phenylalanine-4-hydroxylase)	*pah-1*
Polycystic kidney disease, type 1	*PKD1* (polycystin-1)	*lov-1*
Polycystic kidney disease, type 2	*PKD2* (polycystin-1)	*pkd-2*
Spastic paraplegia 4	*SPAST* (spastin, AAA ATPase)	spas-1
Spinal muscular atrophy	*SMN* (survival motor neuron, an mRNA splicing protein	*smn-1*
Spinocerebellarataxia 1	*SCA1* (ataxin-1)	*K04F10.1*
Spinocerebellarataxia 2	*SCA2* (ataxin-2)	*atx-2*
Stargardt disease	*ABCA4* (ABC transporter)	*abt-4*
Waardenburg syndrome	*PAX3* (paired homeobox domain)	*vab-3*
Werner syndrome	*WRN* (RecQ DNA helicase)	*wrn-1*
Wernicke-Korsakoff syndrome	*TKT* (transketolase)	*D2007.2*
Wilson disease	*ATP7B* (Cu2+ transporting ATPase)	*cua-1*
Zellweger syndrome 3/Refsum disease	*PXMP3* (peroxisomal membrane protein 3)	*prx-2*
CANCER		
Adenomatous polyposis coli	*APC* (tumor suppressor in beta-catenin signaling pathway	*apr-1*
Cowden disease	*PTEN* (tumor suppressor, phosphatase and tensin)	*daf-18*
Hereditary non-polyposis colon cancer	q*MLH1* (DNA mismatch repair)	*mlh-1*
	MSH2 (MutS DNA repair)	*msh-2*
Leukemia, juvenile myelomonocytic	*GRAF* (GTPase regulator associated with focal adhesion kinase)	*T04C9.1*
Li-Fraumenisyndrome	*TP53* (p53 tumorsuppressor)	*cep-1*
Multiple endocrine neoplasia, type 2a	*RET* (receptor tyrosine kinase)	*egl-15*
Nevoid basal cell carcinoma syndrome	*PTCH* (SSD patched membrane protein)	*ptc-1*
Neurofibromatosis, type 2	*NF2* (talin family)	*nfm-1*
Pancreatic carcinoma	*PC4* (TGFβ signal transducer)	*sma-4*
Retinoblastoma	*RB1* (tumor suppressor)	*lin-35*

Modified from Silverman *et al.*,2010

Finding *C.elegans* orthologues of human disease genes can offer rapid and unforeseen insights into the functions of the human gene. For example, it may be possible to uncover genes which, when mutated, could either enhance or suppress a particular biochemical pathway and, as such, their gene products may represent novel candidate drug targets. Also, by screening for and analyzing mutants that either suppress or enhance the phenotypic effect of already characterized mutations, functionally interacting gene products can be identified. Both strategies can be deployed to identify the different components of a novel signaling pathway. For example, the tyrosine kinase receptor–RAS signaling pathway is involved in *C.elegans* vulval development. The corresponding human signaling cascade is involved in cell proliferation processes in general, and research in this area is proving to be of considerable interest in understanding the control of cell proliferation.

1.4.3 RAS/LET-60 signaling and vulval development in *C. elegans*

The RAS-MAPK pathway plays a central role during the metazoans development controlling various biological processes (Schlessinger, 2000) .The RAS proteins and many of RAS regulatory proteins are highly conserved during evolution. In *C. elegans*, *let-60* is the ortholog of the human genes *HRAS*, *KRAS* and *NRAS* (Han and Sternberg, 1990), and the only known role of the protein encoded by this gene is to activate the MAPK cascade. LET-60 acts downstream at least two different tyrosine kinase receptors, LET-23 (corresponding to the human epidermal growth factor receptor, EGFR; Aroian *et al.*, 1990) and EGL-15 (corresponding to the human fibroblasts growth factor receptor, FGFR; De Vore *et al.*, 1995) (Figure 8). Following the binding of the respective ligands, these receptors dimerize and autophosphorylate at the C-terminal, by generating binding sites for adapter proteins such as SEM-5/GRB2 or SOC-1 (similar to GAB1). These proteins, in turn, recruit the GEF proteins such as SOS-1, which activate LET-60. It follows the cascade activation of LIN-45/RAF (Han *et al.*, 1993), MEK-2/MEK (Churc *et al.*, 1995; Kornfeld *et al.*, 1995; Wu *et al.*, 1995) and MPK-1/ERK (Lackner *et al.*, 1994; Wu and Han, 1994). The latter, when activated, modulates the activity of a large number of substrates (Figure 8).

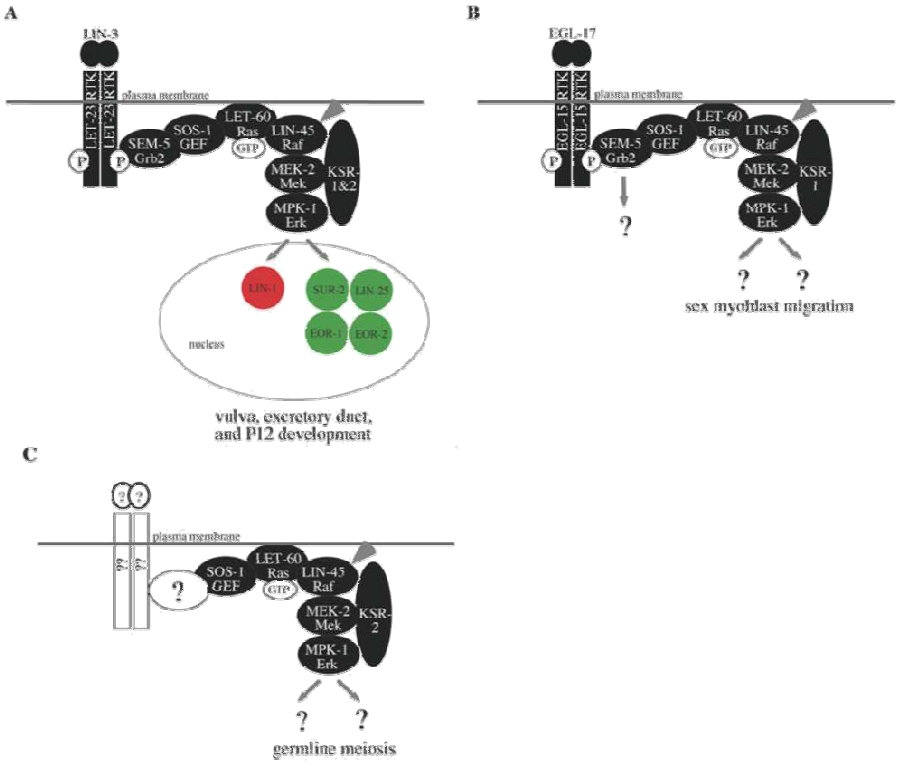

Figure 8. In *C. elegans* RAS-MAPK signalling controls different processes. LET-23/EGFR and EGL-15/FGFR are activated by different ligands, and control different biological processes. A) The processes depending on LIN-3/LET-23 include the vulva and the excretory duct formation through the regulation of nuclear proteins (LIN-1, SUR-2, LIN-25, EOR-1, EOR-2. B) The processes depending on EGL-17/FGF-EGL-15/FGFR refer the sexual myoblasts migration, but the target proteins of MPK-1 are unknown; C) other receptors control the cell progression in meiosis. The signal is mediated by SEM-5 protein adapter (GRB2) who recruits the GEF proteins that activate LET-60 and the MAPK cascade (Sundaram, 2013).

Due to the crucial role played by LET-60 during nematode development, it is not surprising that many different defects can be generated by mutations in *let-60* and other genes involved in this pathway. In particular, the excretory duct formation, necessary for osmoregulation, vulva formation and its connection with the uterus, spicule formation in male meiosis and progression in germline cells from pachytene stage are very important processes regulated by this pathway (Sundaram, 2013).

The development of the vulva is certainly the most intensively studied and better understood among the various mechanisms regulated by this pathway (Sternberg, 2005). In the adult animals the vulva is required for the eggs deposition and for mating. Vulval development occurs since the specification of six precursor cells called *Vulval Precursors Cells* (VPC), P3.p, P4.p, P5.p, P6.p, P7.p and P8.p, at the larval stage L1/L2 . The action of the *hox* genes, in particular *lin-39*, is required for the differentiation of the six VPC. In L3, these cells will face three different fates (fate 1st, 2nd and 3rd) by forming a different cell progeny. The P5.p, P6.p and P7.p cells will form the vulval cells (fate 1° and fate 2°), while P3.p, P4 .p and P8.p cells will become epidermal cells (fate 3°). These different cellular fates depend on the action of a single cell called *Anchor cell* (AC).

This cell activates MAPK pathway through the production of LET-23/EGFR receptor ligand LIN-3/EGF. LIN-3 binds primarily to the LET-23 receptors on P6.p, the nearest cell to AC, and to a lesser extent to receptors on the of P5.p and P7.p surface. In normal conditions, the AC signal will not be able to reach the P3.p, P4.p and P8.p cells, that will fuse with the epidermal syncytium hyp7. The massive activation of the LET-23/LET-60/MPK-1 pathway in P6.p leads the cell to assume fate 1°. Furthermore, this pathway inhibits the LIN-12/Notch receptor formation in P6.p, while it stimulates the production of the ligand of LIN-12 that are released from the same P6.p and bind to the surface receptors of P5.p and P7.p. In these cells the activation of the LIN-12 pathway causes the MAPK cascade and fate 1° inhibition, and the consequent assumption by P5.p and P7.p of fate 2° (Figure 9).

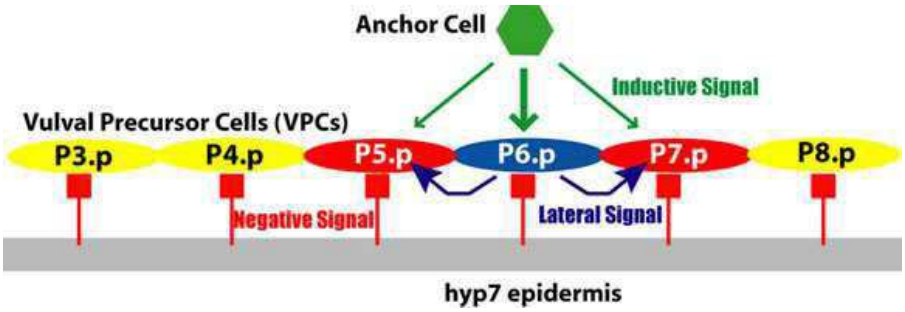

Figure 9. **VPC different cell fates during vulval development.** Yellow, fate 3°; red, fate 2°; blue, fate 1°. The green arr ows indicate the positive regulation by the *Anchor cell* mediated by the release of LIN-3/ EGF. The induction resulting from the *Anchor cell* (LIN-3; Green) is required in order to prevent the fate 3° determination. The lateral s ignalingoriginated from the VPC-induced P6.p (blue) promotes fate 2° in P5.p an d P7.p cells (LIN-12/Notch signaling).
Modified from Herman &Hedgecock, 1990; Horvitz & Sternberg, 1991.

The L4 vulva consists of 22 cells. P6.p will divide symmetrically to generate 8 adult cells, 4 vulE cells e 4 VulF cells, while P5.p and P7.p cells will divide asymmetrically, each generating 2 VulA cells, 2 VulB cells, 2 VulC cells and 1 VulD cell. These different cellular types will have distinct functions and different patterns of gene expression. Finally, during L4 stage, the cells originated from P5.p, P6.p and P7.p will undergo a range of morphogenetic movements leading to the formation of a proper vulva in the adult. The RAC protein, encoded by *ced-10* and *mig-2* genes, seem to be important for the proper execution of this process (Kishore and Sundaram, 2002). VPC induction and morphogenetic defects cause different phenotypes (Sternberg; WormBook, 2005); in particular, reduced LET-23-LET-60 signaling leads to the absence of avulva (*Vulvaless phenotype*, Vul) with failure of egg-laying (Egl phenotype) and consequent accumulation of larvae inside the mother (*Bag-of-worms* phenotype) (Figure 10). In contrast, augmented signaling through this

cascade causes the formation of multiple ectopic pseudovulvae (Muv phenotype). Finally, migration defects of VPCs, as well a loss-of-function mutations in LIN-12,was shown to engender protruding vulva (Pvl phenotype).

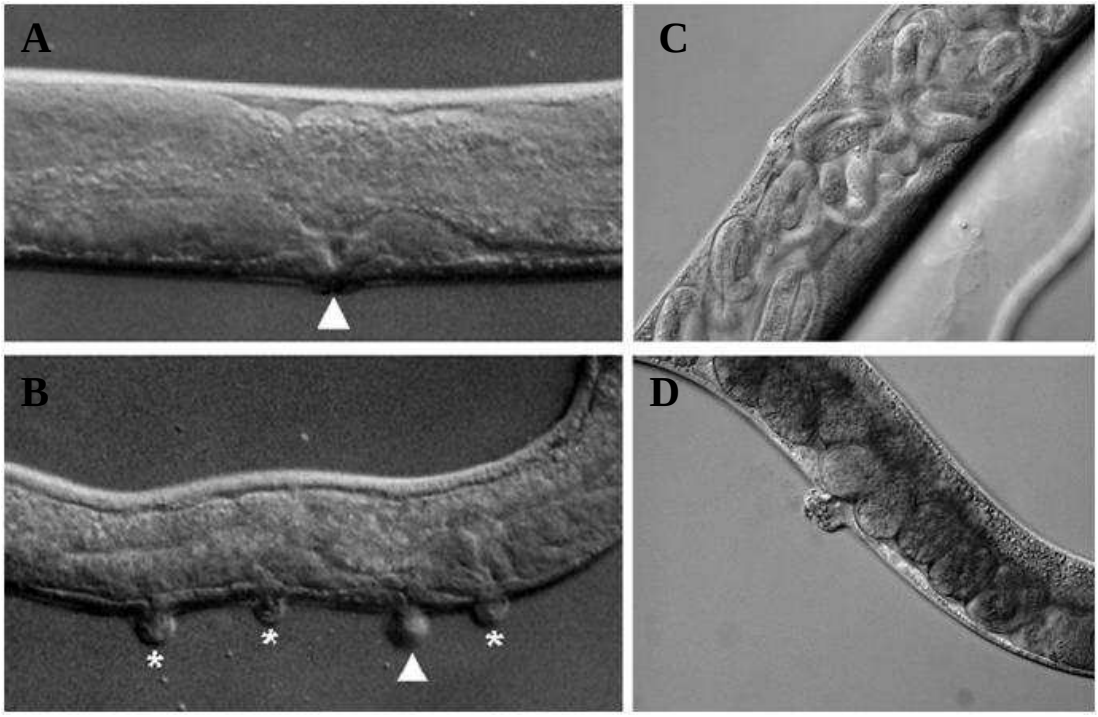

Figure 10.Different defects in the vulval development. A) Adult wild-type hermaphrodite; the white arrow indicates the vulva. B)Adult hermaphrodite presenting ectopic pseudovulvae (Multivulva phenotype, Muv). The white arrow indicates the normal vulva, the asterisks refer to pseudovulvae. C) Hermaphrodite without vulva (Vulvaless phenotype, Vul) in which the vulva absence causes eggs to hatching into the adult (phenotype Bag-of-worms, Bag). D) Hermaphrodite adult with protruding vulva (Pvl). Wormbook and personal observations.

Many aspects of the RAS-MAPK pathway regulation in mammals have been elucidated using *C. elegans* as a model organism because, as previously mentioned, the core of the RAS pathway, and many of its regulators and effctors are highly conserved between *C. elegans* and vertebrates. Overall, *C. elegans* represents an excellent tool to study the effect of novel and previously identified mutations in RASopathy-causing genes on development and intracellular signaling (Tan and Kim, 1999; Wang and Sternberg, 2001; Moghal and Sternberg, 2003; Sundaram, 2004).

1.5 Rho-family GTPases in *C. elegans*

Rho-family GTPases in *C. elegans* and other systems have roles in cytoskeletal organization, cell polarity, cell migration and cell membrane protrusion. The *C. elegans* genome encodes seven members of the Rho family of GTPases, and effector binding regions are typically highly conserved, with some exceptions. Canonical members of the Rho-family GTPases include RHO (*rho-1*), RAC (*ced-10*), and CDC-42 (*cdc-42*). The *rac-2* gene is nearly identical to *ced-10*, but it is unclear if *rac-2* is a functional gene or a non-functional duplication of the *ced-10* locus; *mig-2* encodes an Mtl (MIG-2-like) GTPase, a family found in invertebrates with similarity to both RAC and CDC-42. Functionally, MIG-2 is similar to mammalian RHOG (deBakker *et al.*, 2004). RHO-1, CDC-42 and CED-10 were in one functional cluster, with CDC-42 and CED-10 being closer together, and MIG-2 and CRP-1 were in another, suggesting that CRP-1 and MIG-2 have similar biochemical properties. By similarity of sequence, MIG-2 was closer to CED-10 and CDC-42, followed by RHO-1 and CRP-1.

RNAi-mediated knockdown of RHO-1 activity resulted in early embryonic arrest (http://www.wormbase.org/), and embryos that arrested later in development displayed severe defects in tissue morphogenesis. These phenotypes could be explained by defects in Rho-mediated actin cytoskeleton organization (e.g., actin forms the contractile ring during cytokinesis and is involved in cellular migration and morphogenesis) (Schonegg and Hyman, 2006). Furthermore, RHO-1 is involved in establishing and maintaining the position of the PAR complex proteins in early embryonic polarity (Schonegg and Hyman, 2006). RHO-1 also controls neuronal cell shape after the establishment of the normal axon and dendrite morphology of the neuron.

CDC-42 is required for an assortment of developmental events involving the cytoskeleton, cell polarity, and protrusion. A conserved signaling module of CDC-42 with the polarity proteins PAR-3/PAR-6/PKC-3 is iteratively used in multiple developmental events, and CDC-42 acts upstream of the Rac GTPases CED-10 and MIG-2 in protrusive events in a Rho GTPase hierarchy of signaling. *cdc-42*-directed RNAi caused defects in embryonic cytokinesis similar to *rho-1(RNAi)* (Kay and Hunter, 2001). *cdc-42(RNAi)* also perturbed the polarity of the single-celled zygote and resulted in defects in anterior-posterior axis formation and mitotic spindle orientation (Gotta *et al.*, 2001; Kay and Hunter, 2001). A conserved CDC-42/PAR-3/PAR-6/PKC-3 module acts in multiple cellular events beyond embryonic polarization, including neuronal morphogenesis and cell migration during vulval development (Welchman *et al.*, 2007). CDC-42 acts as a negative regulator of LIN-12/Notch function in VPC fate specification, and in this case is necessary and sufficient for 2° cell fate specification (Choi *et al.*, 2010).

CED-10 and MIG-2 act redundantly in multiple aspects of vulval development and morphogenesis. *mig-2* and *ced-10* single mutant vulvae are largely wild-type, whereas *mig-2; ced-10* double loss-of-function mutants display defects in the orientation of asymmetric divisions of the 1° and 2° vulval cells (Figure 11), indicating that *mig-2* and *ced-10* might redundantly control spindle orientation (Kishore and Sundaram, 2002). *mig-2; ced-10* doubles also display a failure in the migrations of 2° vulval cells toward the 1° vulval cells to form a functional vulva (Kishore and Sundaram, 2002).

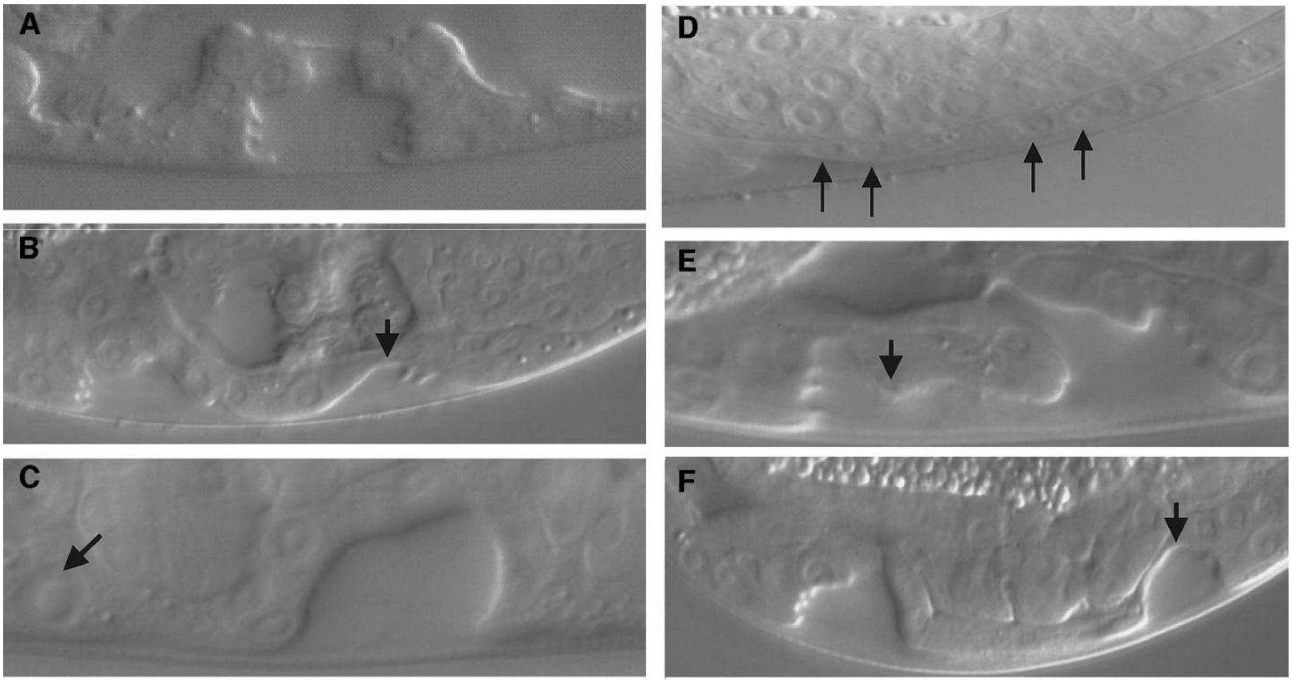

Figure 11 . Vulval defects in *ced-10* Rac and *mig-2* mutants. Nomarski photomicrographs of L4 animals showing vulval cell nuclei and the vulval invagination. Anterior of the worm is to the left and ventral is down. (A) Wild-type; (B) *ced-10(n1993lf)*;*mig-2(mu28lf)*; (C–F) *ced-10(n1993lf)*; *mig-2(RNAi)*; (B) P7.p descendants have formed a separate invagination (arrow). (C) Vul animal in which P5.p adopted a hybrid fate. Arrow points to non vulval anterior daughter of P5.p. (D) Early L4 animal immediately following the last round of division; P6.ppp and P7.pap have divided longitudinally, resulting in adjacent daughter nuclei (arrows). (E) P5.p descendants have failed to migrate toward P6.p descendants, resulting in an extended invagination (arrow). (F) P7.p descendants have formed a separate invagination (arrow).
Kishore and Sundaram, 2002

1.6 Rho-family GTPases in mammals

Rho GTPases are members of the Ras superfamily of monomeric 20-30 kDa GTP-binding proteins. Ten different mammalian Rho GTPases, some with multiple isoforms, have been identified to date: Rho (A, B, C isoforms), Rac (1, 2, 3 isoforms), Cdc42 (Cdc42Hs, G25K isoforms), Rnd1/Rho6, Rnd2/Rho7, Rnd/RhoE, RhoD, RhoG, TC10 and TTF (Ridley, 2000). Different members of the large Ras superfamily regulate a diverse array of cellular processes, from vesicle trafficking to signal transduction. They all have in common the ability to bind and hydrolyse GTP, creating a

switch between an active GTP-bound conformation and an inactive GDP-bound conformation (Figure 12). The structure of Rho GTPases is highly conserved and the presence of the Rho-specific insert domain distinguishes them from other small G proteins (Madaule and Axel, 1985; Jaffe and Hall 2005). All Rho GTPases contain the effector domain and some possess a CAAX box (C-cysteine, A- aliphatic amino acid, X- any amino acid) on the C-terminal tail. The CAAX box is a potential substrate for geranyl- or farnesyltransferases (Foster *et al.*, 1996; Liang *et al.*, 2002) (Figure 13). These enzymes catalyze a lipidation of the CAAX box, which facilitates protein anchoring in the membrane. A hypervariable region is situated upstream of the CAAX box and in some Rho GTPases this contains a polybasic sequence.

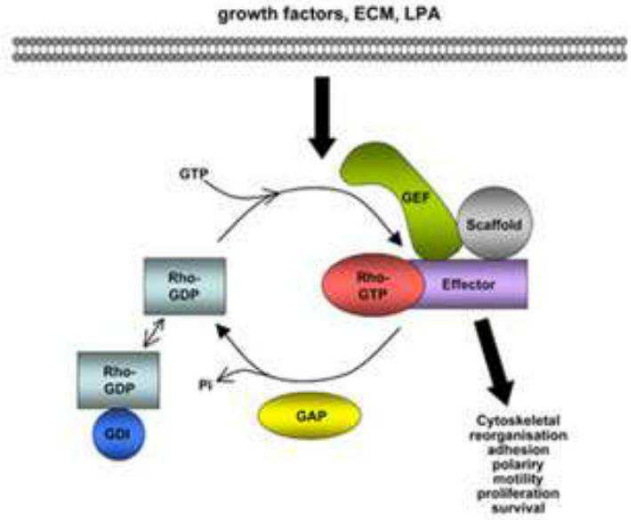

Figure 12. The Rho GTPase cycle. Rho-like GTPases cycle between an active GTP-bound and an inactive GDP-bound form. This is regulated by guanine nucleotide exchange factors (GEFs) and GTPase-activating proteins (GAPs). Guanine nucleotide dissociation inhibitors (GDIs) inhibit nucleotide dissociation and control cycling of Rho GTPases between membrane and cytosol. Signals like growth factors, extracellular matrix (ECM) or lysophosphatidic acid (LPA) are able to activate Rho-like GTPases. Active GTPases interact with effector molecules to elicit various cellular responses. Additionally GEFs could work as scaffold proteins by either binding directly to Rac effectors or other scaffold proteins that bind to effectors. http://www.cruk.manchester.ac.uk

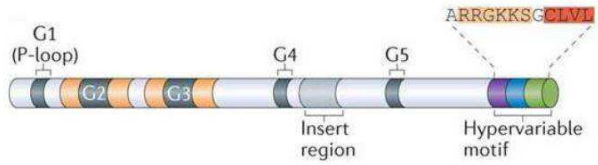

Figure 13. A general schematic diagram of Rho GTPase domain architecture. The G domain in Rho GTPases is highly conserved and is responsible for binding to guanine nucleotides. The G domain contains a variety of amino acid motifs responsible for GTP and GDP binding and coordinating conformational changes. The P-loop (phosphate-binding loop), also known as the G1 domain, is a conserved GXXXXGKS/T motif that is responsible for binding to the β,γ-phosphate of the guanine nucleotide. Rho GTPase specificity is imparted through the hypervariable domain at the carboxyl terminus, which contains several important sequences (and shows the highest level of variability between Rho proteins). The highlighted sequence shown is taken from RhoA as an example. The CAAX motif (red) at the C terminus undergoes a variety of post-translational lipid modifications that are crucial for membrane targeting. Some Rho GTPases also contain a C-terminal polybasic region (orange) that immediately precedes the CAAX motif, containing several Lys and Arg residues, which provide a positively charged interface for membrane association.
Hodge and Ridley, 2006

Over the intervening years, many more activities of Rho GTPases have been demonstrated (Figure 14).

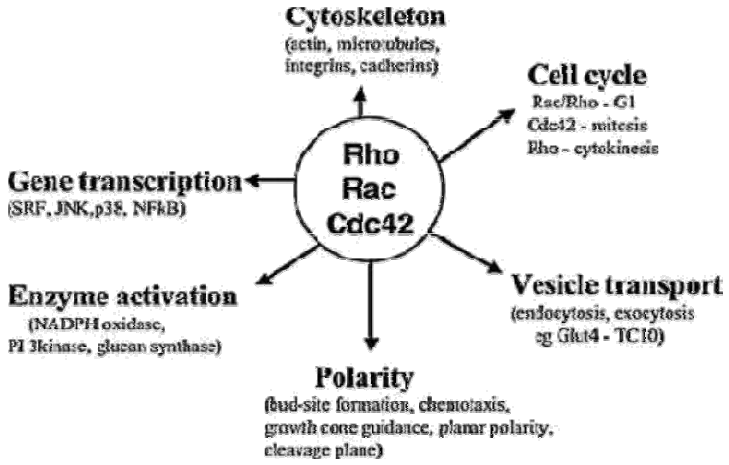

Figure 14. Cellular effects of Rho GTPases. In addition to controlling the assembly of filamentous actin and the organization of the actin cytoskeleton, Rho GTPases have been shown to contribute to the regulation of gene transcription, cell cycle, microtubule dynamics, vesicle transport and numerous enzymatic activities such as phosphoinositide 3-kinase and NADPH oxidase in mammalian cells and glucan synthase in yeast. A special relationship appears to exist between Cdc42 and the establishment of polarity in all eukaryotic cells. Hall, 2005.

The major role of Rho GTPases is to control the assembly and organization of the actin cytoskeleton (Hall, 1998) and, consequently, the cell migration and polarity. Directional cell migration is dependent on cell polarity which influences the formation of the leading and trailing cell edges. A typical polarized migrating cell exhibits cell protrusions, such as filopodia and lamellipodia at the front and large focal adhesion complex at the back (Mayor and Carmona-Fontaine, 2010). Directional cell migration is achieved by the polarized formation of cell protrusions at the front and the contraction of stress fibres at the trailing edge. The typical Rho GTPases – RHOA, RAC1 and CDC42 – play a crucial role in controlling cell polarity. These three Rho GTPases regulate different aspects of cytoskeleton dynamics. CDC42 has been shown to be involved in controlling the actin cytoskeleton present in protrusions known as filopodia (Gupton and Gertler, 2007). RAC1 promotes the formation of lamellipodia – large, flattened and ruffling protrusions – by regulating actin polymerization (Jaffe and Hall, 2005). The three Rho isoforms – RhoA, RhoB and RhoC – can induce stress fibres form action (Wheeler and Ridley, 2004) (Figure 15). In addition to their role in actin dynamics, the Rho GTPases also control polarized adhesion to the substratum during directional migration. Small focal complex structures are localized in the lamellipodia of most migrating cells, and are important for the attachment of the extending lamellipodium to the extracellular matrix (Lauffenburger and Horwitz, 1996).

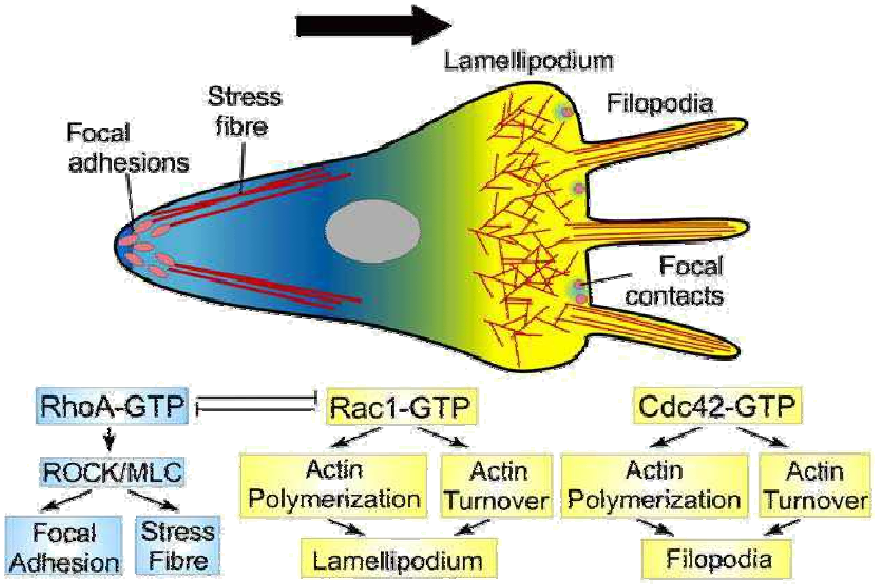

Figure 15. Rho GTPases and cell protrusion control.
Mayor and Carmona-Fontaine, 2010

It is not surprising, therefore, that Rho GTPases have been found to play a role in a variety of cellular processes that are dependent on the actin cytoskeleton, such as cytokinesis (Mabuchi *et al.*, 1993; Drechsel *et al.*,1997; Prokopenko *et al.*, 2000), phagocytosis (Cox D *et al.*, 1997; Caron and Hall, 1998), cell migration (Allen *et al.*, 1998; Nobes and Hall, 1999), morphogenesis (Settleman, 1999) and axon guidance (Luo *et al.*, 1997). Therefore, although Rho GTPases are best characterized for their effects on the actin cytoskeleton, there is now much interest in their ability to affect cell proliferation and gene transcription, and the contributions of all of these activities to malignant transformation is an important field of study. Although members of Rho GTPase family are relatively homologous in their structure, the selectivity in their binding of different effector proteins is significant; Rho GTPases can interact with a wide range of structurally different proteins; these include various scaffold proteins, serine/threonine kinases, tyrosine kinases, lipid kinases, lipases and oxidases (Jaffe and Hall, 2005).

On the basis of the crucial role of these Rho GTPases regulating cell migration and polarity, we assume that dysregulation of their proper functions in these mechanisms it may underlie clinical features characteristic of RASopathies, such as cardiac defects, lymphedema and lymphocytes infiltration in non-hematopoietic tissues (JMML).

2. Aim of the thesis

Noonan syndrome and other RASopathies present a high genetic heterogeneity. In recent years, the research conducted by our group and others allowed the identification of numerous disease genes, which are mutated in about 75% of affected individuals. Because of the absence of sufficiently large families for linkage analyses, gene hunting was performed by using a gene candidacy approach based on mutation scanning of candidate genes with a role in RAS-MAPK pathway. The crucial role of this cascade in the pathogenesis of NS and related phenotypes, and the genetic heterogeneity of the disease, suggest a continuous research of new disease genes within this signaling pathway. The recent discovery of mutations in *RIT1* and *LZTR1* underlying Noonan syndrome suggests that research should not be confined to genes that are part of the RAS-MAPK backbone, but should be extended to genes that encode for proteins contributing to the propagation of signal flow downstream/parallel to RAS.

During my PhD studies, efforts have been directed to identify novel disease genes underlying orphan RASopathies and characterize the molecular mechanisms of pathogenesis, using *C. elegans* as an experimental tool.

3. Material and Methods

3.1 *In silico* prediction of RASopathy candidate genes

A web-based tool, Genes2FANs (http://actin.pharm.mssm.edu/ genes2FANs), using a large-scale protein-protein interaction network coupled to a panel of functional association networks (FANs) was utilized to build a subnetwork connecting proteins to the known RASopathy genes (i.e. *PTPN11*, *SOS1*, *NF1*, *SPRED1*, *CBL*, *NRAS*, *KRAS*, *HRAS*, *RAF1*, *BRAF*, *SHOC2*,*MAP2K1*and *MAP2K2*), as seed proteins. Gene Ontology (biological process tree), mammalian phenotype browser, and Connectivity Map (drug-associated gene expression signatures), ChEA and TRANSFAC (transcription factor networks) databases were selected to construct the functional subnetworks utilized for prioritization of candidates (Dannenfelser *et al.*, 2012).

3.2 Patients and mutation analysis

Three cohorts of patients were considered in the *RRAS* study. A first group including 96 subjects with clinical features within the RASopathy spectrum and without mutation in previously identified RASopathy genes was screened for a selected panel of candidates. A second cohort including 408 subjects with NS or a strictly related phenotype previously tested negative for mutations in a heterogeneous subset of RASopathy genes was scanned for *RRAS* mutations. In both cohorts, the clinical diagnosis was made on the basis of standardized clinical criteria assessed by experienced clinical geneticists and pediatricians. *RRAS* mutation analysis was also carried out on a cohort including 110 subjects with non-syndromic JMML that had prospectively been collected and genotyped (Perez *et al.,* 2010). Mutation screening was performed on the entire *RRAS* coding sequence and flanking intronic stretches (NC_000019.10, 49635295.. 49640143, complement; NM_006270.3; NP_006261.1) on genomic DNA extracted from circulating leukocytes (cohorts I, II and III) or bone marrow aspirates (cohort III) by denaturing high-performance liquid chromatography (DHPLC) (3100 or 3500HT WAVE DNA fragment analysis system, Transgenomic) and/or direct bidirectional sequencing (ABI Prism 3130, 3730 and 3500 Genetic Analyzers). Primer pairs, PCR and DHPLC conditions are available upon request. dbSNP137 (http://www.ncbi.nlm.nih.gov/projects/ SNP/snp_summary.cgi), HapMap (rel.27) (http://hapmap.ncbi. nlm.nih.gov/) and 1000 Genomes (http://www.1000genomes. org/) databases were used to annotate the identified sequence variants. SIFT (http://sift.jcvi.org/), PolyPhen-2 (http://genetics. bwh.harvard.edu/pph2/) and MutationTaster (http://www.muta tiontaster.org/) were used to predict the functional impact of the identified variants. Paternity was confirmed by STR genotyping, using the PowerPlex 16 System (Promega). DNA from leukocytes, hair bulb cells, bone

marrow aspirates and skin fibroblasts was extracted using standard protocols. DNA specimens were collected under Institutional Review Board-approved protocols. Informed consent for DNA storage and genetic analyses was obtained from all subjects.

Targeted enrichment and massively parallel sequencing were performed on genomic DNA extracted from circulating leukocytes and fibroblasts of patient 9802. Exome capture was carried out using the SureSelect Human All Exon V4+UTRs (Agilent), and sequencing with a HiSeq2000 instrument (Illumina). Image analysis and base calling were performed using the Real Time Analysis (RTA) pipeline v. 1.14 (Illumina). Paired-end reads alignment to the reference human genome (UCSC GRCh37/hg19) and variant calling were carried out using the CASAVA v. 1.8 pipeline (Illumina). Variant annotation,SNP filtering (dbSNP135, 1000 Genomes, HapMap and IntegraGen Exome databases) and patient-matched germline variant filtering were attained using an in-house pipeline by IntegraGen (Evry, France).

CDC42 was analyzed by targeted resequencing performed on a large cohort of patients with clinical features within the RASopathy phenotypic spectrum. Clinical exome sequencing was conducted on single families with syndromic intellectual disabilities by our collaborators Dr. Marco Seri (University of Bologna), Dr. Raoul Hennekam (University of Amsterdam Medical Center) and Ghayda Mirzaa (University of Washington). Sanger sequencing was performed to validate genetic variants and perform segregation analyses.

3.3 Structural analysis of RRAS and CDC42 mutants

Structural analysis of RRAS and CDC42 mutants was performed by Prof. Lorenzo Stella (Dipartimento di Scienze e Tecnologie Chimiche, Università di Roma 'Tor Vergata', Rome, Italy.) and Prof. Reza Ahmadian (Heinrich-Heine University, Düsseldorf, Germany), respectively.

Briefly, starting coordinates for MD simulations were obtained from the RRAS crystallographic structure in complex with GDP and Mg^{2+} (PDB: 2FN4; RCSB Protein Data Bank, http://www. rcsb.org/pdb/home/home.do). The N-terminus and C-terminus of RRAS, absent in the crystal, were not considered in simulations. All MD simulations were performed with GROMACS 4.5 package, by using the GROMOS96 43a1 force field parameters for the protein. Parameters for GDP were taken from the GROMACS website (http://www.gromacs.org). Simulations were performed as previously described (Bocchinfuso *et al.*, 2007; Martinelli *et al.*, 2008), except for some details. UCSF Chimera (http://www.cgl.ucsf.edu/chimera/) was used for molecular graphics and structures superposition, by using the MatchMaker option.

Binding interfaces of p50GAP, intersectin and WASP, used as representatives for CDC42 GAPs, GEFs and effectors, respectively,were mapped, using CDC42 in both its inactive and active

states. Structures with PDB codes 1CEE (CDC42-WASP), 1grn (CDC42-p50GAP) and 1ki1 (CDC42- intersectin) were illustrated by using Pymol molecular viewer (DeLano, 2002). Residues in reciprocal vicinity up to 4Å were considered as part of the binding interface. Structures with PDB codes 1AN0 (inactive CDC42) and 2QRZ (active CDCD42) were used for indicating the molecular surfaces with color coded binding interface and mutated residues.

3.4 Biochemical studies of RRAS and CDC42 mutants

Biochemical analysis of RRAS and CDC42 mutants was performed by Prof. Reza Ahmadian (Heinrich-Heine University, Düsseldorf, Germany). Briefly, the generation of constructs, and preparation and purification of proteins were as previously described (Gremer *et al.*, 2011). The intrinsic activities of the RAS proteins, their modulation by GEFs and GAPs and their interaction with different effector proteins were determined as described earlier (Hemsath and Ahmadian, 2005; Jaiswal *et al.*, 2012). Dissociation of mantGDP from RAS proteins was measured using a Perkin Elmer fluorimeter at 366 nm (excitation wavelength) and 450 nm (emission wavelength). GEF-accelerated mantGDP dissociation from RAS proteins (0.1 mM) was measured as mentioned earlier, in the presence of the catalytic domain of SOS1, Cdc25 (5 mM), using stopped-flow instrument. The intrinsic GTPase reaction was performed by mixing 70 mM nucleotide-free RAS proteins (HRAS, $RRAS^{WT}$, $RRAS^{V55M}$ and $RRAS^{G39dup}$) with 50 mM GTP using HPLC assay as previously described (Eberth and Ahmadian, 2009). Samples were taken at different time points and analyzed by HPLC for their GDP and GTP contents to determine the relative GTP content [(GTP)/(GDP + GTP)]. For determination of GAP (neurofibromin, residues 1–333)-stimulated GTPase activity, GDP bound to HRAS and RRAS proteins was exchanged with excess mantGTP in the presence of alkaline phosphatase. Reactions measured the decrease in fluorescence owing to hydrolysis of mantGTP. Effector binding assays were performed using a Fluoromax 4 fluorimeter in polarization mode.

pGEX vectors were used for bacterial expression of $CDC42^{WT}$, $CDC42^{R68Q}$ and $CDC42^{E171K}$, as well as the GTPase-binding domain (GBD) of WASP (aa 154-321), the catalytic domains of CDC42-intersectin (aa 1229-1580), and p50RHOGAP (aa 198-439), as previously described (Jaiswal *et al.*, 2005, 2014; Hemsath *et al.*, 2015). Proteins were isolated as glutathione S-transferase (GST) fusion proteins in *E. coli* BL21 (DE3) cells purified after cleavage of the GST tag *via* gel filtration (Superdex 75 or 200, Pharmacia, Uppsala, Sweden) (Hemsath *et al.*, 2005). Nucleotide-free and fluorescent nucleotide-bound CDC42 variants were prepared using alkaline phosphatase (Roche) and phosphodiesterase (Sigma Aldrich) at 4° C, as described (Hemsath and Ahmadian , 2005; Eberth and Ahmadian, 2009). Fluorescent nucleotides were methylanthraniloyl

(mant-) GDP and mantGppNHp (guanosine 5'- β,γ-imidotriphosphate), a non-hydrolysable GTP analog, and tetramethylrhodamine (tamra-) GTP (Eberth *et al.*, 2005). All purified proteins were analyzed by SDS-PAGE and stored at -80°C. Kinetic m easurements of the CDC42-WASP(GBD) interaction, GEF-catalyzed nucleotide exchange and GAP-stimulated GTP hydrolysis were performed using a stopped-flow apparatus (Hi-Tech Scientific SF-61 with a mercury xenon light source and TgK Scientific Kinetic Studio software), as described (Hemsath *et al.*, 2005; Jaiswal *et al.*, 2013, 2014).

3.5 *Caenorhabditis elegans* studies

Culture and maintenance of animals were as previously described (Sulston and Hodgkin, 1988). The *let-60(n1046)* (*let-60*/*RAS* gain-of-function allele), *let-23(sy1)* (*let-23*/*EGFR* hypomorphic allele), *soc-2 (ku167)* (*soc-2/SHOC 2* loss-of-function allele), *ras-1 (gk237)* (*ras-1/RRAS* loss-of-function allele), *ras-2 (ok682)* (*ras-2/MRAS* loss-of-function allele), *ced-10 (n1993)* (*ced-10/RAC1* loss-of-function allele), *mig-2 (mu28)* (*mig-2/RAC1* loss-of-function allele), *cdc-42 (gk388)* (*cdc-42/CDC42* loss-of-function allele), *rho-1 (ok2418)* (*rho-1/RHOA* loss-of-function allele) strains were provided by the *Caenorhabditis Genetics Center* (University of Minnesota). The three-nucleotide insertion, c.81_82insGGC *(ras-1*^{G27dup}), corresponding to c.116_118dup in *RRAS*, was introduced in the wild-type cDNA (*ras-1*^{WT}) (*C. elegans* ORF clone AAB03320, Thermo Scientific) by site-directed mutagenesis (QuikChange Site-Directed Mutagenesis Kit, Stratagene). *ras-1* cDNAs were subcloned into the pPD49.83 heat shock-inducible vector (a gift of A. Fire, Stanford University School of Medicine). In the same vector we subcloned the wild-type *cdc-42* cDNA (*C. elegans* ORF clone R07G3.1, Thermo Scientific) and c.68A>G (p.Tyr23Cys), c.247T>C (p.Ser83Pro), c.476C>T (p.Ala159Val), c.511G>A (p.Glu171Lys) nucleotide substitutions, as well as the double c.202A>C/c.203G>A (p.Arg68Gln) change, were introduced by site directed mutagenesis. Germline transformation was performed as described (Mello *et al.*, 1991). pJM371 plasmid [p*elt-2*:: NLS::*RFP*] (a gift from J.D. McGhee, University of Calgary), which drives red fluorescent protein (RFP) expression in intestinal cell nuclei, and pJM371 plasmid [*pelt-2::NLS::GFP*] (a gift from J.D. McGhee, University of Calgary), which drives green fluorescent protein (GFP) expression in intestinal cell nuclei, was used as co-injection marker (30 ng/ml). Two different doses of constructs were injected (30 and 100 ng/ml).

Synchronized embryos were heat shocked (30 min at 30° C) to study the effects of transgene expression on embryonic and early larval development (embryonic lethality was measured as the percentage of unhatched eggs), while L1/L2 larvae were heat shocked (60 min at 30° C) to study the consequences on later larval development, movement and fertility. To analyze vulval induction

and morphogenesis, synchronized animals from at least three independent lines for each construct were grown at 20° C and heat-shocked (90 min at 33° C followed by 30 min at 30° C) in parallel at early L3 larval stage and scored for vulval induction from late L3 to mid L4 stages, as well as for the presence of a protruding vulva (Pvl phenotype), multiple ectopic pseudovulvae (Muv phenotype) and lack of a vulva (Vul phenotype) at the adult stage. All the animals were scored blindly at a Leica MZ10F dissecting microscope. Isogenic worms that had lost the transgene were cloned separately and used as controls. All the screened lines exhibited a variable prevalence of these phenotypes upon heath shock. Lines *gbEx555a*[*hsp-16.41*::*ras-1*^{WT};*pelt-2*::NLS::*RFP*], *gbEx557a*[*hsp-16.41*::*ras-1*^{G27dup};*pelt-2*::NLS::*RFP*], gbEx620c[*hsp-16.41*::*cdc-42*^{WT};p*elt-2*::NLS::*GFP*], gbEx637a[*hsp-16.41*::*cdc-42*^{Y23C};p*elt-2*::NLS::*GFP*], gbEx622a[*hsp-16.41*::*cdc-42*^{R68Q};p*elt-2*::NLS::*GFP*], gbEx634b[*hsp-16.41*::*cdc-42*^{S83P};p*elt-2*::NLS::*GFP*], gbEx635a[*hsp-16.41*::*cdc-42*^{A159V};p*elt-2*::NLS::*GFP*] and gbEx623b[*hsp-16.41*::*cdc-42*^{E171K};p*elt-2*::NLS::*GFP*] were scored quantitatively in triplicate experiments at the compound microscope and used for further analyses and crosses.

Genetic crosses were performed according to standard methods (Sulston and Hodgkin, 1988). After each cross, the genotype of individual alleles was confirmed by direct sequencing of the appropriate genomic region. Isogenic animals that had lost the transgene (control groups) were cloned separately and used as controls in each experiment. Vulval induction was evaluated using a Nikon Eclipse 80i instrument equipped with Nomarski differential interference contrast optics. Live animals were mounted on 2% agarose pads containing 10 mM sodium azide as anesthetic.

RNAi was performed by feeding as previously described (Kamath *et al.*, 2001), with minor modifications. Briefly, plates containing NGM agar, 1 mM IPTG and 25 μg/ml carbenicillin were seeded with *E. coli* bacteria expressing double stranded RNA (Addgene) and grown overnight at 37°C. To reduce both maternal and zygotic activities of the gene and overcome lethality, we carried out RNAi of mothers for short periods and looked for phenotypes in their progeny. Synchronized adults were placed on plates seeded with RNAi bacteria at 20°C for 0, 2, 4 or 8 hours. Longer incubations result in variable degree of embryonic lethality. Adults were then transferred to fresh RNAi plates and allowed to lay eggs for 2 hours before removal. Progeny were incubated at 20°C until they reached the required stage for heat shock (early L3). Phenotypic analysis was performed at the adult stage. The RNAi clone was sequenced prior to use. As a control of the efficiency of the modified RNAi protocol, *let-60* RNAi experiments were performed on animals carrying the *let-60* gain-of-function allele *n1046* (p.Gly13Glu), and the prevalence of the Muv phenotype was scored at a dissecting microscope (Table 7).

P-values were calculated using two-tailed Fisher's exact test.

3.6 Cellular studies

Cellular studies was performed by Prof. Reza Ahmadian (Heinrich-Heine University, Düsseldorf, Germany), and Elisabetta Flex (Department of Hematology, Oncology and Molecular Medicine, Istituto Superiore di Sanità, Rome, Italy) and Simona Coppola (Italian National Centre for Rare Diseases, Istituto Superiore di Sanità, Rome, Italy) of our research group.

For cell-based assays in *RRAS* study, COS-7 cells were transiently transfected with FLAG-tagged $RRAS^{WT}$,$RRAS^{V55M}$ or $RRAS^{G39dup}$ by the DEAE-dextran method. Cleared cell lysates were incubated with GSH-beads loaded with GST-RAF1-RBD. GTP-bound proteins and total recombinant proteins were analyzed by immunoblotting with anti-FLAG antibody. Antibodies against MEK1/2, ERK1/2, AKT, phospho-MEK1/2 (Ser217/221), phospho-ERK1/2 (Thr202/Tyr204) and phospho-AKT (Thr308) were purchased from Cell Signaling Technology.

In *CDC42* study, the wild-type human *CDC42* variant 1 cloned into a pcDNA3-FLAG was generated by PCR and cloned *via* BamHI and EcoRI restriction sites. Mutant constructs carrying the Y23C, R68Q, S83P, A159V and E171K were generated by site-directed mutagenesis using the QuikChange XL kit (Agilent Technologies) in accordance with the manufacturer's protocol. All generated constructs were checked by direct sequencing. 3T3 murine cell line was obtained from American Type Culture Collection (ATCC). FLAG-tagged CDC42 mutants, wild-type protein or the empty vector (pcDNA3-FLAG, 2 µg/35mm dish) was transfected using Fugene 6 (Roche, Basel, Switzerland). Twenty-four hours after transfection, cells were assayed for cell growth or processed for wound healing assays. Transfection efficiency was verified by western blot analysis of the protein lysate as previously described (Magini *et al.,* 2014).

Motility of 3T3 cells on fibronectin-coated wells (10ug/ml; SIGMA, St Louis, MO) was evaluated by wound-healing assays. Monolayers of 3T3 cells transfected for 24 hours with the indicated plasmids were scratched with a 200-µl micropipette tip and incubated in the presence of thymidine (10 mM; Sigma) to inhibit cell proliferation. Images were acquired at different time points using a Nikon Eclipse TS100 microscope, a Nikon Plan Fluor 10×0.13 objective and a Nikon Coolpix 990 digital camera (Nikon, UK). Cells that had migrated in the wounded area were counted in four fields per well and the fold increase of migratory cells compared to the WT counterpart was evaluated 4 hours after scratch.

Proliferation and viability of transiently transfected 3T3 cells were quantified by manual counting using a Neubauer hemocytometer. Cell viability was detected by the exclusion of the Trypan Blue dye (5 g/ml in PBS; Sigma). Cells were counted at different time points using a LeitzOrtholux II microscope, a Leitz 10×0.13 objective (Leitz, Germa ny).

P-values were calculated using student's t Test.

4. Results

4.1 Activating mutations in *RRAS* underlie a phenotype within the RASopathy spectrum and contribute to leukaemogenesis (Flex *et al.*, 2014)

4.1.1 Identification of candidate disease genes and *RRAS* mutation analysis

While the core of the machinery implicated in RAS signaling has been characterized widely, signal propagation through this network is likely to include a larger number of proteins playing a modulatory or structural role (McKay and Morrison, 2007), whose aberrant or defective function is expected to perturb development and contribute to oncogenesis. Based on this supposition, we used a protein interaction/functional association network analysis to select a panel of genes encoding proteins functionally linked to the RAS signaling network as candidates for NS or a related RASopathy (Dannenfelser *et al.*, 2012) (Figure 16).

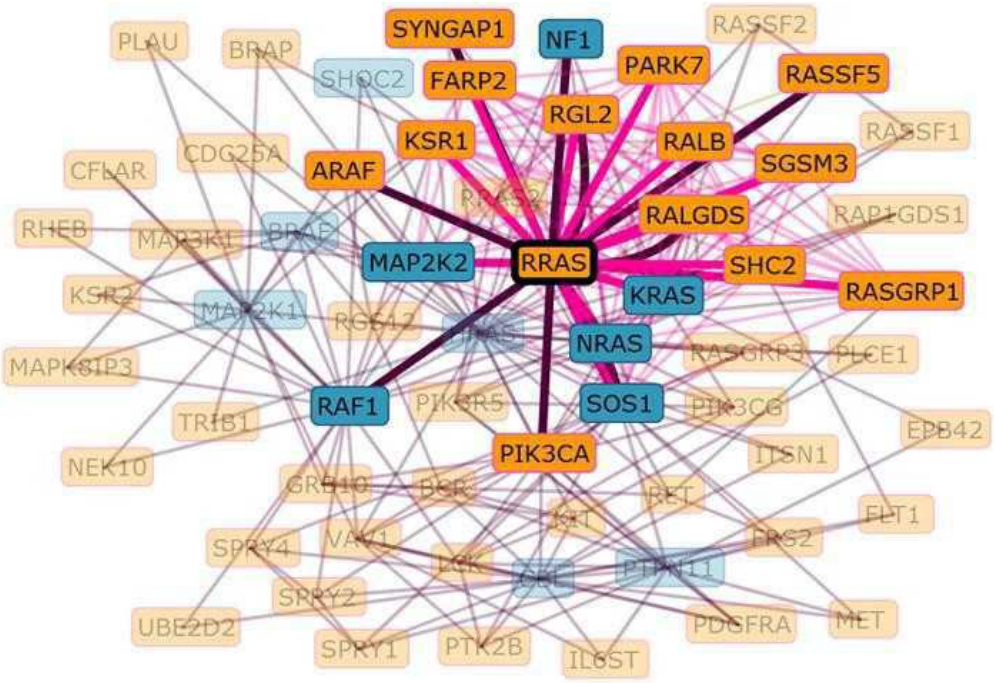

Figure 16. Mammalian protein interaction/functional association network analysis constructed by using proteins known to be mutated in RASopathies as seed proteins. The analysis was performed by using Genes2FANs (Dannenfelser *et al.*, 2012) (http://actin.pharm.mssm.edu/genes2FANs). Connections are based on Protein-Protein Interaction (PPI) and Connectivity Map (CMAP) networks, Mammalian Phenotype (MP) Browser, and Gene Ontology (GO), ChIP Enrichment Analysis (ChEA) and TRANSFAC databases. Connections involving RRAS are highlighted. Purple lines indicate protein-protein interactions; magenta lines indicate GO-biological process links. RASopathy genes are in blue.

Candidate gene selection was based on the use of the previously identified RASopathy genes as 'seed' proteins (*i.e.*, proteins used to build the interaction/functional networks), and considering a panel of databases to construct functional subnetworks (Figure 16). Sequence scanning of the best candidates in a RASopathy cohort including 96 unrelated subjects negative for mutations in known disease-genes allowed the identification of a functionally relevant *RRAS* change (c.163G>A, p.Val55Met) (Figure 17) in an adult subject with clinical features suggestive of NS but lacking sufficient characteristics to allow a definitive diagnosis (Table 3).

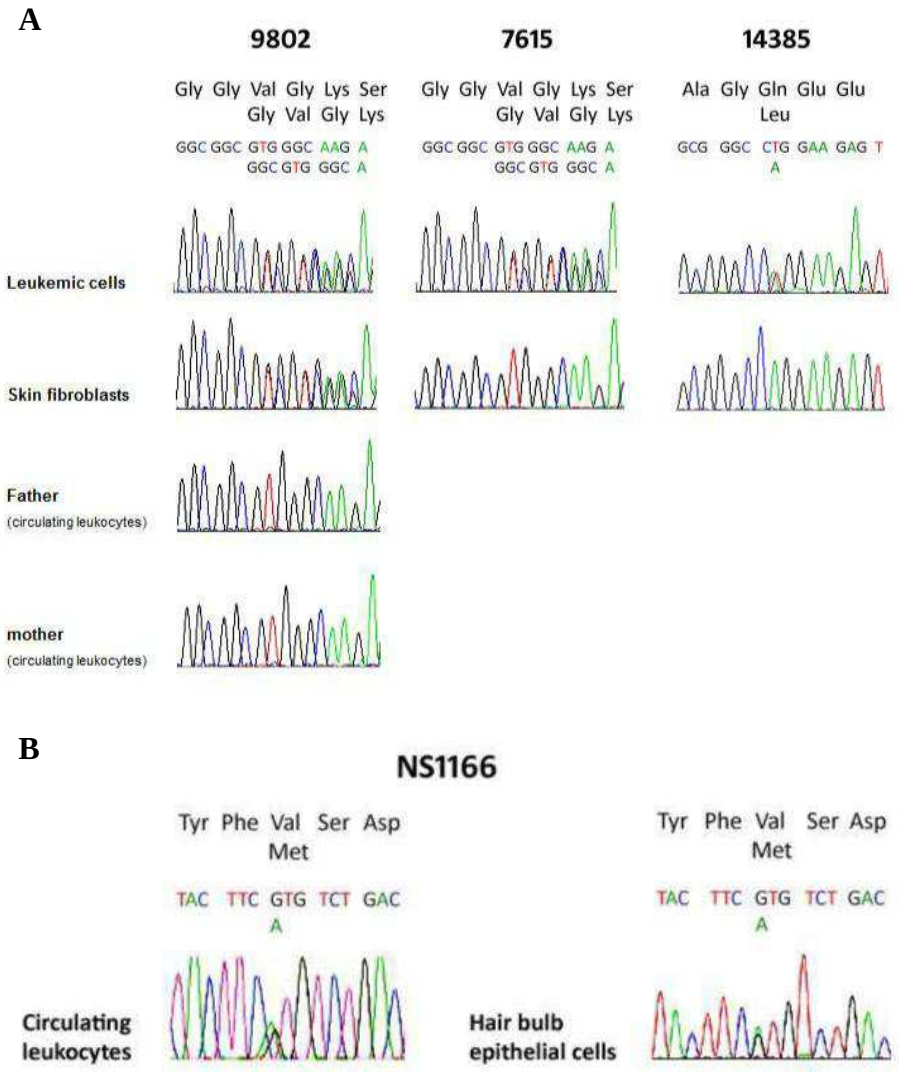

Figure 17. Germline and somatic disease-associated *RRAS* mutations. (A) Electropherograms showing the *de novo*, germline origin of the c.116_118dup change (p.Gly39dup) in sporadic case 9802 (RASopathy with AML), and the somatic origin of the same in-frame duplication and the c.260A>T missense substitution (p.Gln87Leu) in subjects 7615 and 14385 (non-syndromic JMML). (B) Electropherograms of the germline c.163G>A missense substitution (p.Val55Met) in subject NS1166.

Parental DNA was not available for segregation analysis. The mutation was not identified among >400 population-matched unaffected individuals, indicating that it did not represent a common polymorphic nucleotide substitution.

Table 3. Clinical features of the subjects heterozygous for germline *RRAS* mutations.

Patient #	NS1166	9802
Nucleotide change	c.163G	c.116_118dup
Amino acid change	p.Val55	p.Gly39dup
Sporadic/familial	unknow	sporadic
Origin of mutation	-	*de novo*
Age at last evaluation (years)	51	16
Sex	female	female
Prenatal findings	NA	polyhydramnio
Feeding difficulties	NA	+
Growth failure	NA	+
Short stature (<3rd centile)	-[1]	+
Facial features	triangular face, downslanting palpebral fissures, low-set ears, thick lips	triangular face, downslanting palpebral fissures, ptosis[2], low-set ears, thick lips
Low posterior hairline	+	+
Congenital heart defect	-	pulmonic
Hypertrophic cardiomyopathy	-	-
Short/webbed neck	-	-
Broad chest	+	+
Pectus deformity	-	-
Coagulation defects	-	-
Postnatal lymphedema	-	-
Ophthalmological problems	-	-
Motor delay / muscular hypotonia	-	delayed acquisition of walking
Cognitive deficits	-[3]	-
Ectodermal anomalies	-	-
Lentigines	-	-
Nevi	-	-
Café-au-lait spots	-	+
Malignancy	+[4]	+[5]
Other		Crowded teeth, pyloric stenosis, glomerulonephritis, arthritis

NA, not available.
[1]10th centile.
[2]Congenital, surgically treated.
[3]Borderline cognitive abilities.
[4]Unspecified bone tumour (left leg) diagnosed during childhood.
[5]AML suspected to be secondary to JMML, with onset at 13 years (Supplementary Table S3). The condition was not associated with any germline/somatic mutation affecting previously identified RASopathy genes. Several complications occurred during treatment (renal failure, pulmonar infection, vein-occlusive disease), without complete remission. Death occurred at age of 16 by recurrence of the disease after 2 years of palliative treatment.

This change, rs368625677 (dbSNP 138), had been described in 1/13,006 alleles in the NHLBI Exome Sequencing Project (http://eversusgs.washington.edu/EVS/). Of note, similar frequencies have been reported in the same database for recurrent RASopathy-causing mutations (*e.g.*,

c.922A>G in *PTPN11* and c.1259G>A in *CBL*). Mutation analysis was extended to additional 408 patients with NS or a clinically related phenotype tested negative for mutations in the major NS disease genes, allowing to identify one sporadic case heterozygous for a three nucleotide duplication (c.116_118dup, p.Gly39dup) (Figure 17). Parental DNA sequencing of the relevant exon demonstrated the *de novo* origin of the variant, and STR genotyping confirmed paternity. In this subject, the duplication was documented in DNA obtained from skin fibroblasts, excluding a somatic event restricted to haematopoietic cells. The subject had features reminiscent of NS (Figure 18 and Table 3), with onset of AML suspected to represent a blast crisis of JMML.

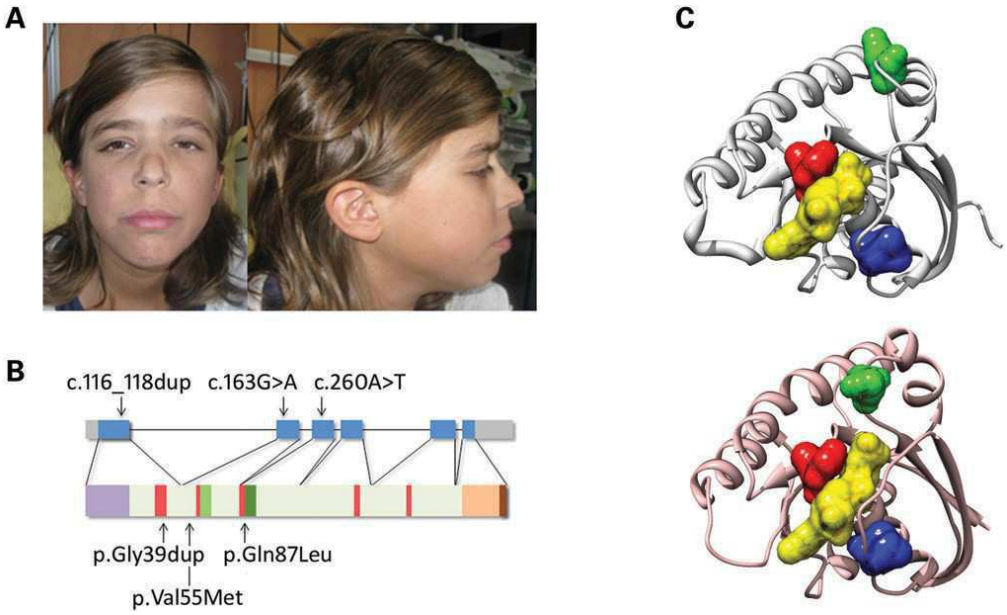

Figure 18. RASopathy causing and leukaemia associated *RRAS* mutations. (A) Facial features of the affected subject (9802) heterozygous for the *de novo* germline c.116_118dup. (B) *RRAS* exon-intron arrangement with coding exons as blue boxes. RRAS functional motifs include the GTP/GDP binding domain (G1 to G5, starting from the *N*-terminus) (red), switch I (light green), switch II (dark green) and hypervariable region (light brown) with the *C*-terminal CAAX motif (dark brown). The unique *N*-terminal region is also shown (violet). Location of disease-associated mutations is reported. (C) Position of affected residues on the three-dimensional structure of RRAS in its GDP-bound, inactive state (PDB: 2FN4) (above) and that of non-hydrolysable GTP analogue (GppNHp)-bound, active HRAS (PDB: 5P21) (below). The red surface indicates Gly^{39} and Val^{40} (Gly^{13} and Val^{14}, in HRAS), whereas Val^{55} (Val^{29}) and Gln^{87} (Gln^{61}) are shown in blue and green, respectively. GDP is reported as semi-transparent yellow surface.

In this patient, exome sequencing performed on leukaemic and non-leukaemic DNA failed to reveal any additional relevant germline/somatic change affecting genes known to be mutated in RASopathies and JMML, as well as genes directly linked to the RAS signaling network, further

supporting the causal role of the identified *RRAS* lesion. Based on this association, the occurrence of *RRAS* mutations was also explored in a panel of genomic DNAs obtained from bone marrow aspirates/circulating leukocytes of 110 subjects with JMML. Heterozygosity for the previously identified Gly[39] duplication and the c.260A>T (p.Gln87Leu) change was observed in two patients with JMML rapidly progressing to AML (Table 4). Both lesions were absent in non-leukaemic DNA, indicating their somatic origin (Figure 17).

Table 4. Haematological features associated with germline or somatically acquired *RRAS* mutations. Mutations characterize a subset of myeloid neoplasms with classical features of JMML (*i.e.*, monocytosis, low blast counts, presence of circulating myeloid progenitors, and elevated basophil counts) combined with atypical features, including late onset and rapid progression to AML.

Patient	**9802**	**7615**	**14385**
Diagnosis	AML[1]	JMML[2]	JMML[2]
Gender	F	F	F
Age at onset (years)	13	10	13
Splenomegaly	yes	yes	no
Peripheral blood cell counts ($x10^9$/L)			
Platelets	663	47	180
White blood cells	11	7.4	14
Monocytes	1.3	1.5	4.6
Basophils	0.2	0.18	0.77
Myeloid precursors in peripheral blood (%)	14	15	10
Circulating undifferentiated myeloid blasts (%)	8	3.5	10
Bone marrow smear cytomorphology			
Undifferentiated myeloid blasts (%)	38	12	18
Myelodysplasia	+	+	+
In vitro growth of myeloid progenitors	microclusters only	microclusters only	+
Haemoglobin (g/L)	86	104	120
Fetal Haemoglobin	NA	5%	-
RRAS mutation	c.116_118dup p.Gly39dup (germline)	c.116_118dup p.Gly39dup (somatic)	c.260A>T p.Gln87eu (somatic)
Concomitant RAS pathway mutations	-	*NRAS*, c.82A>G p.Q61R (somatic)	*NRAS*,c.35GA p.G12D (somatic)
BCR-ABL transcript	-	-	-
Karyotype (blasts)	46,XX,t(3;6)(q26;q26)[24]	/46,XX[1]	45,XX -7

NA, not available. [1]Secondary to JMML. [2]Rapidly progressed to AML.
[3]The clonal architecture was investigated by sequencing the somatic *RRAS* and *NRAS* mutations in 62 individual colonies obtained by *in vitro* culture of myeloid precursors (30 CFU-GM and 32 CFU-M). All colonies exhibited both mutations.

These subjects also carried a somatic *NRAS* mutation, suggesting that the two hits might cooperate with this severe form of disease. Sequencing of isolated JMML myeloid colonies in patient 14385 showed that *NRAS* and *RRAS* mutations coexisted in the same progenitors but failed to establish their sequence of appearance during leukaemogenesis, not allowing to discriminate whether the latter was involved in initiation or progression of disease.

4.1.2 Structural analyses

RRAS encodes a 23-kD membrane-bound monomeric GTPase with 55-60% amino acid identity to RAS proteins (Lowe *et al.,* 1987). This highly conserved structure is flanked by a unique 26-amino acid region at the *N*-terminus (Figure 18B). Similarly to the other RAS family proteins, RRAS binds to GTP and GDP with high affinity and specificity and functions as a molecular switch by cycling between active, GTP-bound and inactive, GDP-bound states (Wennerberg *et al.,* 2005). RRAS is activated by guanine nucleotide exchange factors (GEFs) in response to signals elicited by cell surface receptors. In the GTP-bound state, two functionally conserved regions, switch I and switch II (Figure 18B), undergo a conformational change enabling RRAS to bind to and activate effector proteins. This interaction is terminated by hydrolysis of GTP to GDP, which is promoted by GTPase-activating proteins (GAPs) and results in switching towards the inactive conformation. Disease-associated *RRAS* mutations affected residues highly conserved among orthologs and paralogs (Figure 19) residing in the GTP-binding pocket (Figure 18C) and were predicted to be damaging with high confidence.

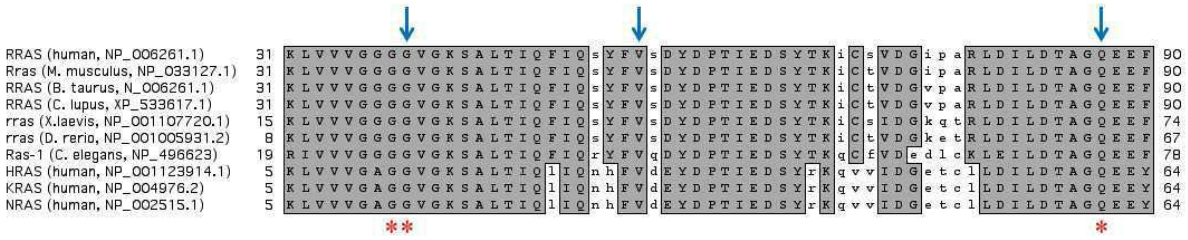

Figure 19. Partial amino acid sequence alignment of human RRAS, KRAS, NRAS and HRAS proteins, together with representative RRAS orthologs showing conservation of the RRAS mutated residues. Blue arrows on top of the alignment mark amino acids affected by disease-associated *RRAS* mutations, while the red asterisks below the alignment indicate the positions of the cancer-associated mutation hot spots in RAS proteins.

Among them, Gln^{87}, homolog of Gln^{61} in RAS proteins, is directly involved in catalysis (Krengel *et al.,* 1990; Saez *et al.,* 1994).The p.Gln87Leu substitution had previously been reported as a rare somatic event in lung carcinoma, and mutations affecting Gln^{61} are among the most recurrent oncogenic lesions in *RAS* genes (COSMIC database, http://cancer.sanger.ac.uk/cosmic). Likewise, p.Gly39dup altered the G1 motif participating in GTP/GDP binding and GTPase activity (Figure

18B). Within this motif, Gly^{12} and Gly^{13} (Gly^{38} and Gly^{39} in RRAS) represent major mutation hot-spots in human cancer (COSMIC database) and account for the majority of germline *HRAS* mutations causing Costello syndrome (Aoki *et al.*, 2005). In contrast, no somatic/germline *RAS* mutation affecting Val^{29}, homolog of Val^{55} in RRAS, had previously been reported.

Molecular dynamics (MD) simulations were performed to predict *in silico* the effects of p.Val55Met on the structure and dynamics of RRAS (Figure 20). The mutation was introduced in the available crystallographic structure of RRAS in complex with GDP and Mg^{2+}, and the system was simulated in water for 200 ns. For comparison, MD simulations were also performed using the wild-type protein, which maintained a stable structure along the whole simulation, as expected (Figure 20A, left panel). In contrast, a dramatic local structural transition extending up to the switch I region (residues 58-64), which mediates effector binding, was documented for the $RRAS^{V55M}$ mutant, after ~80 ns (Figure 20A, right panel).

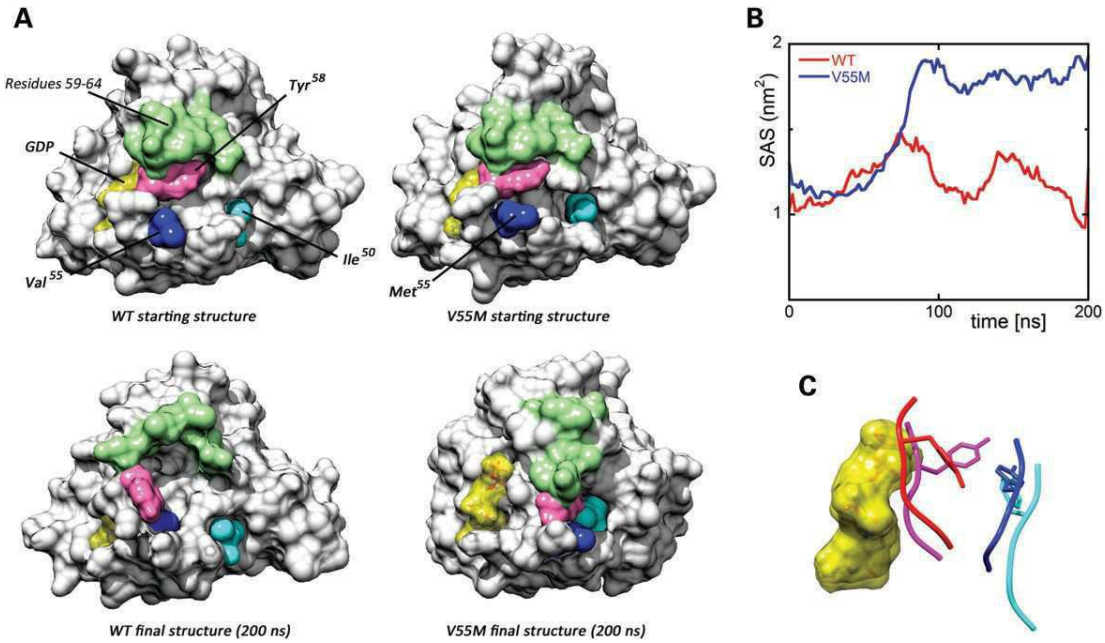

Figure 20. Molecular dynamics (MD) simulations. (A) Structural perturbations promoted by the p.Val55Met substitution as obtained from MD simulations of the RRAS/GDP complex. The wild-type (WT) protein is also shown for comparison. Top panels report the protein structures at the beginning of simulations, whereas the final structures (200 ns) are shown at the bottom. The final structure of $RRAS^{V55M}$ is well representative of the last 120 ns of the trajectory. The protein surface of RRAS is shown with GDP (yellow). The mutated residues and those forming a cluster in the simulation of mutated RRAS are coloured as follows: Val^{55}/Met^{55} (blue), Tyr^{58} (pink) and Ile^{50} (cyan). Residues 59-64, which, together with Tyr^{58}, form the switch I region, are coloured in green. (B) Solvent accessible surface of GDP in the MD simulations of wild-type (red) and mutant (blue) RRAS/GDP complexes. (C) Conformation of the loop comprised between Val^{55}/Met^{55} and Asp^{59} in wild-type (red) and mutant (blue) RRAS/GDP complexes obtained from MD simulations. GDP is reported as semi-transparent yellow surface. Superimposed conformations of the corresponding loop (residues 29-33) in GDP-bound HRAS (violet) (PDB: 4Q21) and GDP-bound HRAS complexed with SOS1 (cyan) (PDB: 1BKD) are shown for comparison. The side chains of Tyr^{58} and the corresponding residue in HRAS, Tyr^{32}, are displayed as sticks.

This conformational transition resulted in an increased solvent exposure of Met^{55}, in agreement with the higher hydrophilicity of this residue compared with Val, and was accompanied by the formation of a stable cluster involving residues Ile^{50}, Met^{55} and Tyr^{58} (Figure 20A) permitted by the unbranched and long side-chain of Met^{55}.The major effect of this structural rearrangement was to increase exposure of GDP to the solvent (Figure 20B) and a loss of the H-bonds between residues at codons 55 and 56, and GDP. We also observed that after the conformational rearrangement, the RRAS^{V55M} region implicated in GEF binding populated a structure similar to that assumed in RAS/GEF complexes (Figure 20C), suggesting a possible enhanced interaction of the disease-associated RRAS mutant with GEFs. Overall, these data supported an activating role of p.Val55Met through enhanced GDP release as a result of a decreased affinity for the nucleotide and/or enhanced interaction with a GEF.

4.1.3 Biochemical and functional characterization of RRAS mutants

To characterize the impact of p.Val55Met and p.Gly39dup on protein function, we analyzed the intrinsic and GEF-accelerated nucleotide exchange reaction of these mutants. Dissociation kinetics analysis demonstrated a dramatically increased intrinsic (RRAS^{G39dup}) and GEF-stimulated (RRAS^{G39dup} and RRAS^{V55M}) dissociation rate of mantGDP, indicating a facilitated nucleotide release in both mutants (Figure 21A).

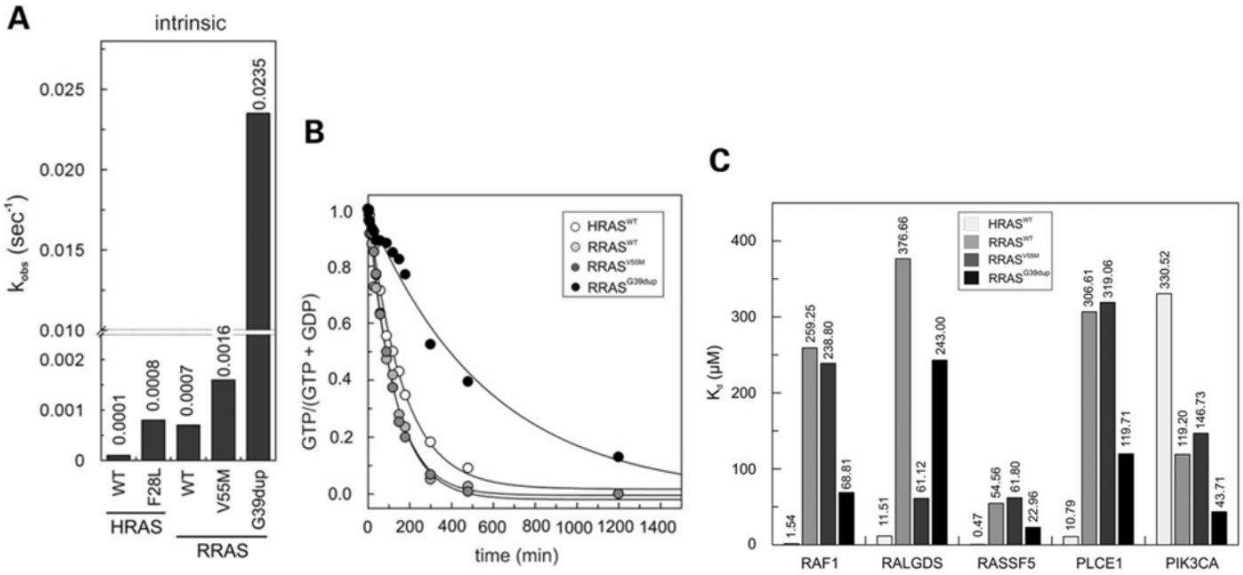

Figure 21. *In vitro* biochemical characterization of the RRAS^{G39dup} and RRAS^{V55M} mutants. (A) Intrinsic mantGDP nucleotide dissociation measured in the presence of 20-fold excess of non-labelled GDP. RRAS^{G39dup} exhibited a 35-fold increased intrinsic dissociation of mantGDP. (B) Intrinsic GTP hydrolysis kinetics of RRASG^{39dup} and RRAS^{V55M} proteins, documenting the impaired catalytic activity in the former. (C) Dissociation constants (Kd) for the interaction of HRAS^{WT} and RRAS proteins to the RBDs of RAF1, RALGDS, PLCE1, PIK3CA and RASSF5. Of note, RRAS^{WT} binds to RAF1, RALGDS, RASSF5 and PLCE1 less efficiently than HRAS, whereas an increased binding affinity to PIK3CA is observed.

Assessment of RRAS^{G39dup} and RRAS^{V55M} GTPase activity documented a significantly reduced intrinsic and GAP-stimulated GTP hydrolysis in the former (Figure 21B). Finally, the interaction of RRAS proteins with various effectors was analyzed (Figure 21C) and an aberrant binding behavior of the two RRAS mutants was demonstrated, with RRASG^{39dup} exhibiting an increased binding affinity towards PIK3CA, RAF1, PLCE1 and RASSF5, and RRAS^{V55M} to RALGDS. To gain further insights into the impact of disease-causing mutations on RRAS functional dysregulation and explore their effects on RAS signaling, the activation state of RRAS proteins and extent of signaling through the MAPK and PI3K/AKT cascades were evaluated using transient expression in COS-7 cells. Consistent with the above-mentioned findings, pull-down assays revealed a variably higher proportion of active, GTP-bound form for both mutants (Figure 22A). Moreover, similarly to what observed under cell-free conditions, RRAS^{G39dup} was resistant to GAP stimulation. Expression of both mutants promoted enhanced serum-dependent MEK, ERK and AKT phosphorylation (Figure 22B), which was more evident in cells expressing the RRAS^{G39dup} mutant.

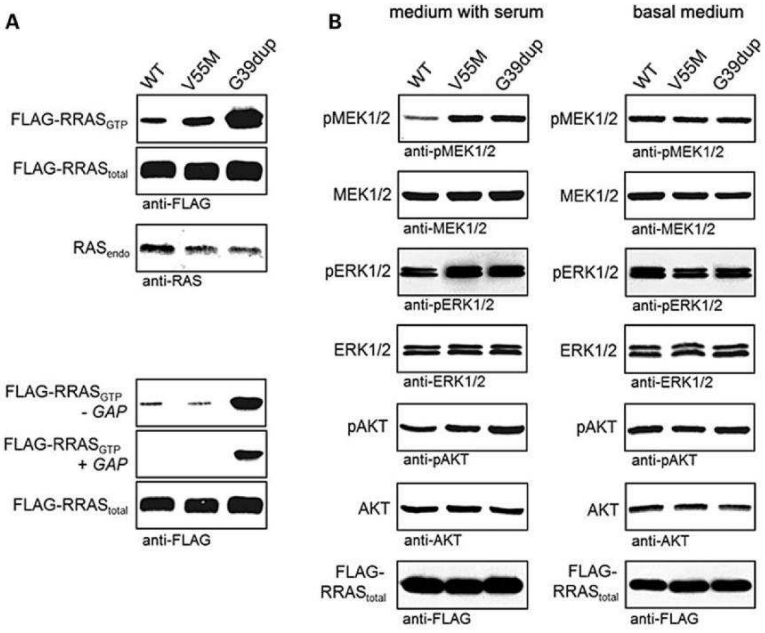

Figure 22. RRAS^{G39dup} and RRAS^{V55M} signalling activities in cells.(A) Determination of GTP-bound RRAS levels in COS-7 cells transiently expressing wild-type or mutant FLAG-tagged RRAS proteins. Assays were performed in the presence of serum (above), and in serum-free conditions (2GAP) or in the presence of the neurofibromin GAP domain (+GAP) (below). RRAS^{G39dup} was predominantly present in the active GTP-bound form and was resistant to GAP stimulation, whereas a slightly increased level of GTP-bound RRAS^{V55M} was observed in the presence of serum. Representative blots of three performed experiments are shown.
(B) Determination of MEK, ERK and AKT phosphorylation levels (pMEK, pERK and pAKT) in transiently transfected COS-7 in medium with serum (left) or basal medium (right). Expression of each RRAS mutant resulted in variably enhanced MEK, ERK and also partially AKT phosphorylation after stimulation. Total MEK, ERK and AKT in cell lysates are shown for equal protein expression and loading. Expression levels of exogenous, FLAG-tagged RRAS in cell lysates are shown for each experiment. Representative blots of three performed experiments are shown.

4.1.4 *Caenorhabditis elegans* studies

To explore further the functional impact of the RASopathy causative RRAS mutants on RAS signaling *in vivo*, we used the nematode *C. elegans* as an experimental model. In *C. elegans*, the role

of *ras-1*, the *RRAS* ortholog (Lundquist, 2006), has not been characterized yet. On the contrary, as described in the introduction, proper signaling through *let-60*, the *C. elegans* ortholog of the human *RAS* genes, has been established to play a crucial role in vulval development (Stenberg, 2005). In particular, LET-60/RAS is known to mediate the priming signal (LIN-3/EGF) released by the anchor cell to induce the three nearby vulval precursor cells (VPCs), P5.p, P6.p and P7.p, to generate a normal vulva. Enhanced and decreased signaling through LET-60 and the MAPK cassette results in multiple ectopic pseudovulvae (multivulva phenotype) and a failure in VPC induction (vulvaless phenotype), respectively (Stenberg, 2005; Sundaram, 2016). Multiple transgenic lines were generated to conditionally express the wild-type *ras-1* cDNA (*ras-1*^{WT}) or the allele homologous to the disease-associated three-nucleotide duplication (*ras-1*^{G27dup}), which was identified to occur both as a germline and somatic event. Exogenous RAS-1 expression was induced by heat shock at early L3 larval stage to investigate the effects of the mutant protein on vulval development. Animals expressing *ras-1*^{G27dup} displayed abnormal vulval morphogenesis resulting in the formation of a protruding vulva (Pvl) (Figure 23A and B; Table 5), a phenotype associated with aberrant traffic through different signaling cascades (Eisenmann and Kim, 2000; Kishore and Sundaram, 2002).Of note, this phenotype had previously been reported in worms expressing the RASopathy causative SHOC2^{S2G} mutant (Cordeddu *et al.*, 2009).

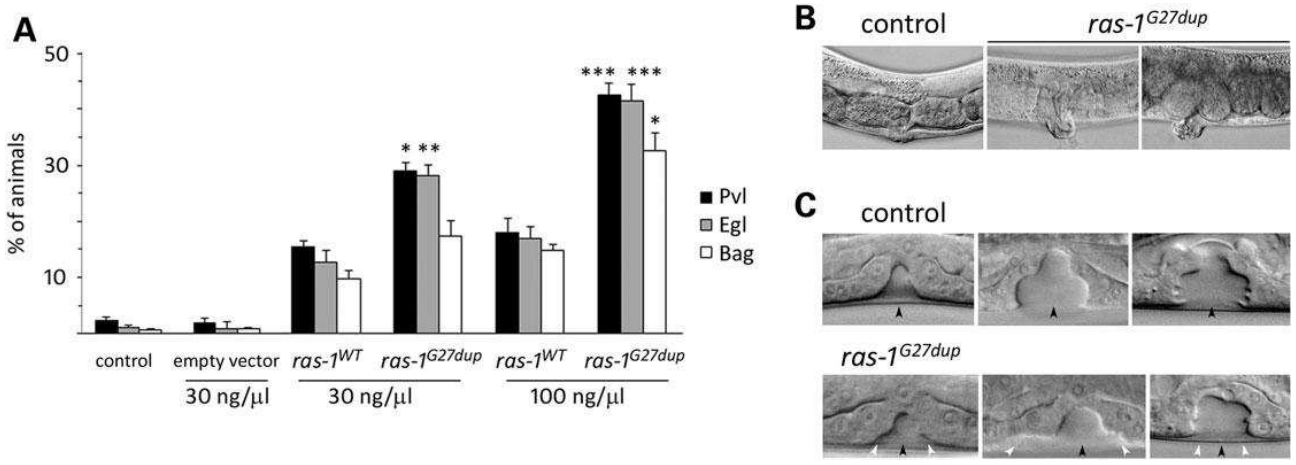

Figure 23. Consequences of *ras-1*^{G27dup}expression on *C. elegans* vulval development. (A) Heat-shock-driven expression of *ras-1*^{WT} and *ras-1*^{G27dup} at early L3 stage results in protruding vulva (Pvl), egg laying defective (Egl) and bag-of-worms (Bag) phenotypes. Isogenic animals that had lost the transgene (control group) and worms expressing the heat shock-inducible vector (empty vector) were subjected to heat shock and scored in parallel for comparison. The dose at which the transgene has been injected is reported at the bottom. Error bars indicate SD of three independent experiments. Asterisks indicate significant differences compared with *ras-1*^{WT} at the corresponding dose of injection ($^{*}P< 0.05$; $^{**}P< 0.005$; $^{***}P< 0.0005$; Fisher's Exact Test). (B) A proper vulva develops in heat-shocked control animals (left), whereas a protruding vulva is observed in heat-shocked *ras-1*^{G27dup} young adults (middle) and adult worms (right). (C) Nomarski images of vulval precursor cells in late L3 (left), early L4 (middle) and mid-late L4 (right) stages from synchronized animals heat-shocked at early L3.
In control animals (N= 48), only P6.p descendants invaginate (upper panel), whereas in 10 of 30 analysed *ras-1*^{G27dup}-expressing worms, P5.p and/or P7.p descendants also detach from the cuticle, generating asymmetric invaginations (lower panel). Black arrowhead spot into P6.p descendant invagination, whereas white arrowheads point to P5.p and P7.p descendant invagination. Anterior is to the left and dorsal is up, in all images.

Like those animals, *ras-1*^{G27dup} worms showed decreased egg-laying efficiency (Egl phenotype), and accumulation of larvae inside the mother (Bag-of-worms phenotype). A significantly less penetrant phenotype was observed in animals expressing *ras-1*^{WT}. These findings, together with the observation that animals lacking *ras-1* do not exhibit any vulval defect (WormBase, http://www.wormbase.org/, and our personal assessment), supported the gain-of-function role of the mutation on RAS-1 function. At the late L3/early L4 larval stage, vulva morphogenesis normally begins with the descendants of VPC P6.p detaching from the cuticle and forming a symmetric invagination (Figure 23) (Stenberg, 2005). Animals in which the expression of *ras-1*^{WT} had been induced at early L3 largely maintained this pattern (17/20). In contrast, in larvae expressing *ras-1*^{G27dup}, descendants of VPCs P5.p and/or P7.p more frequently detached from the cuticle, resulting in larger and more asymmetric invaginations (10/30). This morphogenesis defect was the earliest detectable effect of the *ras-1*^{G27dup} allele on vulval development, similarly to that previously documented in transgenic lines expressing *SHOC2*^{S2G} (Cordeddu *et al.*, 2009).

Table 5. *C. elegans* phenotypes resulting from expression of wild-type RAS-1 or the disease-associated RAS-1^{G27dup} mutant.

Transgene (dose of injection)	*N*	Pvl (%)	Egl (%)	Bag (%)
none	175	1.1	0.6	0.6
empty vector (30 ng/µl)	106	1.9	0.9	0.9
ras-1^{WT} (30 ng/µl)	103	15.5	12.7	9.7
ras-1^{G27dup} (30 ng/µl)	103	29.1[1]	28.2[2]	17.5
ras-1^{WT} (100 ng/µl)	94	18.1	17.0	14.9
ras-1^{G27dup} (100 ng/µl)	89	42.7[3]	41.6[3]	32.6[4]

Injections were carried out on N2 worms (wild-type background).
Strains: *ras-1*^{WT}and *ras-1*^{G27dup} indicate *hsp-16.41::ras-1*^{WT}and *hsp-16.41::ras-1*^{G27dup}, respectively; *ras-1*^{G27dup} results from the three-nucleotide insertion, c.82_83insGCG, corresponding to the RASopathy causative c.116_118dup in *RRAS*.
The concentration at which the plasmid has been injected is reported in parenthesis.
Worms were grown at 20 °C and heat-shocked at early L3 stage. Isogenic worms that had lost the transgene were cloned separately and used as controls.
N indicates the number of animals scored.
Pvl is the percent of adult worms with a protruding vulva.
Egl is the percent of animals with an increased number of eggs retained in the uterus (N > 22). Bag is the percent of bag-of-worms animals counted up to 6 days post-fertilization.
[1-4]Statistical significance of comparisons with worms expressing *ras-1*^{WT} at the corresponding dose of injection ([1]$P < 0.05$; [2]$P < 0.005$; [3]$P < 0.0005$; [4]$P < 0.01$). *P* values were calculated using 2-Tail Fisher's Exact Test.

Genetic interaction between the RAS-1/RRAS mutant and LET-60/RAS was also investigated. While expression of the RAS-1^{G27dup} mutant was able to exacerbate the multivulva phenotype associated with a hyperactive *let-60* allele (*n1046*), expression of wild-type RAS-1 failed to do so (Table 6). Similarly, a significant, although partial rescue of the VPC induction defect associated with a *let-23/EGFR* hypomorphic allele (*sy1*) was observed in animals expressing the activating RAS-1^{G27dup} mutant, but not in worms expressing the wild-type counterpart (Table).

Table 6. Vulva phenotypes in *C. elegans* mutant strains expressing wild-type RAS-1 or the disease-associated RAS-1^{G27dup} mutant

Genotype	Transgene	*N*	Muv (%)	Vul (%)	Pvl	*N*	P6.p
wild-type	none	207	0	0	1.0	48	100
let-60(*n1046*)	none	201	77.9	–	0.5	50	100
let-60(*n1046*)	*ras-1*^{wt}	244	76.4	–	2.8	43	100
let-60(*n1046*)	*ras-1*^{G27dup}	231	87.1[a]	–	3.0	50	100
let-23(*sy1*)	none	194	–	87.8	3.6	178	13.4
let-23(*sy1*)	*ras-1*^{wt}	169	–	84.3	4.1	156	14.0
let-23(*sy1*)	*ras-1*^{G27dup}	282	–	83.3	10.3[b]	128	24.2[c]

Strains: *let-60(n1046)* is a gain-of-function allele of *let-60* (ortholog of the human *HRAS*, *KRAS* and *NRAS* genes); *let-23(sy1)* is a hypomorphic allele of *let-23* (ortholog of the human *EGFR* gene). *ras-1*^{WT} and *ras-1*^{G27dup} indicate *hsp-16.41::ras-1*^{WT}- and *hsp-16.41::ras-1*^{G27dup}-containing constructs injected at 100 ng/ml, respectively. After each cross, isogenic worms that had lost the transgene were cloned separately and used as controls.
Animals were grown at 20°C and heat-shocked in para llel at early L3 stage. *N* indicates the number of animals scored. Multivulva (Muv), vulvaless (Vul) andprotruding vulva (Pvl) phenotypes are expressed as percentage of worms with ectopic pseudovulvae, animals lacking a vulva and adults with a protruding vulva, respectively. Induction of vulval cell fate is expressed as percentage of P6.p that has been induced to invaginate.
In all comparisons, *P*-values were calculated using two-tailed Fisher's exact test. [a]Significantly different from *let-60(n1046)* ($P < 0.02$).
[b]Significantly different from *let-23(sy1)* ($P < 0.01$) and *let-23(sy1);ras-1*^{WT} ($P < 0.02$).
[c]Significantly different from *let-23(sy1)* ($P = 0.02$) and *let-23(sy1);ras-1*^{WT} ($P < 0.05$).

Overall, these experiments provided evidence of a positive modulatory role of the RAS-1/RRAS mutant on LET-60/RAS signaling.

4.2 RASopathy-causing mutants dysregulate multiple pathways in *C. elegans*

4.2.1 Functional equivalence between SHOC2 and RRAS mutants

Because of the similar impact of the RASopathy-causing SHOC2^{S2G} and RRAS^{G39dup} mutants on *C. elegans* vulval development (*i.e.*, Pvl, Egl and Bag phenotypes) (Cordeddu *et al.*, 2009; Flex *et al.*, 2014), epistatic studies were carried out to further analyze the functional link between these mutants. Genetic crosses set up between worms expressing SHOC2^{S2G} and animals knockout for

ras-1/RRAS or *ras-2/MRAS*, the latter being a SHOC2 interactor mediating RAF activation in mammals (Rodriguez-Viciana *e t al.*, 2006), demonstrated that $SHOC2^{S2G}$-related Pvl is strongly reduced in a *ras-1*$^{-/-}$ genetic background and is completely suppressed in the absence of *ras-2* (Figure 24). In contrast, the prevalence of vulval defects caused by expression of $RAS\text{-}1^{G27dup}$ (homolog of $RRAS^{G39dup}$) did not change in worms knockout for *sur-8/SHOC2* or *ras-2*. Overall, these data established that the RASopathy-causing SHOC2 and RRAS mutants belong to the same pathway. Within this signaling network, both RAS-1 and RAS-2 are downstream to constitutively active SHOC2, with the former being epistatic to the latter.

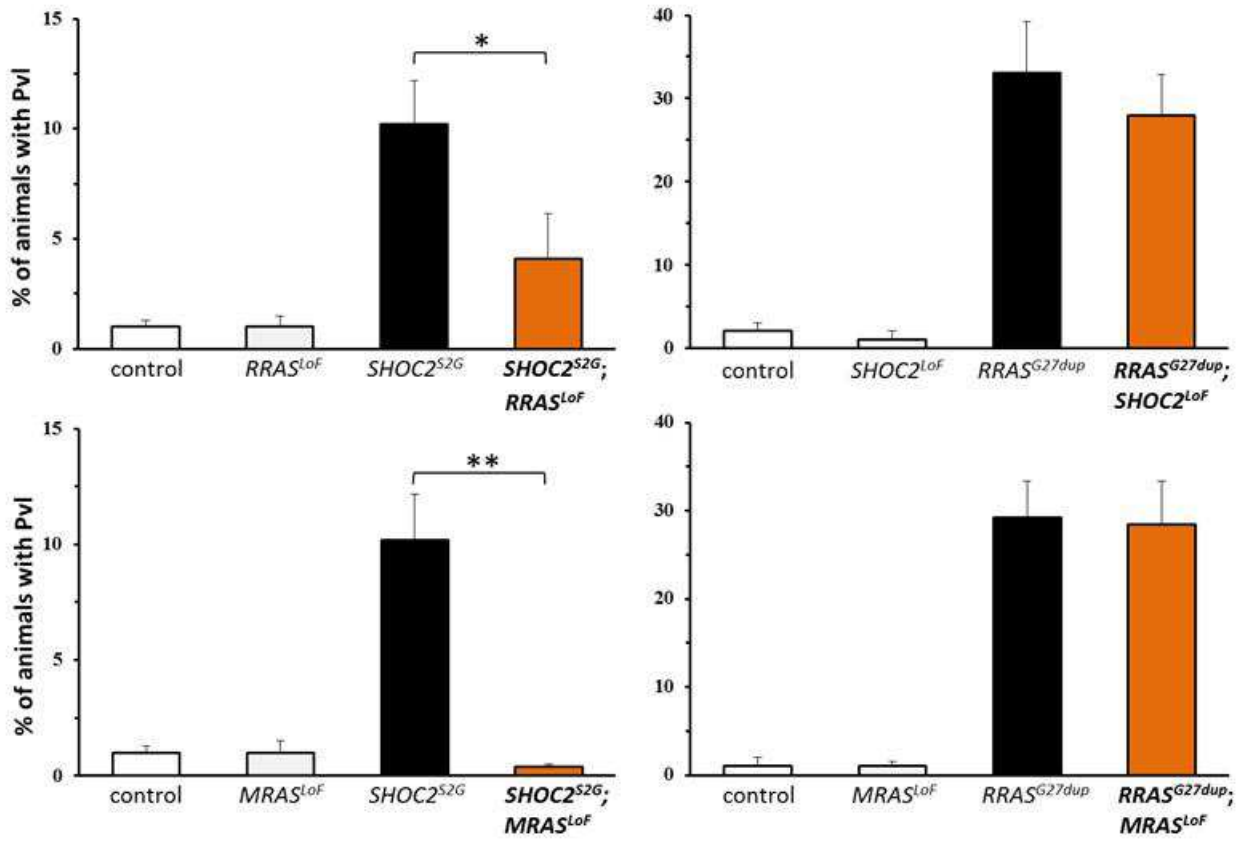

Figure 24. Epistatic analyses showe d that SHOC2, MRAS and RRAS belong to the same pathway.

Accordingly, animals expressing both the mutants showed a slightly higher prevalence of Pvl than worms expressing *ras-1*^{G27dup} only (Figure 25A), confirming that they work within the same pathway (Figure 25B), and su pporting the evidence that Pvl engender ed by expression of $SHOC2^{S2G}$ is largely due to *ras-1* hyperactivation.

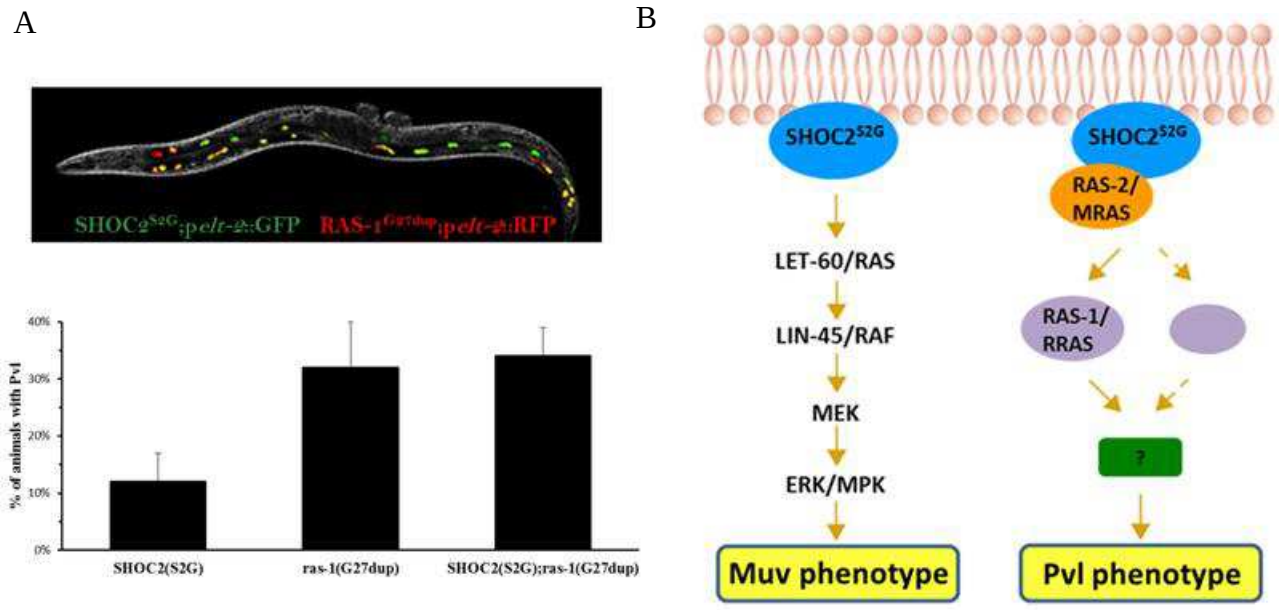

Figure 25. (A) Co-expression of SHOC2 and RRAS mutants did not increase thhe prevalence of the Pvl phenotype supporting their function within the same pathway. (B) The Muv phenotype is LET-60/RAS-dependent, whereas the Pvl phe notype is not; it depends on proper function of ras-1/RRAS and ras-2/MRAS that are downstream of S HOC2^{S2G}, RRAS being epistatic to MRAS.

4.2.2 Exploring the role of LE T-60/RAS and Rho-family GTPases in med iating vulval defects

To define the genes and signaling cascades controlling the cellular processes underlying the Pvl and Muv phenotypes, RNA interference (RNAi) experiments of candidate genes were carried out on animals expressing SHOC2^{S2G} under the control of the *lin-31* promoter, which drives expression in VPCs. As expected, expression of SHOC2^{S2G} and RAS-1^{G27dup} engendered both Pvl and Muv phenotypes, while expression of the wild-type counterparts did not (% of Pvl and Muv associated with p*lin-31*::*SHOC2*^{S2G}: 12% and 3%, respectively; % of Pvl associated with p*lin-31*::*ras-1*^{G27dup}: 5% and 3%, respectively). Sincee RASopathy-causing SHOC2 and RRAS mutants are expected to promote vulval defects by altering LET-60/RAS-MAPK signaling (Muv phenotype), or perturbing pathways downstream of cell fate specification involved in the control of VPC migration and/or polarity (Pvl phenotype), a selected panel of genes (*let-60/RAS*, *age-1/p110*, *cdc-42/CDC42*, *rho-1/RHOA* and *mig-2*, *ced-10/RAC1*) has been interfered in transgenic lines to identify the genes placed downstream to *SHOC2*, *MRAS* and *RRAS* mediating these phenotypes.To find the common effectors mediating the Pvl phenotype, we focused on the RHO-family small GTPases RHO, RAC and CDC42 which, in mammals, play a role in promoting plasma membrane protrusions regulating cell migration (Wozniak *et al.*, 2005). In *C. elegans*, they control cell polarity and migration in the embryos and VPCs (Kishore and Sundaram, 2002; Schonegg and Hyman, 20006).

To explore this hypothesis, we used a reverse genetic approach. RNA interference can be performed in *C. elegans* by feeding worms with bacteria expressing the double stranded RNA corresponding to the gene to be silenced. RNAi experiments were carried out in the context of partial gene knockdown (see the Materials and Methods section) because complete inhibition of these genes was shown to result in embryonic lethality (http://www.wormbase.org/). To validate such a protocol, we performed *let-60* RNAi on both N2 and let-60 (*n1046*) worms, the latter carrying a *let-60* gain-of-function allele, and the number of animals without a vulva (Vul phenotype) or with multiple ectopic pseudovulvae (Muv) were counted (Table 7). This assay demonstrated the effectiveness of such an approach.

Table 7. Partial RNAi performed on N2 and *let-60 (n1046)* worms

Genotype	RNAi[a]	Vul (%)	Muv (%)	Embryonal/Larval Letality (%)	N
N2	0	0	0	0	125
N2	2	3	0	0	150
N2	4	32	0	5	171
N2	6	41	0	10	179
N2	8	55	0	36	103
N2	72	10	0	80	144
let-60(n1046)	0	0	73	2	205
let-60(n1046)	2	12	44	1	150
let-60(n1046)	4	14	39	2	174
let-60(n1046)	6	15	34	10	117
let-60(n1046)	8	21	26	15	120
let-60(n1046)	72	10	10	50	115

[a]Time of exposure (hours) of animals to RNAi bacteria. Screening of the Vul and Muv phenotypes was carried out on F1 (0–8 hs) or F2 (72 hs) hermap hrodites. Percentage of the phenotype was calculated on survival animals.

By using this strategy, we found that silencing of *cdc-42*, *rho-1* and *rac* genes in wild-type animals caused vulval defects *per se,* whose prevalence increased with the length of exposure to dsRNA, confirming previous data on the role of RAC and CDC-42 in vulval development and provided first evidence indicating that RHO is also involved in this process (Figure 26).

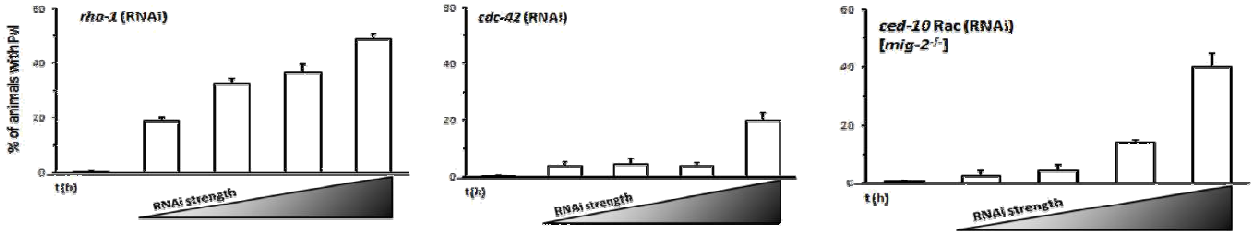

Figure 26. RNAi experiments sho wed that silencing of *cdc-42*, *rho-1* and *rac* gene s in wild-type animals caused vulval defects *per se*.

In animals expressing SHOC^{S2G}, we showed that *rho-1* RNAi had no effect on the penetrance of the Pvl phenotype. In contrast, the penetrance of Pvl was significantly increased by *cdc-42* RNAi and completely suppressed by *RAC1* RNAi, demonstrating that SHOC2^{S2G} elicits Pvl through RAC hyperactivation in VPCs (Figure 27). All the data are present in Table 8, Tabl e 9 and Table 10.

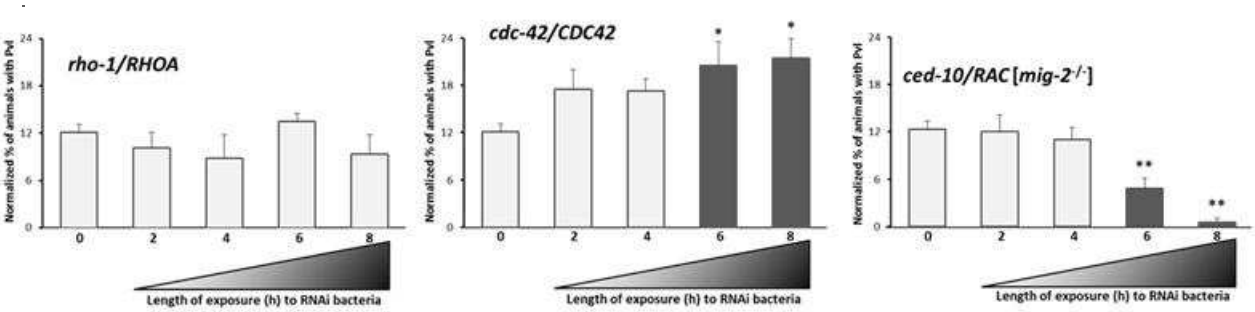

Figue 27. RNAi experiments showi ng the role of CDC-42 and RAC1 in modulating the Pvl phenotype.

Table 8. *rho-1* RNAi.

Genotype	RNAi[a]	Pvl (%)	Muv (%)	Embryonal Letality (%)	Sterility (%)	Gonad D efects (%)	N
N2	0	0.7	0	0	0	0	150
N2	2	12.9	0	0	85	60	289
N2	72			98			180
rho-1(ok2418)$^{+/-}$	0	1.7	0	0	0	0	303
p*lin-31::SHOC2*^{S2G}	0	12.4	2.6	0	0	0	499
isogenic animals	0	0.3	0	0	0	0	302
p*lin-31::SHOC2*^{S2G}	2	28.9	5.6	0	na	na	308
isogenic animals	2	18.8	0.6	0	na	na	361
p*lin-31::SHOC2*^{S2G}	4	41.3	3.3	7	na	na	92
isogenic animals	4	32.5	0	4	na	na	117
p*lin-31::SHOC2*^{S2G}	6	51.0	1.2	15	na	na	48
isogenic animals	6	36.5	0	8	na	na	63
p*lin-31::SHOC2*^{S2G}	8	58.1	0	33	na	na	86
isogenic animals	8	48.8	0	23	na	na	69

[a]Time of exposure (hours) of animals to RNAi bacteria. Screening of the Pvl and Mu v phenotypes was carried out on F1 (0– 8 hs) or F2 (72 hs) hermaphrodites. Percentage of the phenoty pe was calculated on survival animals. In all ex periments, isogenic worms that had lost the transgene were used as controls.
na: not ascertained.

Table 9. *cdc-42* RNAi.

Genotype	RNAi[a]	Pvl (%)	Muv (%)	Embryonal/Larval letality (%)	N	*P*
N2	0	0	0	0.7	148	
N2	2	2	0	0	121	
N2	72	10	10	77	266	
cdc-42(gk388)$^{+/-}$	0	0.6	0	0	155	
p*lin-31::SHOC2*^{S2G}	0	9.6	3.3	0	396	
p*lin-31::SHOC2*^{S2G}*;cdc-42(gk388)*$^{+/-}$	0	15.7*	2.5	1	204	*<0.05
p*lin-31::SHOC2*^{S2G}	0	12.3	3.2	0	160	
isogenic animals	0	0.3	0	0	312	
p*lin-31::SHOC2*^{S2G}	2	21.3	0.7	0	140	
isogenic animals	2	3.8	0	0	83	
p*lin-31::SHOC2*^{S2G}	4	21.5	2.4	3	209	
isogenic animals	4	4.2	0	3	120	
p*lin-31::SHOC2*^{S2G}	6	24.3*	2.5	15	120	*<0.005
isogenic animals	6	3.8	1.9	15	90	
p*lin-31::SHOC2*^{S2G}	8	41.0*	1.9	18	156	*<0.001
isogenic animals	8	19.6	0	15	138	

[a]Time of exposure (hours) of animals to RNAi bacteria. Screening of the Pvl and Muv phenotypes was carried out on F1 (0–8 hs) or F2 (72 hs) hermaphrod ites. Percentage of the phenotype was calculated on survival animals. In all experiments, isogenic worms that had lost the transgene were used as controls.
P-values were calculated using two-tailed Fisher's exact test.

Table 10. *ced-10* RNAi.

Genotype	RNAi[a]	Pvl (%)	Muv (%)	Embryonal/Larval letality (%)	N	*P*
N2	0	0	0	0	158	
N2	2	0	0	0	222	
N2	72	0	0	0	95	
mig-2(mu28)	0	0	0	0	100	
mig-2(mu28)	2	7.3	0	2	192	
mig-2(mu28)	72	69	10	59	230	
p*lin-31::SHOC2*^{S2G}*;mig-2(mu28)*	0	11.8	3.3	0	184	
isogenic animals	0	0.5	0	0	142	
p*lin-31::SHOC2*^{S2G}*;mig-2(mu28)*	2	15.3	2.4	0	144	
isogenic animals	2	2.6	0	1	122	
p*lin-31::SHOC2*^{S2G}*;mig-2(mu28)*	4	16.2	4.3	4	190	
isogenic animals	4	4.1	0	3	188	
p*lin-31::SHOC2*^{S2G}*;mig-2(mu28)*	6	18.6*	2.3	10	189	*<0.05
isogenic animals	6	13.8*	0	5	121	
p*lin-31::SHOC2*^{S2G}*;mig-2(mu28)*	8	40.5*	2.0	21	169	*<0.0001
isogenic animals	8	40.0*	0	14	96	

[a]Time of exposure (hours) of animals to RNAi bacteria. Screening of the Pvl and Muv phenotypes was carried out on F1 (0–8 hs) or F2 (72 hs) hermaphro dites. Percentage of the phenotype was calculated on survival animals. In all experiments, isogenic worms that had lost the transgene were used as controls.
P-values were calculated using two-tailed Fisher's exact
test. na: not ascertained.

We then confirmed these results by performing genetic crosses betweeen males expressing SHOC2^{S2G} and females heterozygous for a cdc-42 loss-of-function mutation or a mig-2/RAC1 gain-of-function mutation (Figure 28).

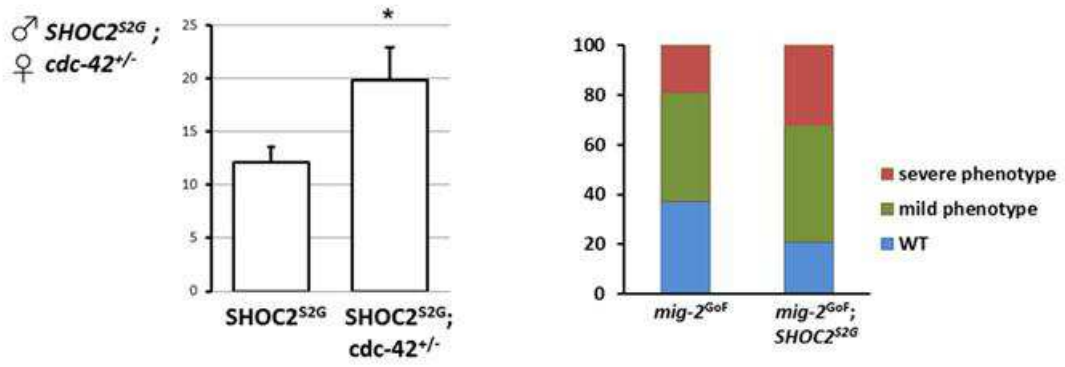

Figure 28. Genetic cros ses indicating that *cdc-42* haploinsufficiency increased the SHOC2 phenotype, and that SHOC2^{S2G} was also able to worsen the vulval defects observed in animals carrying a gain-of-function mutation in *mig-2*, one of the two RAC1 homologs**.**

To validate these results in humans, we evaluated RAC1 activity and RAC- dependent cytoskeletal alterations in patient-derived fibroblasts. As shown in Figure 29, we observed constitutive RAC1 activation in pull-down experiments, and consistent with the role of RAC1 in promoting lamellipodia formation, these structures were more extended in S2G fibroblasts compared to wild-type cells. Next, we confirmed these results in transfected cells. Here, you can easily recognize loosely adherent actin projections on the leading edge of the cell, indicating increased lamellipodia extensions in S2G cells, and what's also interesting is that SHOC2 co-localized with lamellipodia.

Figure 29. Constitutive RAC1 activation (pull-down experiments) and lamellipodia formation were more extended in SHOC2^{S2G} fibroblasts compared to wild-type cells (upper panels). Loosely adherent actin projections on the leading edge of the cell were more extended in SHOC2^{S2G} transfected cells (lower panel).

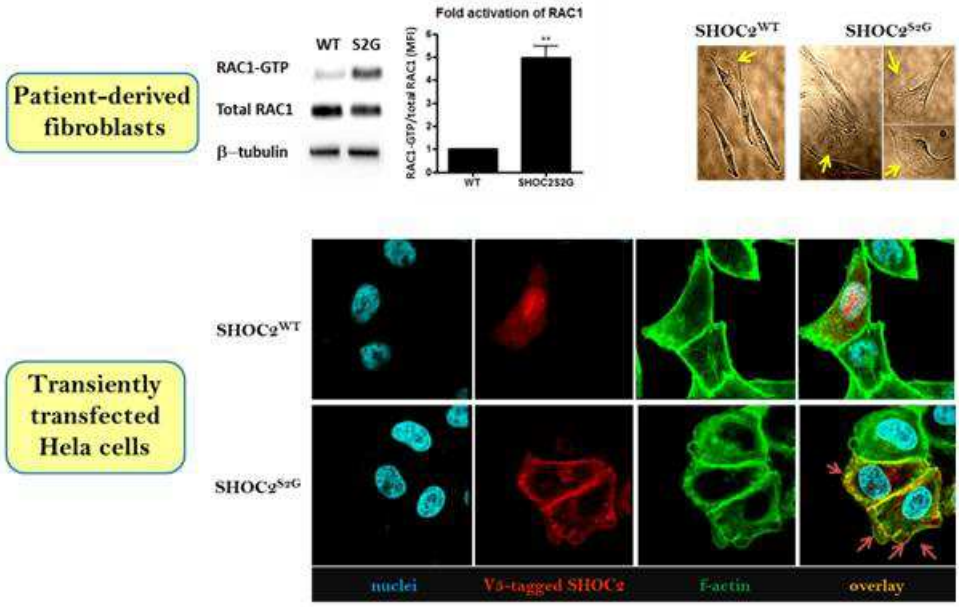

Overall, *C. elegans* studies showed that SHOC2 and RRAS mutants enhance signal flow through RAS and RAC in VPCs, that CDC42 and RAC have counteracting effects on vulval defects, and confirmed RAC1 hyperactivation in patient-derived fibroblasts (Figure 30).

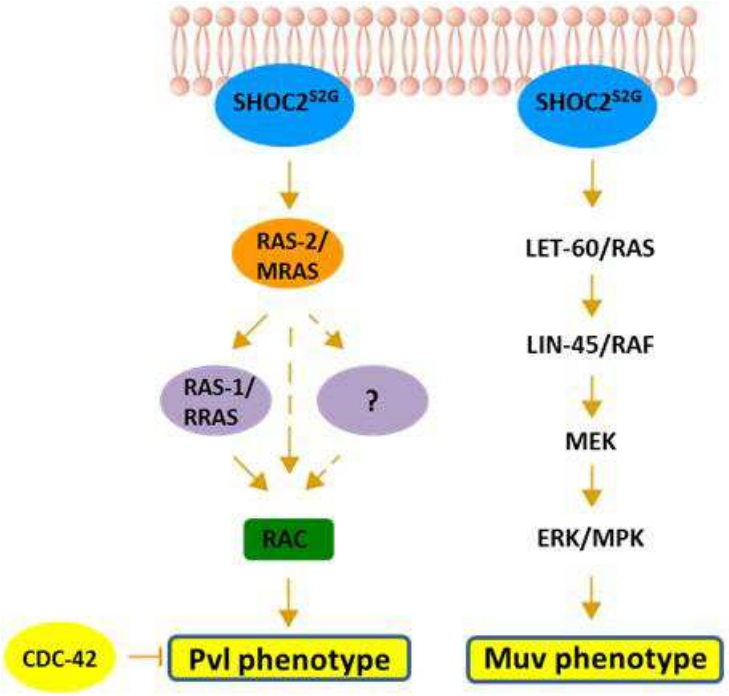

Figure 30. Scheme indicating the proteins mediating induction of the Pvl and Muv phenotype.

Finally, these findings also suggest RHO-family small GTPases as excellent candidate genes to be mutated in RASopathies. Interestingly, a RAC2 mutation has recently been reported in JMML (Caye *et al.*, 2015), and a single CDC42 change was found in two patients with thrombocytopenia and developmental delay (Takenouchi *et al.*, 2015).

4.3 Germline *CDC42* mutations cause a phenotype partially overlapping NS

4.3.1 Identification of *CDC42* mutations and clinical characterization

Based on our findings derived from *in vivo* and *in vitro* studies indicating that *RAC1*, *RAC2* and *CDC42* are excellent candidate genes for RASopathies, mutation scanning of the entire coding sequence of these genes was performed on a cohort of patients with clinical features suggestive of NS or a clinically related phenotype, and negative for mutations in known disease genes. Such a screening effort allowed us to identify two germline *CDC42* mutations in three unrelated subjects (two *de novo* and one segregating with the disease in a single family). Thanks to the wide network established in the last decade by Dr. Marco Tartaglia, as well as to the use of available software (*i.e.*, GeneMatcher, https://genematcher.org/), we started collaborating with Dr. Ghayda Mirzaa (Seattle Children's Research Institute and Department of Pediatrics, University of Washington, Seattle, Washington, USA), Raoul Hennekam (Department of Pediatrics and Translational Genetics, Department of Pediatrics, Academic Medical Center, University of Amsterdam Medical Center, Amsterdam, The Netherlands) and Marco Seri (Department of Medical and Surgical Science, Policlinico Sant' Orsola Malpighi and University of Bologna, Italy), who had been identified by whole exome sequencing (WES) germline *CDC42* mutations in patients with intellectual disability, facial dysmorphisms and thrombocytopenia. Overall, seven functionally relevant *CDC42* changes (c.68A>G, p.Tyr23Cys; c.196A>G, p.Arg66Gly; c.203G>A, p.Arg68Gln; c.242G>T, p.Cys81Phe; c.247T>C, p.Ser83Pro; c.476C>T, p.Ala159Val; c.511G>A, p.Glu171Lys) have been identified in 11 unrelated subjects (Table 11 and Figure 31). Interestingly, two *CDC42* lesions were recently reported by Takenouchi and colleagues (Takenouchi *et al.*, 2015, 2016) in two individuals with a severe form of syndromic thrombocytopenia.

Table 11. Main clinical features of *CDC42* mutation-positive subjects (N=11)

Feature	Number	GI N = 4	GII N = 4	GIII N= 5[a]
Growth				
Prenatal Weight at birth ≤–2SD	2/11	1/4	1/4	0/3
OFC at birth ≤–2SD	2/5	0/2	1/2	1/2
PostnatalLength/height ≤–2SD	6/10	3/4	3/4	1/5
OFC ≤–2SD	4/9	3/4	1/4	2/3
OFC ≥+2 SD	1/9	0/4	1/4	0/3
Signs resembling Noonan syndrome[b]	3/11	0/4	1/4	2/5
Other facial signs				
Sparse hair	6/8	2/4	4/4	1/2
Sparse eyebrows	4/11	2/4	2/4	1/5
Epicanthal folds	4/11	1/4	0/4	3/5
Strabismus	7/10	4/4	3/4	2/4
Long philtrum	5/11	1/4	2/4	2/5
Thin upper vermillion	8/11	4/4	2/4	4/5
Hearing loss	**2/11**	**2/4**	**0/4**	**0/5**
Optic atrophy	3/9	1/3	0/3	2/5
Scoliosis; vertebral anomalies	9/11	1/2	1/4	1/4
Digital anomalies (camtodactyly, syndactyly)	4/11	1/3	3/4	1/5
Cardiac defects	5/11	2/4	3/4	1/5
Recurrent infections	**4/11**	**3/3**	**2/4**	**0/5**
Platelet abnormalities				
Thrombocytopenia	**3/11**	**3/4**	**2/3**	**0/5**
Macrothrombocytes	**2/11**	**2/4**	**1/3**	**0/5**
Neurologic abnormalities				
Intellectual disability	**6/11**	**4/4**	**3/4**	**1/5**
Seizures	**4/11**	**0/4**	**3/4**	**1/5**
Brain MRI abnormalities[c]	**7/7**	**3/3**	**4/4**	**1/1**
Tone abnormalities	**6/11**	**4/4**	**3/4**	**1/5**

[a]Group III also include the two previously published patients by Takenouchi *et al.*, 2015, 2016.

[b]Scored positively if 6 or more of the following 12 signs were present: extra hair whorls; ptosis; wide nasal bridge; flaring nostrils; broad nasal tip; low-set ears; webbed neck; pectus excavatum; PS or HCM; multiple nevi; peripheral lymphedema; lymphangiectasia.

[c]ventriculomegaly (5x), Dandy-Walker malformation, crowded posterior fossa (2x), small cerebellum, thin corpus callosum, dysmyelination, heterotopias.

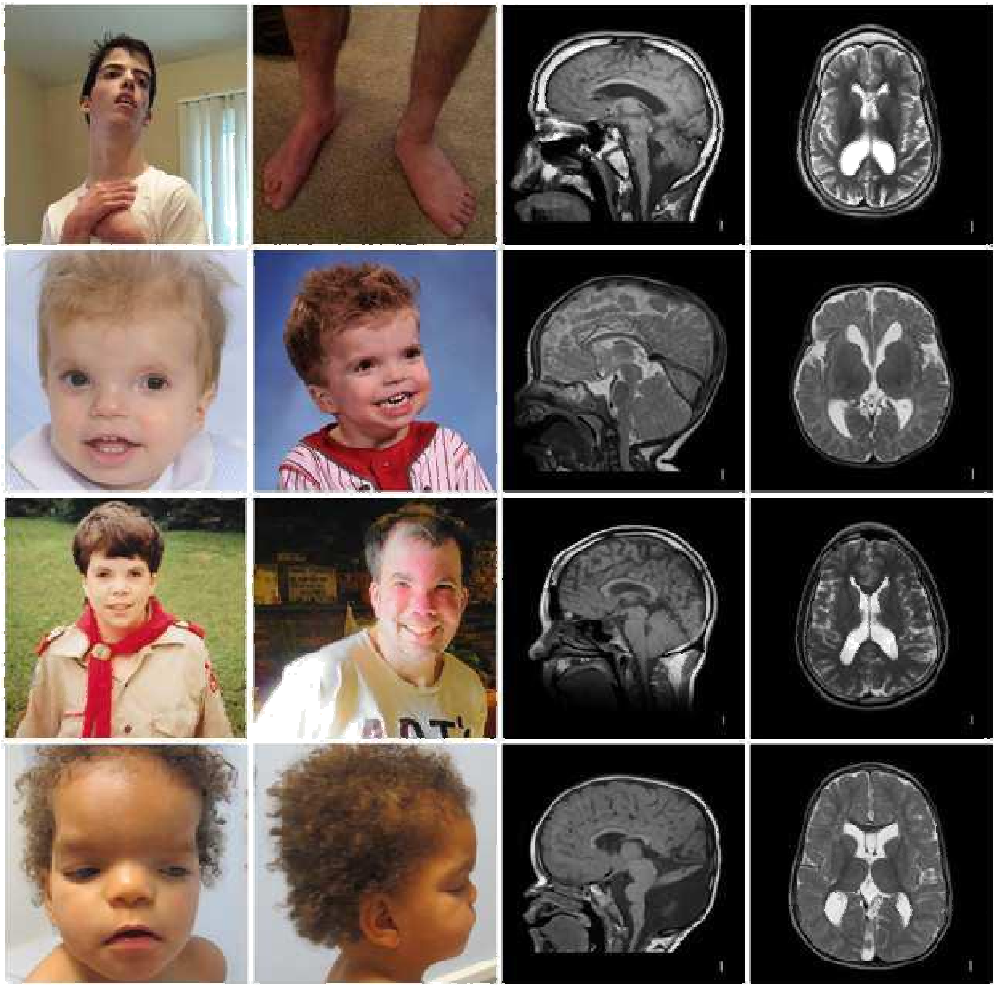

Figure 31. Facial dysmorphism and MRI scans of four patients with *de novo* mutation in *CDC42* gene. Patient 1 has a p.Y23C mutation, patients 2 and 3 have a p.S83P mutation and patient 4 has a A159V mutation. We have received the declaration of informed consent for the publication of the photos.

4.3.2 Structural and biochemical analysis of CDC42 mutants

In collaboration with the group of Reza Ahmadian, based on the location of the affected residues and the available information on CDC42 structure and function, we have structurally and functionally divided the identified missense mutations in *CDC42* into three major classes.

Group I includes the mutations affecting the switch II region (Tyr64Cys, Arg66Gly and Arg68Gln), which mediates the interaction of CDC42 with its binding partners (Dvorsky and Ahmadian, 2004). Tyr^{64} and Arg^{66} are solvent exposed residues, and are directly involved in the interaction with GEFs, GAPs and effectors (Figure 32). Differently, the invariant Arg^{68} is a buried residue that contributes to the non-polar intramolecular binding network with multiple residues (Ala^{59}, Gln^{61}, Glu^{64} and Glu^{100}) stabilizing the conformation of the switch II region. Its substitution to the hydrophilic glutamine is predicted to have a disrupting impact locally. These residues are also relatively close to the active site of the GTPase, which suggests a possible impact of these changes

on the intrinsic and stimulated catalytic activity of the mutants and/or on their perturbed binding to GTP/GDP.

Group II includes mutations affecting residues mapping at the pocket of the GTPase mediating GTP/GDP binding (Ser83Pro and Ala159Val). These mutations were predicted to affect the nucleotide binding properties of CDC42 (Figure 32). Specifically, Ala^{159} is directly facing the guanine base and its replacement by valine is expected to promote fast GDP/GTP cycling, a well-established aberrant behavior reported in members of the RAS subfamily (Tartaglia *et al.,* 2011). Similarly, Ser^{83} is indirectly involved in binding and stabilizing Gln^{116}, which covers the guanine base. Its substitution to proline is also predicted to increase the intrinsic nucleotide exchange.

Finally, group III includes the "rear mutations" (Tyr23Cys, Thr25Ile and Glu171Lys), which lie outside of the main interacting interface (Figure 32). All three residues are exposed to the solvent, but quite far from both nucleotide binding site and the switch regions. These residues, however, map in a region that has been implicated in the binding of CDC42 to effectors containing a CDC42/RAC-interacting binding (CRIB) motif, such as WASP and PAK1 (Hemsath *et al.,* 2005). Due to their vicinity to the CRIB motif binding sites, these residues were predicted to perturb CDC42 binding to these interactors. In particular, Glu^{171} maps in the region mediating binding to WASP (Figure 33). We hypothesize that Glu^{171} is a major part of the electrostatic mechanism favoring an accelerated WASP-CDC42 association reaction (Hemsath *et al.,* 2005). This process is a prerequisite for WASP activation and a critical step in temporal regulation and integration of WASP-mediated cellular responses.

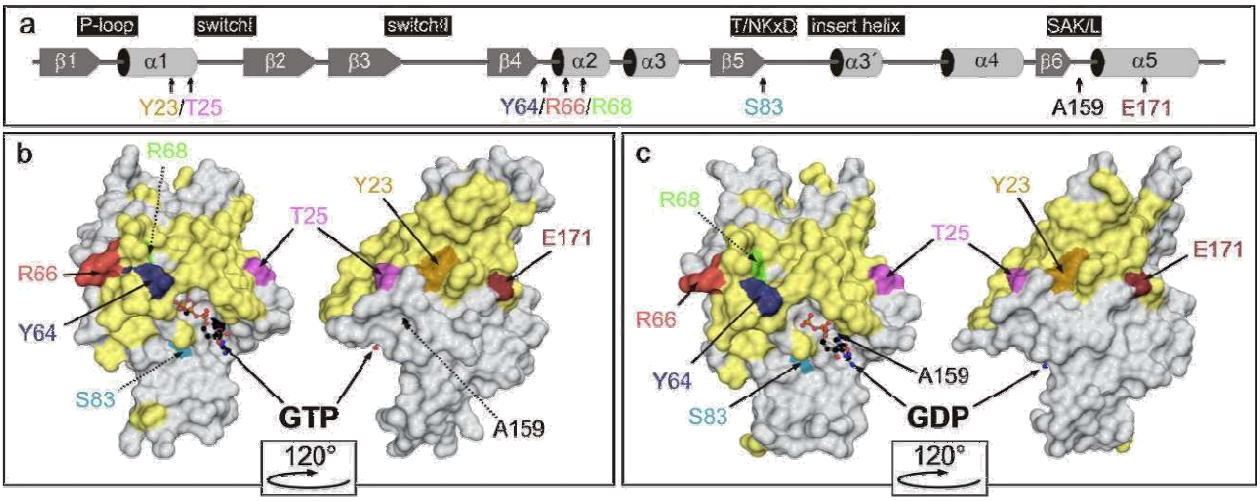

Figure 32. Relative positions of amino acids in CDC42 altered in patients with NS. (**a**) Secondary structure elements and conserved motifs of CDC42. The α-helices and β-strands are illustrated as cylinders and arrows, respectively. The G-domain of CDC42 also consists of five conserved motifs (black boxes) that are responsible for specific and tight nucleotide binding and hydrolysis. (**b-c**) Solvent accessible surfaces of CDC42 molecules are shown in the active GTP-bound state (**b**) and the inactive GDP-bound state (**c**). For clarity, structures are illustrated in two different views. Therefore, left panels are rotated 120° around the vertical ax es to the left (right panel). Amino acids altered in patients with NS are color-coded. Dashed arrows depict critical residues buried within the hydrophobic core of the CDC42. Residues of CDC42 that mediate the interactions with guanine nucleotide-dissociation inhibitors (GDIs), guanine nucleotide-exchange factors (GEFs), GTPase-activating proteins (GAPs) and effectors, such as WASP, are colored in yellow.

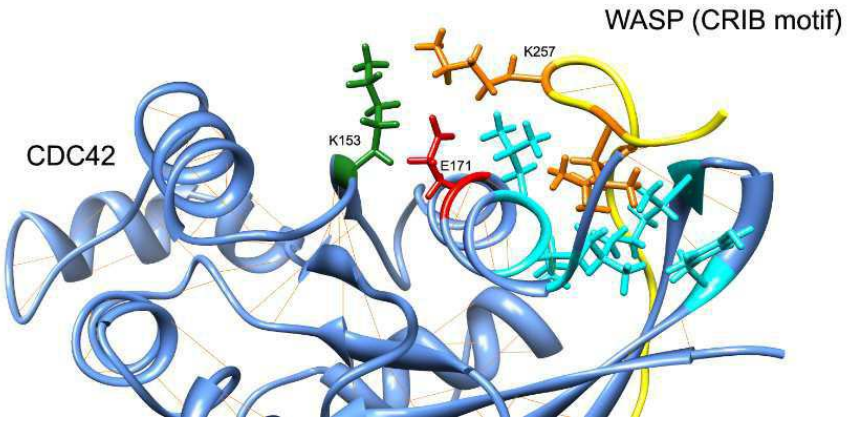

Figure 33. Localization of group III "rear mutation" Glu171Lys in the region of CDC42 mediating binding to WASP effector.

Consistent with *in silico* structural predictions, biochemical characterization of purified $CDC42^{R68Q}$ revealed that replacement of Arg^{68} by glutamine had no significant effects on the GEF-catalyzed nucleotide exchange, but led to a drastic impairment of both intrinsic (9-fold) and GAP-stimulated (240-fold) GTP hydrolysis (Figure 34).

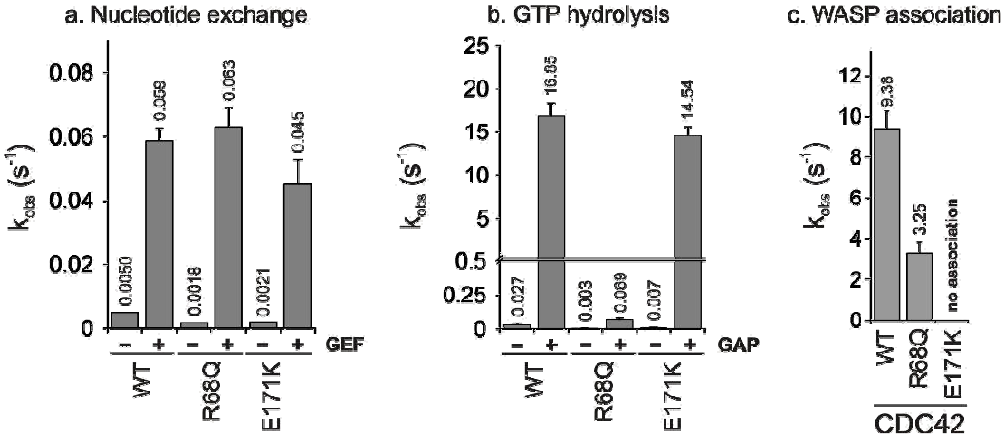

Figure 34. Gain-of-function of CDC42 due to mutation of Arg68 to Glutamine and a loss-of-function effect in CDC42^{E171K} in effector binding. WASP-GBD associates with CDC42^{WT} and R68Q proteins. Association rates (k_{on}) of WASP-GBD binding CDC42^{WT} and R68Q. Various CDC42 proteins were analyzed regarding (**a**) the GEF-catalyzed nucleotide exchange, (**b**) the GAP-stimulated GTP hydrolysis and (**c**) effector association. Therefore, purified catalytic domain of the CDC42-specific GEF (intersectin), the catalytic domain of the CDC42-specific GAP (p150GAP), and (**c**) the GTPase-binding domain (GBD) of the CDC42 effector (WASP) were used along with appropriate fluorescent nucleotides. Obtained data (for more details see Figs. S1 and S2) were evaluated and depicted as numbers and bars. A mean value of at least three different experiments was single exponentially fitted to obtain the observed rate constants (k_{obs} values) for the reactions in the absence (intrinsic) and in the presence of GEF and GAP, and the effector association.

These data indicate that the destabilization of the switch II region of CDC42 promoted by the Arg68Gln change leads to an accumulation of CDC42 in its active, GTP-bound state, and consequently would contribute in principle to an increased and persistent signaling. On the other hand, biochemical characterization of CDC42^{E171K} documented that substitution of Glu^{171} by lysine had no effects on both GEF-catalyzed nucleotide exchange and GAP-stimulated GTP hydrolysis, but completely abolished association of WASP, which was consistent with structural data.

Counteracting effects of amino acid substitutions affecting the switch I and II regions resulting in only mildly activated behavior have been documented for RASopathy-causing RAS gene mutations (Gremer *et al.*, 2010). Based on these considerations, to evaluate a possible impact of group I mutations on binding to effectors, CDC42^{R68Q} binding to WASP was investigated. Quantification of the binding properties of CDC42^{R68Q} showed a decreased association with and an increased dissociation from the GTPase-binding domain (GBD) of WASP, leading to an overall reduction in affinity of 7.5 fold (Figure 34)

4.3.3 Impact of disease-causing mutants on cell migration and proliferation

CDC42 is a master regulator of cell polarization, and plays a critical role in controlling cell migration and growth (Melendez *et al.*, 2011, 2013; Zegers and Friedl, 2014). Based on these evidences, in collaboration with Simona Coppola, we investigated the impact of disease-causing *CDC42* mutations on polarized migration and cell proliferation. To this goal, *in vitro* wound-healing assays and cell growth analyses were performed using NIH3T3 cells transiently transfected to express $CDC42^{WT}$ and the disease-causing $CDC42^{Y23C}$, $CDC42^{R68Q}$, $CDC42^{S83P}$, $CDC42^{A159V}$ and $CDC42^{E171K}$ mutants. As expected, cells expressing exogenous wild-type CDC42 were documented to migrate more rapidly into the scratched area than cells transfected with the empty vector (Figure 35A, B). Notably, mutants appeared to differentially perturb polarized migration. In particular, $CDC42^{S83P}$ and $CDC42^{A159V}$ overexpression variably enhanced the wound closure ability of transfected cells compared to the wild-type protein, whereas expression of $CDC42^{Y23C}$, $CDC42^{R68Q}$ and $CDC42^{E171K}$ failed to increase migration (Figure 35A,B), suggesting a loss-of-function effect of the Y23C, R68Q and E171K amino acid substitutions. A different behavior among mutants was also observed in cell proliferation. Specifically, the $CDC42^{A159V}$ mutant was shown to significantly enhance cell proliferation, compared to cells expressing $CDC42^{WT}$, as well as those expressing the $CDC42^{S83P}$ and $CDC42^{E171K}$ mutants, while a reduced proliferation, suggestive of a dominant negative effect, was documented in cell expressing $CDC42^{Y23C}$ and $CDC42^{R68Q}$ (Figure 35C). Overall, these data indicate that the disease-causing mutations have a diverse impact on CDC42 function, and are able to differentially perturb specific cellular processes controlled by the GTPase.

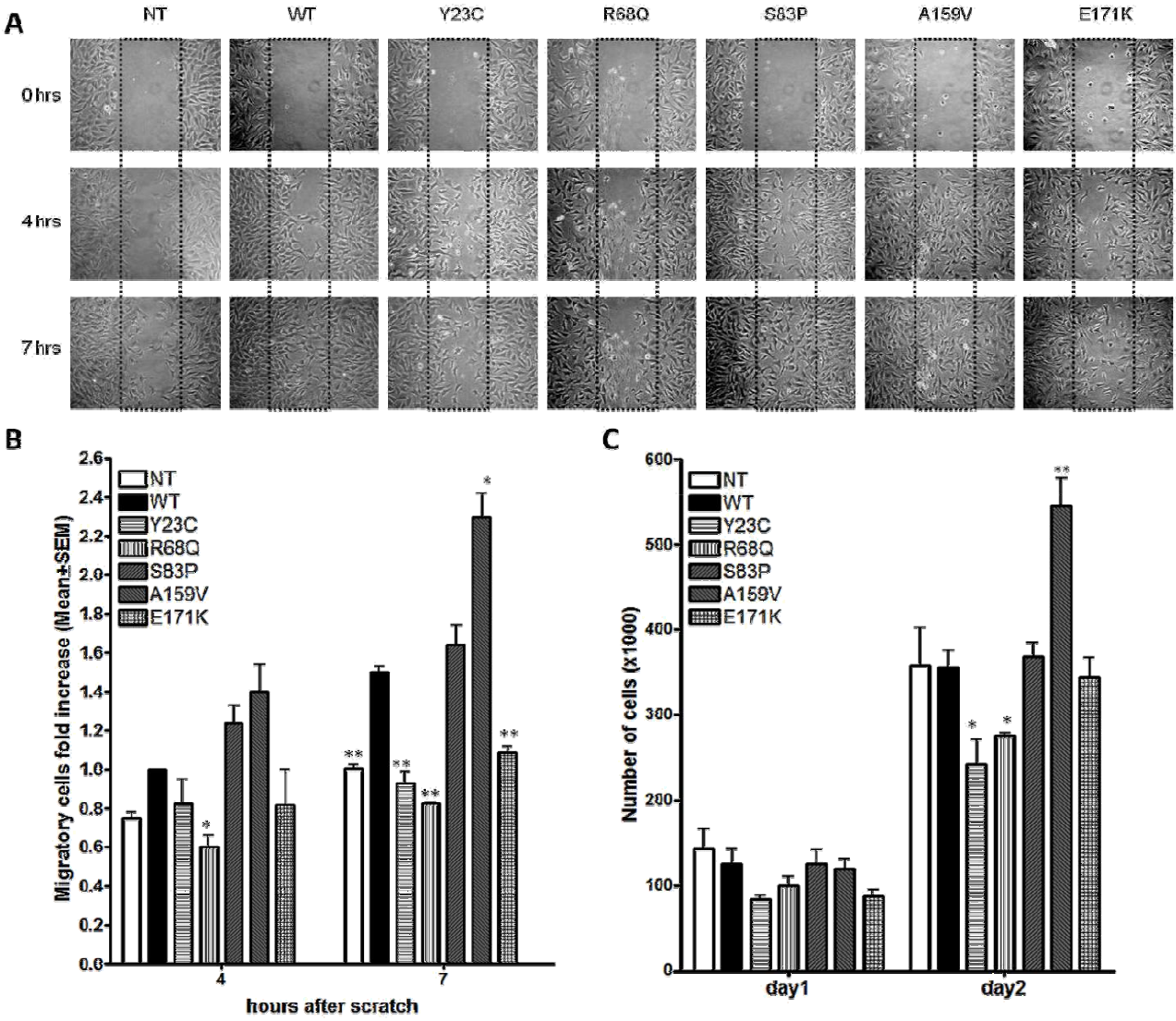

Figure 35. Polarized migratio n and growth in CDC42 overexpressing cells . (A) Migration in the wounded area of 3T3-transfecte d cells at 0,4 and 7hours after creating the scratch. The wound was generated at 24 hours post transfection. A representative experiment out of thre e performed is shown. (**B)** Migratory cells fold increase compared to migratory WT at 4 and 7hours a fter scratch is shown. Cells invading the scratched area were considered as migratory cells. Mean values ± SD relative to WT observed in three separate experiments are reported. (**C)** Cell growth of 3T3-t ransfected cells at the indicated time points. Mean values ± SEM observed in three separate exp eriments are reported (**P*<0.05; ***P* <0.01; student's t Test).

4.3.4 *C. elegans* studies

To explore the functional impact of the disease-causing CDC42 mutants on intracellular signaling *in vivo*, I used the nematode *C. elegans* as an experimental model. Multiple transgenic lines were generated to conditionally express wild-type CDC-42 (CDC-42^{WT}) or CDC-42^{Y23C}, CDC-42^{R68Q}, CDC-42^{S83P}, CDC-42^{A159V} and CDC-42^{E171K}, homologs of the disease-associated mutants (alignments are shown in Figure 36).

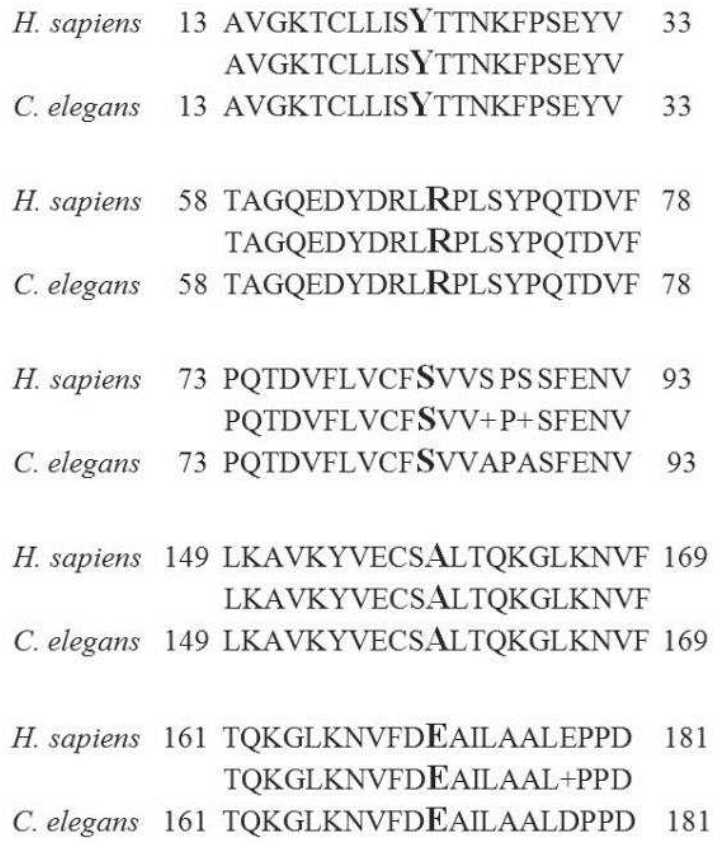

Figure 36. Protein sequence alignments around Tyr[23], Arg[68], Ser[83], Ala[159] and Glu[171] (reported in bold) between *H. sapiens* and *C. elegans*. In the middle row, identity/conservation of individual residues is reported. Alignments were gathered from https://www.ncbi.nlm.nih.gov.

According to the key role played by CDC-42 during embryogenesis, embryonic expression of CDC-42^{WT} caused a full penetrant lethal phenotype ($P<10^{-6}$; two-tailed Fisher's Exact Test), that was significantly higher compared with that observed in embryos expressing CDC-42^{Y23C}, CDC-42^{R68Q} and CDC-42^{E171K} ($P< 0.001$ in all comparisons) (Figure 37), indicating a hypomorphic effect of these lesions in cellular processes mediating embryonic lethality.

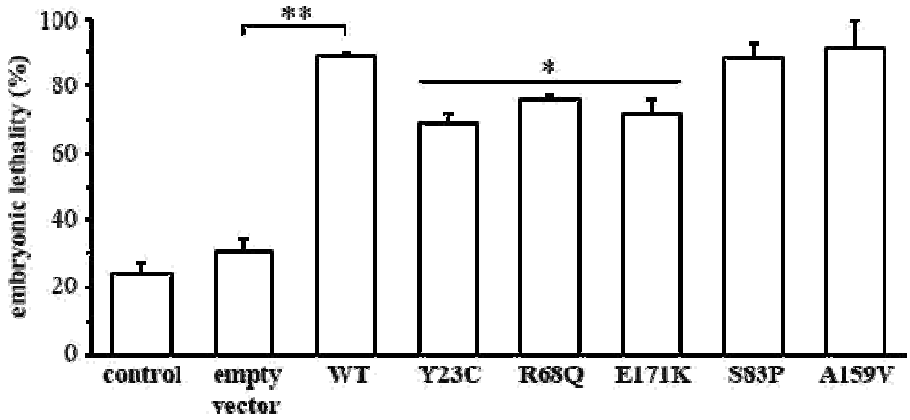

Figure 37. Consequences of CDC-42 expression on *C. elegans* embryonic development. Eggs laid from synchronized animals were heat shocked at 30° C for 30 min and lethality was evalu ated 24 hours later counting the number of unhatched eggs. Isogenic animals that had lost the transgene (control group) and worms expressing the heat shock inducible vector (empty vector) were subjected to heat shock and scored in parallel for comparison. *P*-values were calculated using two-tailed Fisher's exact test ($^{*}P < 0.001$; $^{**}P < 10^{-6}$).

During early larval development (L1 and L2 stages), ectopic expression of wild-type and mutant CDC-42 caused no visible phenotype, whereas at early L3 larval stage, it caused abnormal vulval morphogenesis, resulting in the formation of a protruding vulva (Pvl) (Figure 38A, E and Table 12), a phenotype that had previously been reported in *C. elegans* lines expressing the RASopathy-causing SHOC2^{S2G} and RRAS^{G39dup} mutants (Cordeddu *et al.*, 2009; Flex *et al.*, 2014). Like those animals, a variable proportion of CDC-42 hermaphrodites exhibiting Pvl displayed egg-laying defects (Egl phenotype) and accumulation of larvae inside the mother (Bag-of-worms phenotype). Of note, a significantly less penetrant phenotype was observed in animals expressing CDC-42^{Y23C} ($P< 0.0001$), CDC-42^{R68Q} ($P< 0.05$) and CDC-42^{E171K} ($P< 0.0001$) compared to CDC-42^{WT}, while a more penetrant phenotype was detected in those expressing CDC-42^{S83P} and CDC-42^{A159V} ($P< 0.0001$ in both comparisons) (Figure 38A), indicating a hypomorphic and hypermorphic function in the induction of Pvl of the former and the latter group of mutants, respectively.

Table 12. Vulval phenotypes in *C. elegan*s strains expressing wild-type CDC-42 and the disease-associated mutants.

Genotype	Transgene	Pvl (%)	Muv (%)	Vul (%)	N
wild-type	-	0.5	0	0	>2000
wild-type	empty vector	0.9	0	0	233
wild-type	*cdc-42*^{WT}	18.3[a]	2.3[a]	0	1447
wild-type	*cdc-42*^{Y23C}	8.1[a,b]	2.9[a]	0	588
wild-type	*cdc-42*^{R68Q}	12.6[a,c]	2.0[a]	0	810
wild-type	*cdc-42*^{S83P}	31.0[a,b]	4.5[a,c]	0	749
wild-type	*cdc-42*^{A159V}	34.3[a,b]	5.8[a,e]	0	572
wild-type	*cdc-42*^{E171K}	8.5[a,b]	2.1[d]	0	943
let-60(n1046)	-	na	72.5	0	501
let-60(n1046)	*cdc-42*^{WT}	na	89.2[f]	0	182
let-23(sy1)	-	0	0	80.2	956
let-23(sy1)	*cdc-42*^{WT}	0	0	47.4[g]	475
let-23(sy1)	*cdc-42*^{Y23C}	0	0	47.5[g]	133
let-23(sy1)	*cdc-42*^{R68Q}	0	0	47.8[g]	251
let-23(sy1)	*cdc-42*^{S83P}	0	0	30.2[g,h]	374
let-23(sy1)	*cdc-42*^{A159V}	0	0	21.6[g,h]	236
let-23(sy1)	*cdc-42*^{E171K}	0	0	49.4[g]	166

Strains: *let-60(n1046)* is a gain-of-function allele of *let-60/RAS*;*let-23(sy1)* is a hypomorphic allele of *let-23/EGFR*.

The wild-type and mutant *cdc-42* alleles were expressed under the control of the *hsp16.41* inducible promoter. Animals were grown at 20°C and heat-shocked at early L3 stage. *N* indicates the number of animals scored. Multivulva (Muv), Protruding vulva (Pvl) and Vulvaless (Vul) phenotypes are expressed as percentage of adults with ectopic pseudovulvae, exhibiting a protruding vulva or lacking a vulva, respectively.

na: not ascertained.

In all comparisons, *P*-values were calculated using two-tailed Fisher's exact test.

[a]Significantly different from animals expressing the empty vector ($P<0.00005$).

[b]Significantly different from animals expressing *cdc-42*^{WT} ($P< 0.0001$).

[c]Significantly different from animals expressing *cdc-42*^{WT} ($P< 0.05$).

[d]Significantly different from animals expressing the empty vector ($P<0.05$).

[e]Significantly different from animals expressing *cdc-42*^{WT} ($P< 0.001$).

[f]Significantly different from*let-60(n1046)* animals ($P< 0.00001$).

[g]Significantly different from*let-23(sy1)* animals ($P<10^{-12}$).

[h]Significantly different from*let-23(sy1)* animals expressing *cdc-42*^{WT} ($P< 0.0001$).

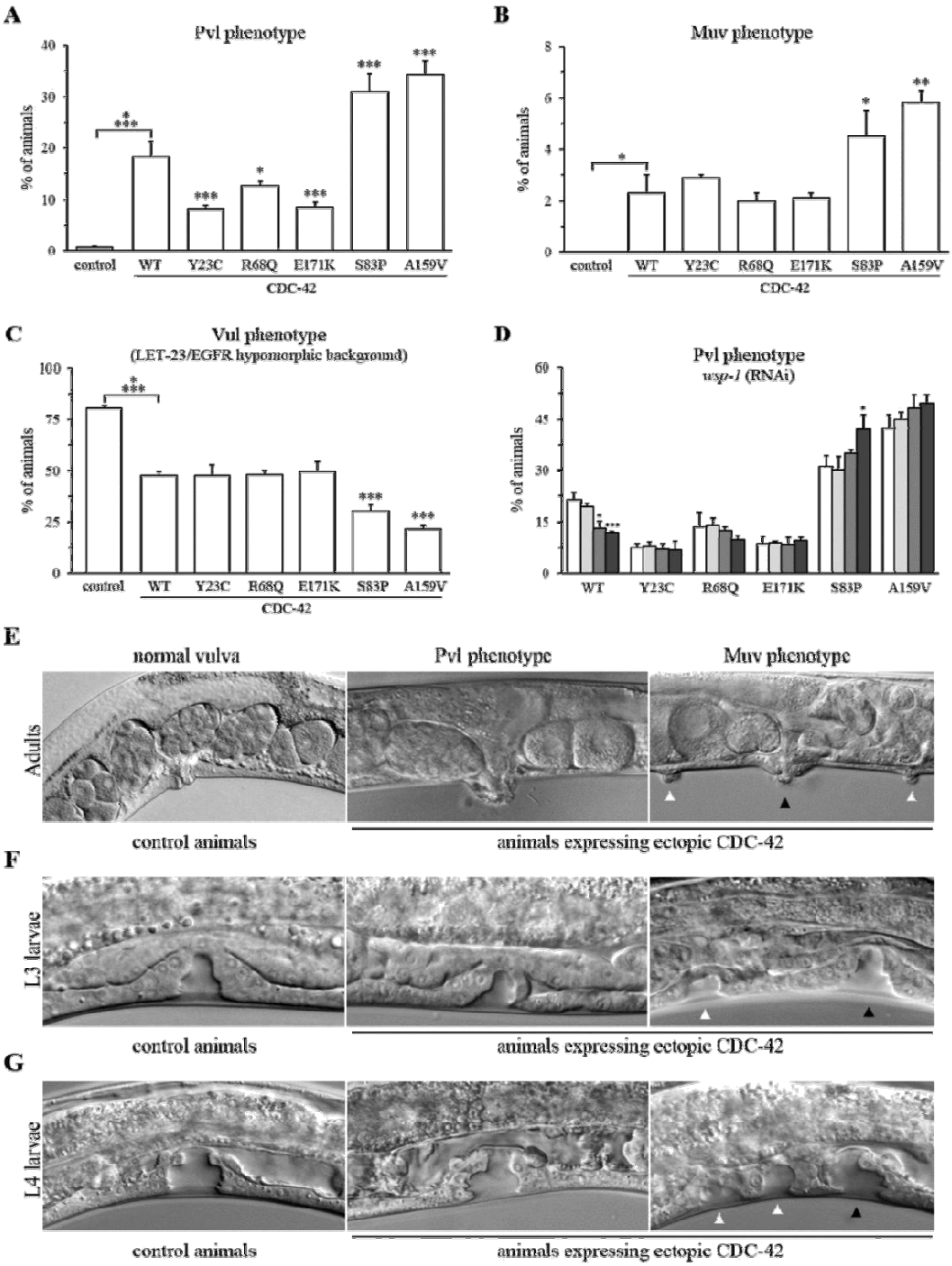

Figure 38. Consequences of CDC-42 expression on *C. elegans* vulval development. Ectopic expression of CDC-42^{WT} at early L3 larval stage elicits protruding vulva (Pvl) (**A**) and multivulva (Muv) (**B**) phenotypes. A less (CDC-42^{Y23C}, CDC-42^{R68Q} and CDC-42^{E171K}) and more (CDC-42^{S83P} and CDC-42^{A159V}) penetrant Pvl phenotype was observed in animals expressing the mutant proteins, while a more penetrant Muv phenotype was observed in CDC-42^{S83P}- and CDC-42^{A159V}-expressing mutants. **(C)** CDC-42 overexpression in a LET-23/EGFR hypomorphic background reduces the penetrance of the vulvaless (Vul) phenotype and supports a gain-of-function role of CDC-42^{S83P} and CDC-42^{A159V} on the RAS-MAPK cascade. **(D)** Modulation of the Pvl phenotype by *wsp-1* RNA interference. White and gray bars indicate the penetrance of Pvl in non-interfered and interfered animals, respectively. The darker the gray, the longer is the exposure time to bacteria expressing *wsp-1* RNAi.Error bars indicate SEM of four independent experiments (A-D). Asterisks specify significant differences

between animals expressing CDC-42^{WT} and control worms orCDC-42 mutants (A-C), and between interfered and non-interfered nematodes (D) ($^{*}P < 0.05$; $^{**}P < 0.001$; $^{***}P < 0.0001$; $^{****}P < 0.00005$; two-tailed Fisher's exact test). **(E)** Nomarski images showing that a normal vulva develops in adult control animals (left), whereas a single protruding vulva (middle) or multiple ectopic pseudovulvae (right) are observed in a variable proportion of CDC-42-expressing animals. Black and white arrowheads point to the vulva and ectopic pseudovulvae, respectively. **(F, G)** Nomarski images of VPCs at late L3 (F) and mid L4 (G) larval stages. In control animals, only P6.p descendants detach from the cuticle generating a single, symmetric invagination (left), whereas in CDC-42 expressing animals, VPCs descendants generates asymmetric invaginations (middle), or additional VPCs assume fate 1 generating multiple invaginations (right). Black and white arrowheads point to P6.p descendants-derived invagination and extra invaginations, respectively. Anterior is to the left and dorsal is up, in all images.

Besides promoting Pvl, ectopic expression of wild-type and mutant CDC-42 at early L3 larval stage caused a low penetrant Muv phenotype (Figure 38B, E and Table 12).Of note, a more severe phenotype was observed in CDC-42^{S83P}- and CDC-42^{A159V}-expressing animals ($P< 0.05$ and $P< 0.001$, respectively), suggesting a gain-of-function effect of these lesions on LET-60/RAS-MAPK signaling. To further explore this hypothesis, I have evaluated vulval phenotypes in *let-60* and *let-23/EGFR* sensitized backgrounds. Phenotypic analysis showed that expression of CDC-42^{WT} was able to exacerbate the Muv phenotype associated with a hyperactive *let-60* allele and to strongly reduce the penetrance of the Vul phenotype associated with a hypomorphic *let-23* allele ($P< 0.0001$, in both comparisons), supporting a positive modulatory role of CDC-42 on VPCs induction and the MAPK cascade (Figure 38C and Table 12). Moreover, expression of CDC-42 mutants provided evidence for a gain-of-function role of CDC-42^{S83P} and CDC-42^{A159V} on this pathway ($P< 0.0001$). As expected, Nomarski observations of L3 and L4 control larvae showed that only P6.p descendants detach from the cuticle generating a single, symmetric, invagination (Figure 38F, G) (Sternberg, 2005). In contrast, a variable proportion of larvae expressing ectopically wild-type and mutant CDC-42 displayed single asymmetric and/or multiple invaginations. These defects represent the earliest detectable effect of *cdc-42* overexpression on vulval development, similarly to what had previously been documented in transgenic lines expressing SHOC2^{S2G} and RRAS^{G39dup} mutants (Cordeddu *et al.*, 2009; Flex *et al.*, 2014).

To explore the genes/pathways working downstream to *cdc-42* and involved in the Pvl phenotype, I performed RNA-mediated interference (RNAi) to inhibit the expression of WSP-1/WASP, a CDC-42 effector required for hypodermal cell migration during morphogenesis (Ouellette *et al.*, 2016) and promoting invadopodia formation during anchor cell (AC) invasion into the vulval epithelium (Lohmer *et al.*, 2016). RNAi experiments were carried out in the context of partial gene knockdown because complete *wsp-1* inhibition was shown to result in embryonic and larval lethality (Sawa *et*

al., 2003).Weak *wsp-1* RNAi had no vulval phenotype *per se* (Table 13) and significantly reduced the prevalence of Pvl associated with CDC-42^{WT} expression ($P< 0.0001$) (Figure 38D and Table 13), indicating that occurrence of this phenotype is mediated, in part, by WSP-1. In contrast, the vulval defect observed in CDC-42^{R68Q} and CDC-42^{E171K} animals was not modulated by *wsp-1* RNAi, supporting biochemical data indicating abolished (CDC-42^{E171K}) or strongly reduced (CDC-42^{R68Q}) association of these mutants with WASP (Figure 34). A similar behavior has been observed for CDC-42^{Y23C}, suggesting a possible WSP-1 binding defect for this mutant. Finally, *wsp-1* RNAi was not able to reduce the Pvl phenotype associated with CDC-42^{S83P} and CDC-42^{A159V} expression, indicating that other CDC-42 effectors are likely to play a major role in mediating abnormal vulval morphogenesis caused by these mutants, although a defective WSP-1 binding cannot be ruled out. Notably, the Muv phenotype was not modulated by *wsp-1* RNAi (Table 13), supporting a model in which ectopic expression of wild-type and mutant *cdc-42* perturbs different pathways involved in vulval induction and morphogenesis.

Table 13. Modulation of vulva phenotypes by *wsp-1* RNA-interference in *C. elegan*s strains expressing wild-type CDC-42 and the disease-associated mutants.

Genotype	Transgene	Gene Modulated by RNAi	Time of exposure to RNAi bacteria (hours)	Pvl (%)	Muv (%)	N
let-60(n1046)	-	*let-60*	0	na	73.2	205
			2	na	44.0[a]	150
			4	na	34.2[a]	117
			8	na	25.8[a]	120
wild-type	-	*wsp-1*	0	0.7	0	150
			8	1.3	0.2	829
wild-type	*cdc-42*^{WT}	*wsp-1*	0	21.4	2.4	627
			2	19.5	1.8	56
			4	13.5[b]	1.8	168
			8	11.7[c]	4.1	410
wild-type	*cdc-42*^{Y23C}	*wsp-1*	0	7.5	2.6	154
			2	8.0	2.5	122
			4	7.1	2.4	85
			8	6.8	2.8	72
wild-type	*cdc-42*^{R68Q}	*wsp-1*	0	13.6	2.7	86
			2	14.1	2.0	105
			4	12.5	2.8	72
			8	9.8	3.2	96
wild-type	*cdc-42*^{S83P}	*wsp-1*	0	31.2	4.2	214
			2	30.0	3.8	78
			4	35.0	4.0	101
			8	42.0[b]	4.9	205
wild-type	*cdc-42*^{A159V}	*wsp-1*	0	42.3	6.3	189
			2	45.0	6.3	79
			4	48.0	5.9	119
			8	49.3	7.7	143
wild-type	*cdc-42*^{E171K}	*wsp-1*	0	8.7	2.3	263
			2	8.8	1.9	54
			4	8.3	2.2	89
			8	9.4	1.6	124

Wild-type and mutant *cdc-42* alleles were expressed in N2 worms under the control of the *hsp16.41* inducible promoter. Adult hermaphrodites were left on agar plates seeded with RNAi bacteria for the indicated time. Screening of the Protruding vulva (Pvl) and Multivulva (Muv) phenotypes was carried out on adult F1 animals grown at 20°C and heat-shocked at early L3 stage. *N* indicates the number of animals scored.
na: not ascertained.
P-values were calculated using two-tailed Fisher's exact test.
[a]Significantly different from non-interfered *let-60(n1046)* animals ($P< 0.0001$).
[b]Significantly different from the corresponding non-interfered animals ($P< 0.05$).
[c]Significantly different from the corresponding non-interfered animals ($P< 0.0001$).

5. Discussion

Mutations of genes coding for proteins with role in RAS signaling and the RAF/MEK/ERK cascade have been identified as the molecular cause underlying a group of clinically related developmental disorders, the RASopathies. Here, we used a gene candidacy approach based on large-scale protein–protein interaction/functional network analysis to identify *RRAS* as a novel gene implicated in a condition with features within the RASopathy spectrum. Disease-causing RRAS mutations are activating and act by maintaining the GTPase in its GTP-bound active state. Aberrant RRAS function was demonstrated to perturb variably intracellular signal flow through the RAF/MEK/ERK cascade, and to a certain extent also the PI3K/AKT pathway. Of note, these gain-of-function mutations are likely to define a novel leukaemia-prone condition. Consistent with this view, the same class of *RRAS* lesions was identified tooccur as acquired somatic event in JMML, characterizing a subset of this myeloproliferative/myelodysplastic disorder with rapid progression to AML. RRAS shares several biochemical properties with HRAS,NRAS and KRAS, as well as some common function, including stimulation of cell proliferation, survival and transformation (Saez *et al.*,1994). Despite these similarities, however, previous observations have emphasized the role of RRAS in cell adhesion, spreading and migration, and its modulatory function on effectors distinct from those used by 'classical' RAS proteins (Osada *et al.,* 1999; Wozniak *et al.,* 2005). While PI3K/AKT has been recognized as a major effector pathway of RRAS, only a minor impact on MAPK signaling had been reported (Osada *et al.,* 1999; Marte *et al.,* 1997). The present in vitro findings provide evidence that disease-associated RRAS mutants enhance the activation of the MAPK cascade, at least in response to specific stimuli. On the other hand, the identification of *RRAS* as a novel disease gene implicated in a RASopathy disorder further emphasizes the relevance of dysregulated signaling controlling cell spreading and migration in certain features of NS (e.g. congenital heart defects and lymphedema) and JMML (leukocyte infiltration in non-haematopoietic tissues) (Marte *et al.,* 2007; Wang *et al.,* 2009; Chen *et al.,* 2010). This hypothesis was strongly supported by the identification of *CDC42* as a novel gene implicated in a syndromic form of thrombocytopenia with clinical features partially resembling NS or a clinically correlated phenotype. CDC42 belongs to the RHO-family GTPases and play a key role in mediating cell migration and polarity (Melendez *et al.,* 2011). Furthermore, a *RAC2* mutation has recently been identified in a patient with sporadic JMML (Caye *et al.,* 2015), further supporting the role of signaling pathways parallel/downstream to RAS and the MAPK cassette in both somatic and germline RASopathies.

Caenorhabditis elegans studies provided evidence for a genetic interaction between the RAS-1^{G27dup}/RRAS^{G39dup} and LET-60/RAS in vivo. Specifically, expression of the RAS-1 mutant protein was able to rescue, in part, the VPC induction defect resulting from a hypomorphic LET-23 mutant and enhanced the multivulva phenotype associated with a LET-60 gain-of-function genetic background. No impact of wild-type RAS-1/RRAS expression was observed in both models. We also observed that worms expressing *ras-1^{G27dup}* displayed abnormal vulval morphogenesis (protruding vulva), possibly resulting from aberrant morphogenetic movements of the VPC descendant cells. Of note, we observed an equivalent phenotype in transgenic lines expressing *SHOC2^{S2G}* (Cordeddu *et al.,* 2009) and a PTPN11/SHP2 gain-of-function mutant (our unpublished data), suggesting functional equivalence of these mutants. This hypothesis was tested by performing epistatic analyses, which allowed us to demonstrate that RAS-1/RRAS and SHOC2 mutants work in the same pathway, the latter being downstream to the former.

Genetic studies support the view that vulval defects arise, in part, through perturbation of signaling mediated by the RHO-related GTPase, RAC and CDC42, which play a critical role in vulval morphogenesis (Kishore and Sundaram, 2002; Welchman *et al.*, 2007) and polarity (Schonegg and Hyman, 2006). This finding is in line with the established role of RRAS on RAC signaling (Osada *et al.,* 1999; Wozniak *et al.,* 2005) and with preliminary data indicating enhanced migration and chemotactic capabilities in cells stably expressing the disease-associated RRAS mutants (our unpublished data).

The biochemical characterization of disease-associated *RRAS* and *CDC42* mutations provided strong evidence for the existence of distinct structural and mechanistic effects resulting in an overall dysregulation of intracellular signaling. Function of RAS family proteins in signal transduction is controlled by two events, the GDP/GTP exchange and GTP hydrolysis. Any perturbation of these processes can affect dramatically the fine-tuned balance of the GTPase interaction with effectors and signal output. The majority of gain-of-function mutations affecting RAS proteins, including those contributing to oncogenesis, trigger the accumulation of these GTPases in the active state by impairing intrinsic GTPase activity, and/or conferring resistance to GAPs (Wennerberg *et al.*, 2005). This is also the case of two of the three mutations identified in RRAS, p.Gly39dup and p.Gln87Leu, as well as of the p.Arg68Gln change of CDC42. The characterization of the biochemical behavior of RRAS^{G39dup}, however, also demonstrated a dramatic increase in both the intrinsic and GEF-catalyzed nucleotide exchange as a process contributing to the accumulation of this mutant in its GTP-bound state. Aberrant GEF-accelerated nucleotide exchange dynamics was identified as the event driving functional dysregulation in the RRAS^{V55M} mutant, which was documented to be hyper responsive to GEF stimulation, but retained stimulus dependency.

Remarkably, the RRAS and CDC42 mutants were demonstrated to exhibit a diverse binding behavior to effectors suggesting a differential impact of mutations on downstream signaling cascades, including PI3K/AKT and RALGDS/RAL, whose biological significance and impact, however, require further studies.

The clinical phenotype of subjects with germline *RRAS* or *CDC42* mutations was reminiscent of NS. Clinical features, however, were distinctive, and not typical of NS in most cases. The patient heterozygous for the p.Val55Met substitution exhibited a very mitigated phenotype characterized by suggestive facial characteristics (triangular face, downslanting palpebral fissures and low-set ears), low posterior hairline, broad chest and borderline cognitive abilities, without cardiac involvement or defective growth, indicating that clinical features associated with *RRAS* mutations might be quite subtle. Of note, the milder phenotype associated with the p.Val55Met change is consistent with the weaker perturbing effect of the $RRAS^{V55M}$ mutant on MAPK and PI3K/AKT signaling compared with the $RRAS^{G39dup}$ protein. Notably, the different effect of individual *CDC42* mutations on RAS signaling is not associated with a clear genotype/phenotype correlation, indicating that altered function (hypo- *versus* hyper-morphic) of CDC42 has similar consequences on development.

JMML is a clonal myeloproliferative/myelodysplastic disorder of childhood characterized by overproduction of immature myeloid cells that variably retain the capacity to differentiate. Upregulation of RAS/MAPK signaling owing to germline and somatic mutations in *PTPN11*, *NRAS, KRAS, NF1* and *CBL* isa major event implicated in this malignancy (Loh, 2011; Emanuel, 2008; Niemeyer and Kratz, 2008). Our data document that upregulated RRAS function represents a novel event contributing to JMML pathogenesis and/or disease progression. Notably, somatic *RRAS* mutations co-occurred with acquired *NRAS* lesions in atypical JMML characterized by late onset and rapid progression to AML. While JMML is generally an aggressive malignancy, a subset of *NRAS*/*KRAS* mutation-positive patients has been reported to exhibit a mild course, with spontaneous remission despite the *RAS*-mutated clone persisting for years (Takagi *et al.,* 2007; Matsuda *et al.,* 2008; Flotho *et al.,* 2013, our unpublished data). This suggests that in some instances, certain *NRAS* mutations are not sufficient to support full leukaemogenesis, requiring synergism with a second RAS signaling targeting event. In line with this view, *NRAS* mutations have been documented to co-exist with defects in other RASopathy genes (e.g. *PTPN11*) in some cases resulting in a particularly aggressive disease resembling AML with myelodysplasia-related changes (Park *et al.*, 2012; Sakaguchi *et al.,* 2013), as that observed in the present cases. Other studies, however, are required to appreciate more precisely the role of enhanced RRAS function in leukaemogenesis as well as its clinical relevance in haematological malignancies.

In conclusion, our findings document that germline activating mutations in *RRAS* and *CDC42* underlie two conditions within the RASopathy family that may resemble, in part, NS phenotypically. In the examined cohorts, *RRAS* and *CDC42* lesions were found to account for only a small portion of cases, which might be related to their severe consequences on embryonic/fetal development and/or to the biased selection of the subjects included in these studies. Based on the present findings, however, *RRAS* mutations are expected to bemore common among subjects with clinical features only partially overlapping NS, and particularly in patients with syndromic JMML/AML not associated with mutations in the *PTPN11*, *NF1*, *CBL*, *KRAS* and *NRAS* genes. Similarly, *CDC42* mutations are expected to be more common among subjects with thrombocytopenia. While further efforts are required to characterize more precisely the clinical impact of germline mutations affecting *RRAS* and *CDC42*, our findings suggest an unpredicted role of these GTPases in development and haematopoiesis. Consistent with the recent identification of *RIT1* and *LZTR1* as disease genes implicated in a significant proportion of NS (Aoki *et al.,* 2013;), our findings further extend the concept of 'RASopathy gene' to transducers whose dysregulated function perturbs signal flow through the MAPK cascade but does not belong to the core RAS/MAPK signaling cassette.

6. References

Abo A, Pick E, Hall A, Totty N, Teahan CG, Segal AW. Activation of the NADPH oxidase involves the small GTP-binding protein p21 rac1.*Nature*. 1991; 353:668-670.

Allen WE, Zicha D, Ridley AJ, Jones GE. A role for Cdc42 in macrophage chemotaxis. *J. Cell. Biol*. 1998; 141:1147-1157,

Anastasaki C, Estep AL, Marais R, Rauen KA, Patton EE. Kinase-activating and kinase-impaired cardio-facio-cutaneous syndrome alleles have activity during zebrafish development and are sensitive to small molecule inhibitors. *Hum. Mol. Genet*. 2009; 18:2543-2554.

Anderson P. Mutagenesis. In *Caenorhabditis elegans*: Modern biological analysis of an organism (ed. Epstein, H.F. and Shakes, D.C.). 1995; Chapter 2. pp 31-54. Academic Press, California.

Aoki Y, Niihori T, Kawame H, Kurosawa K, Ohashi H, Tanaka Y, Filocamo M, Kato K, Suzuki Y, Kure S, Matsubara Y. Germline mutations in HRAS proto oncogene cause Costello syndrome. *Nat. Genet*. 2005; 37:1038-1040.

Aoki Y, Niihori T, Banjo T, Okamoto N, Mizuno S, Kurosawa K, Ogata T, Takada F, Yano M, Ando T, Hoshika T, Barnett C, Ohashi H, Kawame H, Hasegawa T, Okutani T, Nagashima T, Hasegawa S, Funayama R, Nagashima T, Nakayama K, Inoue S, Watanabe Y, Ogura T, Matsubara Y. Gain-of-function mutations in RIT1 cause Noonan syndrome, a RAS/MAPK pathway syndrome. *Am. J. Hum. Genet*. 2013; 93:173-180.

Aoki Y, Niihori T, Inoue S, Matsubara Y. Recent advances in RASopathies. *J. Hum. Genet*. 2016; 61:33-39.

Aroian RV, Koga M, Mendel JE, Ohshima Y, Sternberg PW. The *let-23* gene necessary for *Caenorhabditis elegans* vulval induction encodes a tyrosine kinase of the EGF receptor subfamily. *Nature*. 1990; 348:693-699.

Bocchinfuso G, Stella L, Martinelli S, Flex E, Carta C, Pantaleoni F, Pispisa B, Venanzi M, Tartaglia M, Palleschi A. Structural and functional effects of disease-causing amino acid substitutions affecting residues Ala72 and Glu76 of the protein tyrosine phosphatase SHP-2. *Proteins* 2007; 66:963-974.

Bos JL. *ras* oncogenes in human cancer: a review. *Cancer Res*. 1989; 49:4682-4689.

Brems H, Chmara M, Sahbatou M, Denayer E, Taniguchi K, Kato R, Somers R, Messiaen L, De Schepper S, Fryns JP, Cools J, Marynen P, Thomas G, Yoshimura A, Legius E. Germline loss-of-function mutations in *SPRED1* cause a neurofibromatosis 1–like phenotype. *Nat. Genet*. 2007; 39:1120-1126.

Caron E and Hall A. Identification of two distinct mechanisms of phagocytosis controlled by different Rho GTPases. *Science.* 1998; 282:1717-1721.

Cawthon RM, O'Connell P, Buchberg AM, Viskochil D, Weiss RB, Culver M, Stevens J, Jenkins NA, Copeland NG, White R. Identification and characterization of transcripts from the neurofibromatosis 1 region: the sequence and genomic structure of *EVI2* and mapping of other transcripts. *Genomics*. 1990; 7:555-565.

Caye A, Strullu M, Guidez F, Cassinat B, Gazal S, Fenneteau O, Lainey E, Nouri K, Nakhaei-Rad S, Dvorsky R, Lachenaud J, Pereira S, Vivent J, Verger E, Vidaud D, Galambrun C, Picard C, Petit A, Contet A, Poirée M, Sirvent N, Méchinaud F, Adjaoud D, Paillard C, Nelken B, Reguerre Y, Bertrand Y, Häussinger D, Dalle JH, Ahmadian MR, Baruchel A, Chomienne C, Cavé H. Juvenile myelomonocytic leukemia displays mutations in components of the RAS pathway and the PRC2 network. *Nat. Genet.* 2015; 47(11):1334-40.

Chen PC, Wakimoto H, Conner D, Araki T, Yuan T, Roberts A, Seidman C, Bronson R, Neel B, Seidman JG, Kucherlapati R. Activation of multiple signaling pathways causes developmentaldefects in mice with a Noonan syndrome-associated Sos1 mutation. *J. Clin. Invest.* 2010; 120:4353-4365.

Chen PC, Yin J, Yu HW, Yuan T, Fernandez M, Yung CK, Trinh QM, Peltekova VD, Reid JG, Tworog-Dube E, Morgan MB, Muzny DM, Stein L, McPherson JD, Roberts AE, Gibbs RA, Neel BG, Kucherlapati R. Next-generation sequencing identifies rare variantsassociated with Noonan syndrome. *Proc.Natl. Acad. Sci.U. S. A.* 2014; 111:11473-11478.

Choi MS, Yoo AS, Greenwald I. *sel-11* and *cdc-42*, two negative modulators of LIN-12/Notch activity in *C. elegans*.*PLoS One.* 2010; 5(7):e11885.

Church D, Guan KL, Lambie EJ. Three genes of the MAP kinase cascade, *mek-2*, *mpk-1*/*sur-1* and *let-60* ras, are required for meiotic cell cycle progression in *Caenorhabditis elegans*. *Development.* 1995*;* 121:2525-2535.

Cirstea IC, Kutsche K, Dvorsky R, Gremer L, Carta C,Horn D, Roberts AE, Lepri F, Merbitz-Zahradnik T, König R, Kratz CP, Pantaleoni F, Denti ci ML, Joshi VA, Kucherlapati RS, Mazzanti L, Mundlos S, Patton MA, Silengo MC, Rossi C, Zampino G, Digilio C, Stuppia L, Seemanova E, Pennacchio LA, Gelb BD, Dallapiccola B, Wittinghofer A, Ahmadian MR, Tartaglia M, Zenker M. A restricted spectrum of *NRAS* mutations causes Noonan syndrome. *Nat. Genet*. 2010; 42:27-29.

Cordeddu V, Di Schiavi E, Pennacchio LA, Ma'ayan A, Sarkozy A, Fodale V, Cecchetti S, Cardinale A, Martin J, Schackwitz W, Lipzen A, Zampino G, Mazzanti L, Digilio MC, Martinelli S, Flex E, Lepri F, Bartholdi D, Kutsche K, Ferrero GB, Anichini C, Selicorni A, Rossi C, Tenconi R, Zenker M, Merlo D, Dallapiccola B, Iyengar R, Bazzicalupo P, Gelb BD, Tartaglia M. Mutation of *SHOC2* promotes aberrant protein N-myristoylation and causes Noonan-like syndrome with loose anagenhair. *Nat. Genet*. 2009; 41:1022-1026.

Cordeddu V, Yin JC, Gunnarsson C, Virtanen C, Drunat S, Lepri F, De Luca A, Rossi C, Ciolfi A, Pugh TJ, Bruselles A, Priest JR, Pennacchio LA, Lu Z, Danesh A, Quevedo R, Hamid A, Martinelli S, Pantaleoni F, Gnazzo M, Daniele P, LissewskiC, Bocchinfuso G, Stella L, Odent S, Philip N, Faivre L, Vlckova M, Seemanova E, Digilio C, Zenker M, Zampino G, Verloes A, Dallapiccola B, Roberts AE, Cavé H, Gelb BD, Neel BG, Tartaglia M. Activating Mutations Affecting the Dbl Homology Domain of SOS2 Cause Noonan Syndrome. *Hum. Mutat*. 2015; 36:1080-1087.

Cox D, Chang P, Zhang Q, Reddy PG, Bokoch GM and Greenberg S. Requirements for both Rac1 and Cdc42 in membrane ruffling and phagocytosis inleukocytes. *J. Exp. Med.* 1997; 186:1487-1494.

Dannenfelser R, Clark NR, Ma'ayan A. Genes2FANs:connecting genes through functional association networks. *BMC Bioinformatics*. 2012; 13:156.

deBakker CD, Haney LB, Kinchen JM, Grimsley C, Lu M, Klingele D, Hsu PK, Chou BK, Cheng LC, Blangy A, Sondek J, Hengartner MO, Wu YC, Ravichandran KS. Phagocytosis of apoptotic cells is regulated by a UNC-73/TRIO-MIG-2/RhoG signaling module and armadillo repeats of CED-12/ELMO. *Curr. Biol.* 2004; 14(24):2208-2216.

de Bono M. Molecular approaches to aggregation behavior and social attachment. *J. Neurobiol.* 2003; 54:78-92.

DeLano WL. The PyMOL Molecular Graphics System. 2002.

DeVore DL, Horvitz HR, Stern MJ. An FGF receptor signaling pathway is required for the normal cell migrations of the sex myoblasts in *C. elegans* hermaphrodites. *Cell.* 1995*;* 83:611-620.

Diaz JF, Wroblowsk, B, Schlitter J and Engelborghs Y.Calculation of pathways for the conformational transition between the GTP- and GDP-bound states of the Ha-ras-p21 protein: calculations with explicit solvent simulations and comparison with calculations in vacuum. *Proteins*. 1997; 28:434-451.

Digilio MC, Conti E, Sarkozy A, Mingarelli R, Dottorini T,Marino B, Pizzuti A, Dallapiccola B. Grouping of multiple-lentigines/ LEOPARD and Noonan syndromes on the *PTPN11* gene. *Am. J. Hum. Genet.* 2002; 71:389-394.

Dikic I and Schmidt MH. Malfunctions within the Cbl interactome uncouple receptor tyrosine kinases from destructive transport. *Eur. J. Cell. Biol*. 2007; 86:505-512.

Drechsel DN, Hyman AA, Hall A, Glotzer M. A requirement for Rhoand Cdc42 during cytokinesis in *Xenopus*embryos. *Curr. Biol.* 1997; 7:12-23.

Dvorsky R and Ahmadian MR. Always look on the bright site of Rho: structural implications for a conserved intermolecular interface. *EMBO Rep.* 2004; 5(12):1130-1136.

Dvorsky R and Ahmadian MR. Always look on the bright site of Rho: structural implications for a conserved intermolecular interface. *EMBO Rep.* 2005; 5:1130-1136.

Eberth A, Dvorsky R, Becker CF, Beste A, Goody RS, Ahmadian MR. Monitoring the real-time kinetics of the hydrolysis reaction of guanine nucleotide-binding proteins. *Biol. Chem.* 2005; 386:1105-1114.

Eberth A and Ahmadian MR. In vitro GEF and GAP assays. *Curr. Protoc. Cell Biol.* 2009; 43:14.9.1–14.9.25.

Eerola I, Boon LM, Mulliken JB, Burrows PE, Dompmartin A,Watanabe S, Vanwijck R, Vikkula M. Capillary malformation– arteriovenous malformati on, a new clinical and genetic disorder caused by RASA1 mutations. *Am. J. Hum. Genet.* 2003; 73:1240-1249.

Eisenmann DM and Kim SK. Protruding vulva mutants identify novel loci and Wnt signaling factors that function during *Caenorhabditis elegans* vulva development. *Genetics*.2000; 156:1097-1116.

Emanuel PD. Juvenile myelomonocytic leukemia and chronic myelomonocytic leukemia. *Leukemia*. 2008; 22:1335-1342.

Flex E, Jaiswal M, Pantaleoni F, Martinelli S, Strullu M, Fansa EK, Caye A, De Luca A, Lepri F, Dvorsky R, Pannone L, Paolacci S, Zhang SC, Fodale V, Bocchinfuso G, Rossi C, Burkitt-Wright EM, Farrotti A, Stellacci E, Cecchetti S, Ferese R, Bottero L, Castro S, Fenneteau O, Brethon B, Sanchez M, Roberts AE, Yntema HG, Van DerBurgt I, Cianci P, Bondeson ML, Digilio CM, Zampino G, Kerr B, Aoki Y, Loh ML, Palleschi A, Di Schiavi E, Carè A, Selicorni A, Dallapiccola B, Cirstea IC, Stella L, Zenker M, Gelb BD, Cavé H, Ahmadian MR, Tartaglia M. Activating mutations in *RRAS* underlie a phenotype within the RASopathy spectrum and contribute to leukaemogenesis. *Hum. Mol. Genet.* 2014; 23(16):4315-27.

Flotho C, Kratz CP, Bergsträsser E, Hasle H, Starý J, Trebo M, van den Heuvel-Eibrink MM, Wójcik D, Zecca M, Locatelli F, Niemeyer CM; Europe an Working Group of Myelodysplastic Syndromes in Childhood. Genotype-phenotype correlation in cases of juvenile myelomonocytic leukemia with clonal RAS mutations. *Blood.* 2008; 111:966-967.

Foster R, Hu KQ, Lu Y,Nolan KM, Thissen J, Settleman J. Identification of a novel human Rho protein with unusual properties: GTPase deficiency and in vivo farnesylation. *Mol. Cell. Biol.* 1996; 16(6):2689-2699.

Gibbs JB, Sigal IS, Poe M, Scolnick EM. Intrinsic GTPase activity distinguishes normal and oncogenic ras p21 molecules. *Proc. Natl. Acad. Sci. U. S. A.* 1984; 8:5704-5708.

Gremer L, De Luca A, Merbitz-Zahradnik T, Dallapiccola B, Morlot S, Tartaglia M, Kutsche K, Ahmadian MR, Rosenberger G. Duplication of Glu37 in the switch I region of HRAS impairs effector/GAP binding and underlies Costello syndrome by promoting enhanced growth factor-dependent MAPK and AKT activation. *Hum. Mol. Genet.* 2010; 19(5):790-802.

Gremer L, Merbitz-Zahradnik T, Dvorsky R, Cirstea IC, Kratz CP, Zenker M, Wittinghofer A, Ahmadian MR. Germline *KRAS* mutations cause aberrant biochemical and physical properties leading to developmental disorders. *Hum. Mutat.* 2011; 32:33-43.

Gotta M, Abraham MC, Ahringer J. CDC-42 controls early cell polarity and spindle orientation in *C. elegans*. *Curr. Biol.* 2001; 11(7):482-488.

Gupton SL and Gertler FB. Filopodia: the fingers that do the walking. *Sci. Signal.* 2007:re5.

Hall A. Rho GTPases and the actin cytoskeleton. *Science*. 1998; 279:509-514.

Hall A. Rho GTPases and the control of cell behaviour. *Biochem. Soc. Trans.* 2005; 33(Pt 5):891 895.

Han M and Sternberg PW. let-60, a gene that specifies cell fates during *C. elegans* vulval induction, encodes a ras protein. *Cell.* 1990;63(5):921-31.

Han M, Golden A, Han Y, Sternberg PW. *C. elegans lin-45* raf gene participates in *let-60* ras-stimulated vulval differentiation. *Nature.* 1993; 363:133-140.

Hemsath L, Dvorsky R, Fiegen D, Carlier MF, Ahmadian MR. An electrostatic steering mechanism of Cdc42 recognition by Wiskott-Aldrich syndrome proteins. *Mol. Cell.* 2005; 20:313-324.

Hemsath L and Ahmadian MR. Fluorescence approaches for monitoring interactions of Rho GTPases with nucleotides, regulators, and effectors. *Methods* 2005; 37:173-182.

Herman RK and Hedgecock EM. Limitation of the size of the vulval primordium of *Caenorhabditis elegans* by *lin-15* expression in surrounding hypodermis. *Nature.* 1990; 348:169-171.

Hodge RG and Ridley AJ. Regulating Rho GTPases and their regulators. *Nature Reviews Molecular Cell Biology.* 2016; doi:10.1038/nrm.2016.67.

Hof P, Pluskey S, Dhe-Paganon S, Eck MJ, Shoelson SE. Crystal structure of the tyrosine phosphatase SHP-2. *Cell*. 1998; 92:441-450.

Horvitz HR and Sternberg PW. Multiple intercellular signaling systems control the development of the *Caenorhabditis elegans* vulva. *Nature*. 1991; 351:535-541.

Jaffe AB and Hall A. "Rho GTPases: biochemistry and biology." *Annu. Rev. Cell. Dev. Biol.* 2005; 21:247-269.

Jaiswal M, Dubey BN, Koessmeier KT, Gremer L, Ahmadian MR. Biochemical assays to characterise Rho GTPases. *Methods Mol. Biol.* 2012; 827:37-58.

Jaiswal M, Dvorsky R, Ahmadian MR. Deciphering the molecular and functional basis of Dbl family proteins: a novel systematic approach toward classification of selective activation of the Rho family proteins. *J. Biol. Chem.* 2013; 288:4486-4500.

Jaiswal M, Dvorsky R, Amin E, Risse SL, Fansa EK, Zhang SC, Taha MS, Gauhar AR, Nakhaei-Rad S, Kordes C, Koessmeier KT, Cirstea IC, Olayioye MA, Häussinger D, Ahmadian MR. Functional cross-talk between ras and rho pathways: a Ras-specific GTPase-activating protein (p120RasGAP) competitively inhibits the RhoGAP activity of deleted in liver cancer (DLC) tumor suppressor by masking the catalytic arginine finger. *J. Biol. Chem.* 2014; 289:6839-6849.

Jopling C, van Geemen D, den Hertog J. Shp2 knockdown and Noonan/LEOPARD mutant Shp2-induced gastrulation defects. *PLoS. Genet.* 2007; 3:e225.

Jorgensen EM and Mango SE. The art and design of genetic screens: *Caenorhabditi selegans. Nat. Rev. Gen*. 2002; 3:356-369.

Kamath RS, Martinez-Campos M, Zipperlen P, Fraser AG, Ahringer J. Effectiveness of specific RNA-mediated interference through ingested double-stranded RNA in *Caenorhabditis elegans. Genome Biol.* 2001; 2(1):RESEARCH0002.

Kay AJ and Hunter CP. CDC-42 regulates PAR protein localization and function to control cellular and embryonic polarity in *C. elegans*. *Curr. Biol.* 2001; 11(7):474-481.

Keilhack H, David FS, McGregor M, Cantley LC, Neel BG. Diverse biochemical properties of Shp2 mutants. Implications for disease phenotypes. *J. Biol. Chem*. 2005; 280:30984-30993.

Kishore RS and Sundaram MV. *ced-10*Rac and *mig-2* function redundantly and act with *unc-73* trio to control the orientation of vulval cell divisions and migrations in *Caenorhabditis elegans*. *Dev. Biol.* 2005*;* 241:339-48.

Kornfeld K, Guan KL, Horvitz HR. The *Caenorhabditis elegans* gene *mek-2* is required for vulval induction and encodes a protein similar to the protein kinase MEK. *Genes Dev.* 1995*;* 9: 756-768.

Kratz CP, Niemeyer CM, Zenker M. An unexpected new role of mutant Ras: perturbation of human embryonic development. *J. Mol. Med.* 2007; 85:227-235.

Krengel U, Schlichting I, Scherer A, Schumann R, Frech M, John J, Kabsch W, Pai EF, Wittinghofer A. Three-dimensional structures of H-ras p21 mutants: molecular basis for their inability to function as signal switch molecules. *Cell.* 1990; 62:539-548.

Kozma R, Ahmed S, Best A, Lim L. The Ras-related protein Cdc42Hs and bradykinin promote formation of peripheral actin microspikes and filopodia in Swiss 3T3 fibroblasts. *Mol. Cell. Biol*. 1995; 15:1942-1952

Kuppens S, Dıaz JF, Engelborghs Y. Characterization of the hinges of the effector loop in the reaction pathway of the activation ofras-proteins. Kinetics of binding of beryllium trifluoride to V29G and I36G mutants of Hras-p21. *Prot. Sci*. 1999; 8:1860-1866.

Lackner MR, Kornfeld K, Miller, LM, Horvitz HR, Kim SK. A MAP kinase homolog, *mpk-1*, is involved in ras-mediated induction of vulval cell fates in *Caenorhabditis elegans*. *Genes Dev.* 1994*;* 8:160-173.

Lauffenburger DA and Horwitz AF. Cell migration: aphysically integrated molecular process. *Cell.* 1996; 84:359-369.

Loh ML. Recent advances in the pathogenesis and treatment of juvenile myelomonocytic leukaemia. *Br. J. Haematol.* 2011; 152:677-687.

Liang PH, Ko TP, Wang AH. Structure, mechanism and function of prenyltransferases. *Eur. J. Biochem*. 2002; 269(14):3339-3354.

Lohmer LL, Clay MR, Naegeli KM, Chi Q, Ziel JW, Hagedorn EJ, Park JE, Jayadev R, Sherwood DR. A Sensitized Screen for Genes Promoting Invadopodia Function In Vivo: CDC-42 and Rab GDI-1 Direct Distinct Aspects of Invadopodia Formation. *PLoS Genet.* 2016; 12(1):e1005786.

Lowe DG, Capon DJ, Delwart E, Sakaguchi AY, Naylor SL, Goeddel DV. Structure of the human and murine R-ras genes, novel genes closely related to ras proto-oncogenes. *Cell*. 1987; 48:137-146.

Lundquist EA. Small GTPases. In *WormBook*. The *C. elegans* Research Community, WormBook (ed.), http://www.wormbook.org. 2006;doi:/ 10.1895/wormbook.1.67.1.

Luo L, Jan L Y, Jan YN. Rho family GTP-binding proteins in growth cone signalling. *Curr. Opin. Neurobiol.*1997; 7:81-86.

Madaule P and Axel R. A novel ras-related gene family. *Cell*. 1985; 41(1): 31-40.

Mabuchi I, Hamaguchi Y, Fujimoto H, Morii N, Mishima M, Narumiya S.A rho-like protein is involved in the organisation of the contractile ring individing sand dollar eggs. *Zygote.* 1993; 1: 325-331.

Magini P, Pippucci T, Tsai IC, Coppola S, Stellacci E, Bartoletti-Stella A, Turchetti D, Graziano C, Cenacchi G, Neri I, Cordelli DM, Marchiani V, Bergamaschi R, Gasparre G, Neri G, Mazzanti L, Patrizi A, Franzoni E, Romeo G, Bordo D, Tartaglia M, Katsanis N, Seri M. A mutation in PAK3 with a dual molecular effect deregulates the RAS/MAPK pathway and drives an X linked syndromic phenotype. *Hum. Mol. Genet.* 2014; 23(13):3607-3617.

Marte BM, Rodriguez-Viciana P, Wennstrom S, Warne PH, Downward J. R-Ras can activate the phosphoinositide 3-kinase but not theMAPkinase arm of the Ras effector pathways. *Curr. Biol.* 1997; 7:63-70.

Martinelli S, Torreri P, Tinti M, Stella L, Bocchinfuso G, Flex E, Grottesi A, Ceccarini M, Palleschi A, Cesareni G, Castagnoli L, Petrucci TC, Gelb BD, Tartaglia M. Diverse driving forces underlie the invariant occurrence of the T42A, E139D, I282V and T468M SHP2 amino acid substitutions causing Noonan and LEOPARD syndromes. *Hum. Mol. Genet.* 2008; 17:2018-2029.

Martinelli S, De Luca A, Stellacci E, Rossi C, Checquolo S, Lepri F, Caputo V, Silvano M, Buscherini F, Consoli F, Ferrara G, Digilio MC, Cavaliere ML, van Hagen JM, Zampino G, van derBurgt I, Ferrero GB, Mazzanti L, Screpanti I, Yntema HG, Nillesen WM, Savarirayan R, Zenker M, Dallapiccola B, Gelb BD, Tartaglia M. Heterozygous germline mutations in the *CBL* tumor-suppressor gene cause a Noonan syndrome-like phenotype. *Am. J. Hum. Genet.* 2010; 87:250-257.

Matsuda K, Shimada A, Yoshida N, Ogawa A, Watanabe A, Yajima S, Iizuka S, Koike K, Yanai F, Kawasaki K, Yanagimachi M, Kikuchi A, Ohtsuka Y, Hidaka E, Yamauchi K, Tanaka M, Yanagisawa R, Nakazawa Y, Shiohara M, Manabe A, Kojima S, Koike K. Spontaneous improvement of hematologic abnormalities in patients having juvenile myelomonocytic leukemia with specific RAS mutations. *Blood.* 2007; 109:5477-5480.

Mayor R and Carmona-Fontaine C. Keeping in touch with contact inhibition of locomotion. *Trends in Cell Biology* 2010; 20(6):319-328.

McKay MM and Morrison DK. Integrating signals from RTKs to ERK/MAPK. *Oncogene*.2007; 26:3113-3121.

McGrath JP, Capon DJ, Goeddel DV, Levinson AD. Comparative biochemical properties of normal and activated human ras p21 protein. *Nature*. 1984; 310:644-649.

Melendez J, Grogg M, Zheng Y. Signaling role of Cdc42 in regulating mammalian physiology. *J. Biol. Chem.* 2011; 286(4):2375-2381.

Melendez J, Liu M, Sampson L, Akunuru S, Han X, Vallance J, Witte D, Shroyer N, Zheng Y. Cdc42 coordinates proliferation, polarity, migration, and differentiation of small intestinal epithelial cells in mice. *Gastroenterology.* 2013; 145(4):808-819.

Mello CC, Kramer JM, Stinchcomb D and Ambros V. Efficient gene transfer in *C. elegans*: extrachromosomal maintenance and integration of transforming sequences. *EMBO J.* 1991; 10:3959-3970.

Milburn MV, Tong L, deVos AM, Brunger A, Yamaizumi Z, Nishimura S, Kim SH. Molecular switch for signal transduction: structural differences between active and inactive forms of proto-oncogenic ras proteins. *Science*. 1990; 247:939-945.

Moghal N and Sternberg PW. The epidermal growth factor system in *Caenorhabditis elegans. Exp. Cell. Res.* 2003; 284:150-159.

Nacak TG, Leptien K, Fellner D, Augustin HG, Kroll J. The BTB-kelch protein LZTR-1 is a novel Golgi proteinthat is degraded upon induction of apoptosis. *J. Biol. Chem*. 2006; 281:5065-5071.

Niemeyer CM and Kratz CP. Paediatric myelodysplastic syndromes and juvenile myelomonocytic leukaemia: molecular classification and treatment options. *Br. J. Haematol.* 2008; 140:610-624.

Niemeyer CM, Kang MW, Shin DH, Furlan I, Erlacher M,Bunin NJ, Bunda S, Finklestein JZ, Sakamoto KM, Gorr TA, Mehta P, Schmid I, Kropshofer G, Corbacioglu S, Lang PJ, Klein C, Schlegel PG, Heinzmann A, Schneider M, Starý J, van denHeuvel-Eibrink MM, Hasle H, Locatelli F, Sakai D, Archambeault S, Chen L, Russell RC, Sybingco SS, Ohh M, Braun BS, Flotho C, Loh ML. Germline *CBL* mutations cause developmental abnormalities and predispose to juvenile myelomonocytic leukemia. *Nat. Genet.* 2010; 42:794-800.

Niihori T, Aoki Y, Narumi Y, Neri G, Cavé H,Cavé H,Verloes A, Okamoto N, Hennekam RC, Gillessen-Kaesbach G, Wieczorek D, Kavamura MI, Kurosawa K, Ohashi H, Wilson L, Heron D, Bonneau D, Corona G, Kaname T, Naritomi K, Baumann C, Matsumoto N, Kato K, Kure S, Matsubara Y. Germline KRAS and BRAF mutations in cardio-facio-cutaneous syndrome. *Nat. Genet.* 2006; 38:294-296.

Nobes CD and Hall A. Rho GTPases control polarity, protrusion, andadhesion during cell movement. *J. Cell. Biol.*1999; 144:1235-1244.

Osada M, Tolkacheva T, Li W, Chan TO, Tsichlis PN, Saez R, Kimmelman AC, Chan AM. Differential roles of Akt, Rac, andRal in R-Ras-mediated cellular transformation, adhesion, and survival. *Mol. Cell. Biol.* 1999; 19:6333-6344.

Ouellette MH, Martin E, Lacoste-Caron G, Hamiche K, Jenna S. Spatial control of active CDC-42 during collective migration of hypodermal cells in *Caenorhabditis elegans*. *J. Mol. Cell. Biol.* 2016; 8(4):313-327.

Pandit B, Sarkozy A, Pennacchio LA, Carta C, Oishi K, Martinelli S, Pogna EA, Schackwitz W, Ustaszewska A, Landstrom A, Bos JM, Ommen SR, Esposito G, Lepri F, Faul C, Mundel P, LópezSiguero JP, Tenconi R, Selicorni A, Rossi C, M azzanti L, Torrente I, Marino B, Digilio MC, Zampino G, Ackerman MJ, Dallapiccola B, Tartaglia M, Gelb BD. Gain-of-function RAF1 mutations cause Noonan and LEOPARD syndromes with hypertrophic cardiomyopathy. *Nat. Genet*. 2007; 39:1007-1012.

Park HD, Lee SH, Sung KW, Koo HH, Jung NG, Cho B, Kim HK, Park IA, Lee KO, Ki CS, Kim SH, Yoo KH, Kim HJ. Gene mutations in the Ras pathway and the prognostic implication in Korean patients with juvenile myelomonocytic leukemia. *Ann. Hematol.* 2012; 91:511-517.

Perez B, Kosmider O, Cassinat B, Renneville A, Lachenaud J, Kaltenbach S, Bertrand Y, Baruchel A, Chomienne C, Fontenay M, Preudhomme C, Cavé H. Genetic typing of CBL, ASXL1, RUNX1, TET2 andJAK2 in juvenile myelomonocytic leukaemia reveals a genetic profile distinct from chronic myelomonocytic leukaemia. *Br. J. Haematol.* 2010; 151:460-468.

Pritchard C, Carragher L, Aldridge V, Giblett S, Jin H, Foster C, Andreadi C, Kamata T. Mouse models for *BRAF*-induced cancers. *Biochem. Soc. Trans*. 2007; 35:1329-1333.

Rankin CH. From gene to identified neuron to behaviour in *Caenorhabditis elegans*. *Nat. Rev. Genet*. 2002; 3:622-630.

Prokopenko SN, Saint R, Bellen HJ. Untying the gordian knot of cytokinesis : role of small g proteins and their regulators. *J. Cell. Biol.*2000; 148:843-848.

Rauen KA. The RASopathies. *Annu. Rev. Genomics. Hum. Genet.*2013;14:355-369.

Razzaque MA, Nishizawa T, Komoike Y, Yagi H, Furutani M, Amo R, Kamisago M, Momma K, Katayama H, Nakagawa M, Fujiwara Y, Matsushima M, Mizuno K, Tokuyama M, Hirota H, Muneuchi J, Higashinakagawa T, Matsuoka R. Germline gain-of-function mutations in *RAF1* cause Noonan syndrome. *Nat. Genet*. 2007; 39:1013-1017.

Ridley AJ, Paterson HF, Johnston CL, Diekmann D, Hall A. The small GTP-binding protein rac regulates growth factor-induced membrane ruffling. *Cell.* 1992; 70*:*401-410

Ridley AJ.Rho. In GTPases (Hall, A., ed.). 2000; pp. 89–136, Oxford University Press, Oxford.

Roberts AE, Araki T, Swanson KD, Montgomery KT, Schiripo TA,Joshi VA, Li L, Yassin Y, Tamburino AM, Neel BG, Kucherlapati RS. Germline gain-of function mutations in *SOS1* cause Noonan syndrome. *Nat. Genet*. 2007; 39:70-74.

Roberts AE, Allanson JE, Tartaglia M, Gelb BD. Noonan syndrome. *Lancet.* 2013; 381:333-342.

Rodriguez-Viciana P, Tetsu O, Tidyman WE, Estep AL, Conger BA, Cruz MS, McCormick F, Rauen KA. Germline mutations in genes within the MAPK pathway cause cardio-facio-cutaneous syndrome. *Science*. 2006; 311:1287-1290.

Rodriguez-Viciana P, Oses-Prieto J, Burlingame A, Fried M, McCormick F. A phosphatase holoenzyme comprised of Shoc2/Sur8 and the catalytic subunit of PP1 functions as an M-Ras effector to modulate Raf activity. *Mol. Cell*. 2006; 22:217-230.

Saez R, Chan AM, Miki T, Aaronson SA. Oncogenic activation of human R-ras by point mutations analogousto those of prototype H-ras oncogenes. *Oncogene*. 1994; 9:2977-2982.

Sakaguchi H, Okuno Y, Muramatsu H, Yoshida K, Shiraishi Y, Takahashi M, Kon A, Sanada M, Chiba K, Tanaka H, Makishima H, Wang X, Xu Y, Doisaki S, Hama A, Nakanishi K, Takahashi Y, Yoshida N, Maciejewski JP, Miyano S, Ogawa S, Kojima S. Exome sequencing identifies secondary mutations of SETBP1 and JAK3 in juvenile myelomonocytic leukemia. *Nat. Genet.* 2013; 45:937-941.

Sawa M, Suetsugu S, Sugimoto A, Miki H, Yamamoto M, Takenawa T. Essential role of the *C. elegans* Arp2/3 complex in cell migration during ventral enclosure. *J. Cell. Sci.* 2003; 116(Pt 8):1505-18.

Schlessinger J. Cell signaling by receptor tyrosine kinases. Cell. 2000; 103(2):211-25.

Schonegg S and Hyman AA. CDC-42 and RHO-1 coordinate acto-myosin contractility and PAR protein localization during polarity establishment in *C. elegans* embryos.*Development.* 2006; 133(18):3507-3516.

Schubbert S, Zenker M, Rowe SL, Boll S, Klein C, Bollag G, van der Burgt I, Musante L, Kalscheuer V, Wehner LE, Nguyen H, West B, Zhang KY, Sistermans E, Rauch A, Niemeyer CM, Shannon K, Kratz CP. Germline *KRAS* mutations cause Noonan syndrome. *Nat. Genet*. 2006; 38:331-336.

Schubbert S, Bollag G, Lyubynska N, Nguyen H, Kratz CP, Zenker M, Niemeyer CM, Molven A, Shannon K. Biochemical and functional characterization of germline KRAS mutations. *Mol. Cell.Biol*. 2007; 27:7765-7770.

Schwarz EM. Genomic classification of protein-coding gene families. In: The *C. elegans* Research Community, ed. WormBook 2005, doi/10.1895/wormbook.1.29.1, http://www.wormbook.org.

Settleman J. Rho GTPases in development. *Prog. Mol. Subcell. Biol.*1999; 22:201-229.

Schwartz M. Rho signalling at a glance.*J. Cell. Sci*. 2004;117(Pt 23):5457-5458.

Silverman, Luke CJ, Bhatia SR, Long OS, Vetica AC, Perlmutter DH, Pak SC. Modeling Molecular and Cellular Aspects of Human Disease using the Nematode *Caenorhabditis elegans*. *Pediatr. Res*. 2009; 65(1): 10-18.

Spieth J and Lawson D. Overview of gene structure. *WormBook*. 2006; 18:1-10.

Sternberg PW. Vulval development. *WormBook*. 2005;1-28.

Sulston JE and Hodgkin J. Methods. In Wood, W.B. and The Community of C. elegans Researchers (ed.), 1988. The Nematode *Caenorhabditis Elegans*. Cold Spring Harbor Laboratory Press, Cold Spring Harbor,NY, pp. 587-606.

Sundaram MV. Canonical RTK-Ras-ERK signaling and related alternative pathways. *WormBook*. 2013; 11:1-38.

Sweet RW, Yokoyama S, Kamata T, Feramisco JR, Rosenberg M, Gross M. The product of ras is a GTPase and the T24 oncogenic mutant is deficient in this activity. *Nature*. 1984; 311:273-275.

Takagi M, Piao J, Lin L, Kawaguchi H, Imai C, Ogawa A, Watanabe A, Akiyama K, Kobayashi C, Mori M, Ko K, Sugimoto M, Mizutani S. Autoimmunity and persistent RAS-mutated clones long after the spontaneous regression of JMML. *Leukaemia.* 2013; 27:1926-1928.

Takenouchi T, Kosaki R, Niizuma T, Hata K, Kosaki K. Macrothrombocytopenia and developmental delay with a de novo CDC42 mutation: Yet another locus for thrombocytopenia and developmental delay. *Am. J. Med. Genet. A.* 2015; 167A(11):2822-2825.

Takenouchi T, Okamoto N, Ida S, Uehara T, Kosaki K. Further evidence of a mutation in CDC42 as a cause of a recognizable syndromic form of thrombocytopenia. *Am. J. Med. Genet. A.* 2016; 170A(4):852-855.

Tan P and Kim SK. Signaling specificity: the RTK/Ras/MAP kinase pathway in metazoans. *Trends Genet.* 1999; 15:145-149.

Tartaglia M, Mehler EL, Goldberg R, Zampino G, Brunner HG, Kremer H, van der Burgt I, Crosby AH, Ion A, Jeffery S, Kalidas K, Patton MA, Kucherlapati RS, Gelb BD. Mutations in *PTPN11*, encoding the protein tyrosine phosphatase SHP-2, cause Noonan syndrome. *Nat. Genet*. 2001; 29:465-468.

Tartaglia M, Martinelli S, Stella L, Bocchinfuso G, Fle, E, Cordeddu V, Zampino G, Burgt I, Palleschi A, Petrucci TC,Schoch C, Foa R, Emanuel PD, Gelb BD. Diversity and functional consequences of germline and somatic PTPN11 mutations in human disease. *Am. J. Hum. Genet*. 2006; 78:279-290.

Tartaglia M, Pennacchio LA, Zhao C, Yadav KK, Fodale V,Sarkozy A, Pandit B, Oishi K, Martinelli S, Schackwitz W, Ustaszewska A, Martin J, Bristow J, Carta C, Lepri F, Neri C, Vasta I, Gibson K, Curry CJ, Siguero JP, Digilio MC, Zampino G, Dallapiccola B, Bar-Sagi D, Gelb BD.

Gain-of-function *SOS1* mutations cause a distinctive form of Noonan syndrome. *Nat. Genet*. 2007; 39:75-79.

Tartaglia M, Gelb BD, Zenker M. Noonan syndrome and clinically related disorders. *Best. Pract. Res. Clin. Endocrinol. Metab.* 2011; 25(1):161-79.

Tidyman WE and Rauen KA. Pathogenetics of the RASopathies. *Hum. Mol. Genet*. 2016; 1-10.

Viskochil D, Buchberg AM, Xu G, Cawthon RM, Stevens J, Wolff RK, Culver M, Carey JC, Copeland NG, Jenkins NA, *et al*. Deletions and a trans location interrupt a cloned gene at the neurofibromatosis type 1 locus. *Cell*. 1990; 62:187-192.

Wakioka T, Sasaki A, Kato R, Shouda T, Matsumoto A, Miyoshi K, Tsuneoka M, Komiya S., Baron R, Yoshimura A. Spred is a Sprouty-related suppressor of Ras signalling. *Nature*. 2001; 412:647-651.

Wallace MR, Marchuk DA, Andersen LB, Letcher R, Odeh HM, Saulino AM, Fountain JW, Brereton A, Nicholson J, Mitchell AL, *et al*. Type 1 neurofibromatosis gene: identification of a large transcript disrupted in three NF1 patients. *Science*. 1990; 249:181-186.

Wang M and Sternberg P. Pattern formation during *C. elegans vulval* induction. *Curr. Top. Dev. Biol.* 2001; 51:189-220.

Wang S, Yu WM, Zhang W, McCrae KR, Neel BG, Qu, CK. Noonan syndrome/leukemia-associated gain-of-function mutationsin SHP-2 phosphatase (PTPN11) enhance cell migration and angiogenesis. *J. Biol. Chem.* 2009; 284:913-920.

Welchman DP, Mathies LD, Ahringer J. Similar requirements for CDC-42 and the PAR-3/PAR-6/PKC-3 complex in diverse cell types.*Dev. Biol.* 2007;305(1):347-357.

Wennerberg K and Rossman KL, Der CJ. The Ras superfamily at a glance. *J. Cell. Sci.* 2005; 118:843-846.

Wheeler AP and Ridley AJ. Why three Rho proteins? RhoA, RhoB, RhoC, and cell motility. *Exp. Cell. Res.* 2004; 301:43-49.

Wozniak MA, Kwong L, Chodniewicz D, Klemke RL, Keely PJ. R-Ras controls membrane protrusion and cell migration through the spatial regulation of Rac and Rho. *Mol. Biol. Cell.* 2005; 16:84-96.

Wu Y and Han M. Suppression of activated Let-60 Ras defines a role of *Caenorhabditiselegans sur-1* MAP kinase in vulval differentiation. *Genes Dev.* 1994*;* 8:147-159.

Wu Y, Han M, Guan KL. MEK-2, a *Caenorhabditis elegans* MAP kinase kinase, functions in Ras-mediated vulval induction and other developmental events. *Genes Dev.* 1995*;* 9:742-755.

Yamamoto GL, Aguena M, Gos M, Hung C, Pilch J, Fahiminiya S, Abramowicz A, Cristian I, Buscarilli M, Naslavsky MS,Malaquias AC, Zatz M, Bodamer O, Majewski J, Jorge AA, Pereira AC, Kim CA, Passos-Bueno MR, Bertola DR. Rare variants in SOS2 and LZTR1 are associated with Noonan syndrome. *J. Med. Genet*. 2015; 52: 413-421.

Yamamoto GL, Aguena M, Gos M, Hung C, Pilch J,Fahiminiya S, Abramowicz A, Cristian I, Buscarilli M,Naslavsky MS, Malaquias AC, Zatz M, Bodamer O, Majewski J, Jorge AA, Pereira

AC, Kim CA, Passos-Bueno MR, Bertola DR. Rare variants in SOS2 and LZTR1are associated with Noonan syndrome. *J. Med. Genet*. 2015;52:413-421.

Yoon S and Seger R. The extracellular signal-regulated kinase: multiple substrates regulate diverse cellular functions. *Growth Factors*. 2006; 24:21-44.

Zegers MM and Friedl P. Rho GTPases in collective cell migration. *Small GTPases.* 2014;5:e28997.

Publications

Pannone L, Bocchinfuso G, Flex E, Rossi C, Baldassarre G, Lissewski C, Pantaleoni F, Consoli F, Lepri F, Magliozzi M, Anselmi M, Sorge G, Karaer K, Cuturilo G, Sartorio A, Tinschert S, Accadia M, Digilio MC, Zampino G, De Luca A, Cavé H, ZenkerM, Gelb BD, Dallapiccola B, Stella L, Ferrero GB, Martinelli S, Tartaglia M (2017). Structural, functional and clinical characterization of a novel *PTPN11* mutation cluster underlying Noonan syndrome. ***Hum Mutat***, doi: 10.1002/humu.23175.

Martinelli S, Stellacci E, Pannone L, D'Agostino D, Consoli F, Lissewski C, Silvano M, Cencelli G, Lepri F, Maitz S, Pauli S, Rauch A, Zampino G, Selicorni A, Melançon S, Digilio MC, Gelb BD, De Luca A, Dallapiccola B, Zenker M, Tartaglia M (2015) Molecular diversity and associated phenotypic spectrum of germline *CBL* mutations. ***Hum Mutat***, *36:787-796.*

Edwards JJ, Martinelli S, Pannone L, Lo IF, Shi L, Edelmann L, Tartaglia M, Luk HM, Gelb BD. (2014) A *PTPN11* allele encoding a catalytically impaired SHP2 protein in a patient with a Noonan syndrome phenotype. ***Am J Med Genet***, *164A:2351-2355.*

Flex E, Jaiswal M, Pantaleoni F, Martinelli S, Strullu M, Fansa EK, Caye A, De Luca A, Lepri F, Dvorsky R, Pannone L, Paolacci S, Zhang S, Fodale V, Bocchinfuso G, Rossi C, Burkitt-Wright EMM, Farrotti A, Stellacci E, Cecchetti S, Ferese R, Bottero L, Castro S, Fenneteau O, Brethon B, Sanchez M, Roberts AE, Yntema HG, van der Burgt I, Cianci P, Bondeson ML, Digilio MC, Zampino G, Kerr B, Aoki Y, Loh ML, Palleschi A, Di Schiavi E, Carè A, Selicorni A, Dallapiccola B, Cirstea IC, Stella L, Zenker M, Gelb BD, Cavé H,Ahmadian MR, Tartaglia M (2014) Activating mutations in *RRAS* underlie a phenotype within the RASopathy spectrum and contribute to leukaemogenesis. ***Hum Mol Genet***, *23:4315-27*.